Synthesis and Characterization of Agricultural Waste Carbon-based Structures for Application in Sensing

By

Lindokuhle Precious Magagula

Student number: 1477491

A dissertation submitted to the Faculty of Science, University of the Witwatersrand, Johannesburg, in partial fulfilment of the requirements for the award of the degree of Master of Science in Chemistry.

Supervisor: Dr Cebisa E. Linganiso

Co-Supervisor: Prof. Nosipho Moloto

University of the Witwatersrand, Johannesburg, March 2022

Declaration

I declare that this dissertation is my own, unaided work. It is being submitted for the degree of Master of Science at the University of the Witwatersrand, Johannesburg. It has not been submitted before for any degree or examination at any other University.

UNIVERSITY OF THE
WITWATERSRAND,
JOHANNESBURG

(Signature of candidate)

On this 6th day of August 2022

Abstract

Rapid population and economic growths, excessive use of fossil fuels, and climate change have contributed to a serious turn towards environmental management and sustainability. The agricultural sector is a big contributor to (lignocellulosic) waste, which accumulates in landfills and ultimately gets burnt, polluting the environment. In response to the current climate change crisis, policy makers and researchers are respectively encouraging and seeking ways of creating value-added products from generated waste. Recently, agricultural waste is making a regular appearance in articles communicating about the production of a range of carbon and polymeric materials worldwide, this has led to a promising concept of waste to wealth in the modern world. The use of biomass waste such as corncob (CC) for the extraction of cellulose nanocrystals (CNCs), synthesis of carbon quantum dots (CQDs), and preparation of activated carbon (AC), has recently gained interest in the area of waste recycling and management. Further, the new materials generated from this waste promise to be effective and competitive in emerging markets.

In this study, CC waste was used as a feedstock for preparation of CNCs, CQDs, and AC (shown in figure 1), for sensing applications. CNCs extracted from CC using acid hydrolysis were compared to the CNCs prepared from commercial microcrystalline cellulose (MCC). The CNCs from CC and MCC revealed comparable thermal, surface/structural, and crystallinity. These were confirmed by various characterization techniques including scanning electron microscopy (SEM), transmission electron microscopy (TEM), X-ray diffraction (XRD), thermogravimetric Analysis (TGA), and Fourier transform infrared (FT-IR). For further comparison on the effect of the hydrolysis, nitro -oxidation was used to prepare nitro-oxidized cellulose nanocrystals (NOCNCs) from CC. The crystallinity indexes of the NOCNCs was obtained to be 74.37 %, which was significantly higher than that of MCC-CNCs (70.24 %), and CC-CNCs (69.12 %). TEM analysis confirmed that the CNCs had different morphologies, while SEM was used to determine the morphological properties of the samples prior to acid hydrolysis.

The as-prepared CC-CNCs and MCC-CNCs were then utilized to prepare highly luminescent nitrogen doped carbon materials, with a high degree of functional groups, sensitivity, and selectivity towards Fe^{3+}. CQDs showed great potential for fluorescent sensor applications. Incorporation of surface functional groups such as nitrogen and oxygen containing groups were confirmed by FT-IR and X-ray photoelectron spectroscopy (XPS) analysis which showed that the prepared N-CQDs were highly functionalized with these heteroatoms, resulting in an excitation-dependent fluorescence emission. The

detection limit of Fe^{3+} was obtained to be 70 nM and 75 nM, for the CC-CNCs and MCC-CNCs derived fluorescent carbon materials, respectively.

Due to its natural porous nature, the corncob was also utilized to prepare activated carbons by chemical activation with potassium carbonate (activating agent) at 800 °C using varied ratios of impregnation. Highly porous corncob derived activated carbon (ACC) material with a surface area of 1523.2 m^2 /g and a pore volume = 0.81 cm^3 /g was. The as-prepared ACC was then decorated with various percentage loadings copper oxide nanoparticles (CuO NPs) was achieved, which produced composites with surface areas and porosity. Simple and room temperature operable sensors based on ACC and the composites were designed on gold-plated interdigitated electrodes (IDEs) embedded on a printed-circuit board (PCB) substrate. The results showed that CuO NPs play an important role in enhancing sensor performance of the ACC since its incorporation improved on the conductivity and response when compared to the ACC-based sensor. The ACC/PVA/CuO 15% sensor demonstrated good reproducibility of the sensing signal when exposed to 100 ppm ethanol vapors for up to four cycles. The sensor exhibited a response and recovery of 125 and 130 seconds, respectively, when exposed to 100 ppm of ethanol. Hence, the ACC/CuO composites could be a future candidate for ethanol gas sensing application at room temperature.

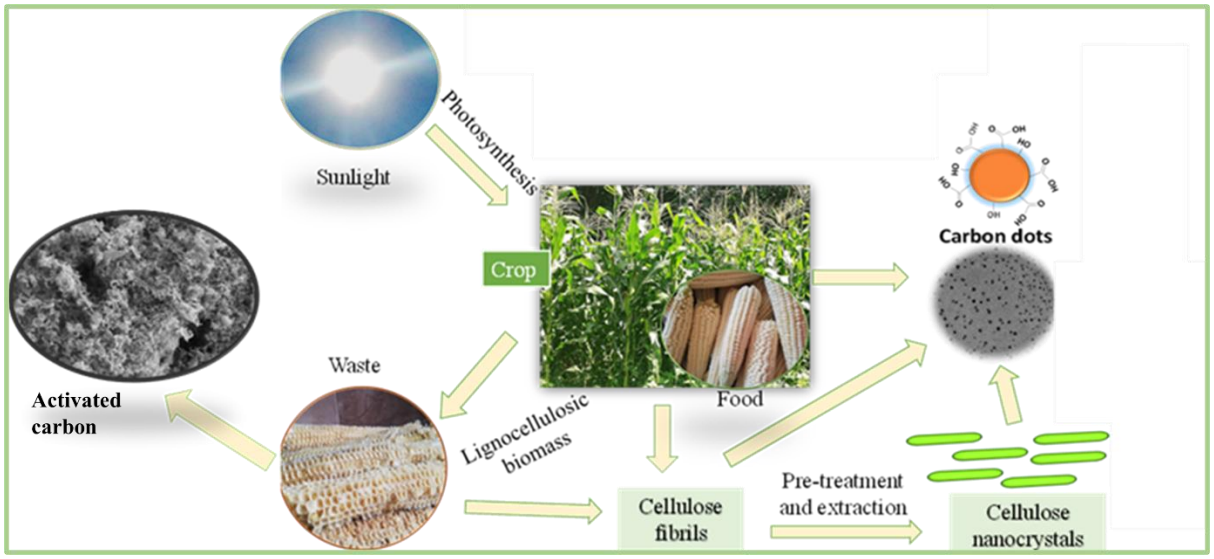

Figure 1: Corncob waste used as a feedstock for preparation of cellulose nanocrystals, carbon quantum dots, and activated carbon.

Dedication

To my mother Agnes Nurse Mlombo, and all the women who never got the opportunity to pursue their studies.

Acknowledgements

- I would like to give my warmest gratitude to my supervisors: Dr. Ella Linganiso and Prof. Nosipho Moloto for their constant support, advice, and guidance during this research project. It has been a wonderful experience to work with you and I am very grateful.
- To the Microscopy and Microanalysis Unit (MMU), thank you for allowing me to access the unit the characterization techniques such as: TEM, SEM and PXRD to analyze my samples.
- I would also like to thank the CATMAT research group especially the following people: Boitumelo Tlhaole, Thulisile Buthelezi, Clinton Masemola, Khanyisile Masemola, Themba Ntuli, Boipelo Mathe, and the others for the support.
- To my friends and family, especially, Agnes Mlombo, Siphesihle Gama, Nomcebo Magagula, Dacod Magagula, Nomthandazo Magagula, Masoka Magagula, and Nonkululeko Magagula. Thank you so much for the support, love, and encouragement.
- To the school of chemistry, thanks for providing me with the laboratories environment to perform my experiments.
- I would also like to thank the National Research Foundation (NRF) for funding. This research project could not be possible without this funding.

Presentations

1. ‘Sustainable conversion of corncob biomass waste into economic, high-performance carbon materials’ (**Oral presentation**), SACI Young Chemist Symposium (National) (July 2021)

2. ‘Sustainable conversion of corncob biomass waste into economic, high-performance carbon materials’ (**Poster presentation**), The 12th Cross-Faculty Postgraduate Symposium 2021 (July 2021)

3. ‘Synthesis of biomass-based fluorescent carbon structures for the detection of Fe (III) in aqueous solutions’ (**Oral presentation**), 10th annual Nanoscience Young Researchers (October 2021)

4. ‘Synthesis of cellulose-based fluorescent carbon quantum dots for the detection of Fe (III) in aqueous solutions’ (**Oral Presentation**), CoSAAMI 2021 (October 2021)

5. ‘Synthesis of fluorescent nitrogen-doped carbon spheres from corncob residue for the detection of Fe (III) in aqueous solutions’ (**Poster presentation**), IEEE Sensors 2021 (November 2021)

6. ‘Sustainable conversion of corncob biomass waste into economic, high-performance carbon materials’ (**Poster presentation**), Carbon Chemistry and Materials conference (November 2021)

Awards

Herman Pistorius Crowd Favourite Award in Oral presentation, SACI Young Chemist Symposium (National) (July 2021) 1.

Publications

1. L. P. Magagula, N. Moloto, S. Gqoba, P. J. Kooyman, T. E. Motaung, and E. C. Linganiso, “Synthesis of fluorescent nitrogen-doped carbon spheres from corncob residue for the detection of Fe (III) in aqueous solutions,” in *2021 IEEE Sensors*, 2021, pp. 1–4, doi: 10.1109/SENSORS47087.2021.9639764.
2. E. C. Linganiso, B. Tlhaole, L. P. Magagula, S. Dziike, L. Z. Linganiso, T. E. Motaung, N. Moloto, and Z. N. Tetana, “Biodiesel Production from Waste Oils: A South African Outlook “, *Sustainability 2022*, 14(4), 1983; https://doi.org/10.3390/su14041983.
3. L. P. Magagula, C. M. Masemola, M. A. Ballim, Z. N. Tetana, N. Moloto, and E. C. Linganiso, “Lignocellulosic biomass waste-derived cellulose nanocrystals and carbon nanomaterials: A review”, International Journal of Molecular Sciences, 23(8), p.4310; https://doi.org/10.3390/ijms23084310.

Table of contents

List of Figures

Chapter 2:

Chapter 3

Chapter 4

Chapter 5

Chapter 6

List of tables:

Chapter 4:

Chapter 5:

Chapter 6:

List of abbreviations:

AC: Activated carbon

ACC: Activated carbon from corncob

A-CC: Alkali treated corncob

B-CC: Bleached corncob

BET: Brunauer-Emmett-Teller

CC: Corncob

CNCs: Cellulose Nanocrystals

CuO NPs: Copper oxide nanoparticles

CVD: Chemical vapour deposition

DTG: Derivative thermal gravimetric

FT-IR: Fourier transform infrared spectroscopy

MCC: Microcrystalline cellulose

NOCNCs: Nitro-oxidised cellulose nanocrystals

N-CQDs: Nitrogen-doped carbon quantum dots

PL: Photoluminescence

PVA: Polyvinyl alcohol

SEM: Scanning electron microscopy

TEM: Transmission electron microscopy

TEMPO: 1-oxo-2,2,6,6-tétraméthylpipyridine 1-oxyle

TGA: Thermal gravimetric analysis

UV-vis: Ultraviolet to visible

XPS: X-ray photoelectron spectroscopy

XRD: X-ray diffraction

Chapter 1: Synopsis

1.1. Background and motivation

The global population size has exponentially risen (approximately 1.5 times) from 5.3 billion in 1990 to 7.3 billion in 2014, with an average annual growth rate of 1.3% [1]. One of the challenges of such a growth is the daunting challenge of food security. In order to fulfil the intense demands of food there has been a significant rise in the production of food which has increased more than three times over the last 50 years [2]. The rapidly increasing food demand, however, has posed tremendous environmental challenges, according to the Food and Agriculture Organization (FAO) an estimated 20–30% of fruits and vegetables are discarded as waste during post-harvest handling contributing towards generation of agricultural wastes [3]. The decomposition of one metric ton of organic agricultural waste can potentially release greenhouse gases including 50–110 m^3 of carbon dioxide and 90–140 m^3 of methane into the atmosphere [4].

Agriculture is an important sector for economic development in South African economy and plays an important role in contributing to household food security. In 2020 the agricultural sector contributed around 10 percent of South Africa's total export earnings at a value of $10.2 billion, with the grain contributing more than 30 percent to the total gross value of agricultural production [5]. Maize (Zea mays), also knowns as corn is the largest locally produced field grain, and the staple source of carbohydrates in the Southern African Development Community (SADC) region for human and animal consumption [5], [6]. South Africa is the main corn producer in the SADC region, with an average production of over 16 million tons produced in the 2019-2020 period, which is 38% higher than the 2018/19 corn crop production of 11.3 million tons [7].

The maize plant is comprised of the stalk, leaf, cob, corn grains, and husk. The corn grains which are the edible corn part of the plant used to produce maize meal, corn flakes, corn flour, and glucose is 20% of the plant's mass and the remaining parts of the plant (cob, husk, leaves, and stalk) are regarded as agricultural waste [8], [9]. The corncob is the central part of the ear maize in which the corn grains are stuck, about 160–180 kg corncobs are generated for every 1 ton of corn, resulting enormous annual corncob yield [10]. Majority of the corncob waste is used for

low value-added applications such as a source of feedstock for livestock, fertilizers, and bedding for small animals, with the remaining portion ending up in dumping sites due to limited space, some of the corncob residues are burnt directly increasing environmental pollution [6], [11]. This is due to the lack of adequate technology and little knowledge about possible value addition on such agricultural wastes, therefore, methods for transforming corncob residues into valuable products are worthy of concern [12]. The utilization these agricultural residues could result in an additional source of revenue for farmers and provide employment opportunities without colliding with the food chain.

In recent years, growing environmental awareness of the society has motivated academic and industrial research in the development towards maximizing the efficiency of the use of raw materials for the development of renewable and suitable materials while minimizing the production of waste [13]. Waste recycling as a waste management strategy in the agricultural sector has cost-saving and ecological implications by reduction of accumulated waste in the environment while converting them into novel, low-cost, high-performance renewable materials[14]. Corncob contains sufficient amount of cellulosic material and has been widely used as a versatile adsorbent for removal of organic pollutants and so on, due to its large specific surface area, porous structure and good adsorption properties [15]. Researchers have reported several studies on the use of corncob residue, including it use as a feedstock for furfural production [16], as a bio-adsorbent [17], for the fabrication of carbon based materials [18], extraction of cellulose [19], and so on. However, the use of corncob to prepare materials suitable to be used as sensing materials is yet to be explored.

Iron (Fe^{3+}) is not only one of the most essential trace elements in biological systems [20]. However, excess iron levels in the living cells and water body had been linked with neurogenerative diseases and pollution [21]. Traditional methods of Fe^{3+} ions detection in water solutions involve relatively expensive Instrument-based detection and electrochemical sensing methods limited by reproducibility, time, and complex preparations [22]. With these limitations, sensitive, simple, and selective detection of Fe^{3+} ions are urgently needed. Recently, quantum dot-based fluorescent sensors have proven to be a very powerful tool for the detection of heavy metal ions in the aqueous solutions, due to their high sensitivity and selectivity, and lower detection limit [23]. Among other quantum dot-based fluorescent sensors, carbon quantum dots (CQDs) have recently gained interest, due to their high biocompatibility, easy availability, low synthesis cost, and low toxicity as compared to their counterparts, semiconductor quantum dots

(QDs) [24]. Despite the fact that many good CQDs sensors have already been reported, there is still a higher demand for simpler, environmentally friendly, and cost-effective methods for the synthesis of CQDs from low cost precursors such as agricultural waste.

Herein, corncob waste was used as a cheap and sustainable precursor to prepare carbon quantum dots (CQDs) and activated carbon (AC), since carbon materials are a promising class of material for potential application in chemical sensors due to their pronounced electrical, optical, and mechanical properties leading to the replacement of less cost-effective and less eco-friendly materials.

1.2 Research objectives

2. Extract cellulose nanocrystals (CNCs) from corncob through acid hydrolysis.
3. Prepare porous carbon structures from corncob using KOH as an activation agent via chemical vapor deposition (CVD) under N_2 conditions.
4. Synthesize N-doped Cdots from the CNCs using microwave-assisted reactions.
5. Synthesize activated carbon/PVA/CuO composites for chemical sensing.
6. Characterize the prepared materials using transmission electron microscopy (TEM), scanning electron microscopy (SEM), thermal gravimetric analysis (TGA), Brunauer-Emmett-Teller (BET), X-ray powder diffraction (XRD), X-ray photoelectron spectroscopy (XPS), ultraviolet–visible spectroscopy (UV-vis), and photoluminescence spectroscopy (PL).
7. Use the prepared N-Cdots for the detection of Fe^{3+}in aqueous solutions.
8. Fabricate sensor devices and use them in the chemical sensing of volatile organic compounds.
9. Test the gas sensing performance of the prepared sensors (sensitivity, selectivity, response/recovery times, stability, and reproducibility) using a home-made gas sensor setup.

1.3 Dissertation outline

The layout of the dissertation followed an order of:

Chapter 1

This chapter gives background information as well as motivation for the proposed research, research objectives are explicitly and briefly stated.

Chapter 2

This chapter gives a review of literature to put things into perspective and provide background information on the production of lignocellulosic waste-derived cellulose nanocrystals and carbon nanomaterials.

Chapter 3

In this chapter procedures for the extraction of cellulose nanocrystals from corncob under different acid hydrolysis media are described in complete detail.

Chapter 4

This chapter gives details on the preparation of activated carbon from corncob by chemical activation with potassium carbonate (activating agent) using varied ratios of impregnation.

Chapter 5

This chapter presents the synthesis and characterization of CuO NPs and ACC/PVA/CuO composites and the gas sensing properties of ACC and the composites towards selected volatile organic compounds.

Chapter 6

This chapter presents the preparation of N-doped fluorescent carbon materials and their sensing properties towards Fe^{3+} ions in aqueous solutions.

Chapter 7

Presented in this chapter are the conclusions and recommendations of the research.

1.4 References

[1] K. Dong, G. Hochman, Y. Zhang, R. Sun, H. Li, and H. Liao, "CO2 emissions, economic and population growth, and renewable energy: Empirical evidence across regions," *Energy Econ.*, vol. 75, pp. 180–192, 2018, doi: 10.1016/J.ENECO.2018.08.017.

[2] M. Duque-Acevedo, L. J. Belmonte-Ureña, F. J. Cortés-García, and F. Camacho-Ferre, "Agricultural waste: Review of the evolution, approaches and perspectives on alternative uses," *Glob. Ecol. Conserv.*, vol. 22, p. e00902, 2020, doi: 10.1016/J.GECCO.2020.E00902.

[3] "Fao.org. 2022. [online] Available at: <https://www.fao.org/3/i3901e/i3901e.pdf> [Accessed 17 March 2022]." .

[4] M. Macias-Corral, Z. Samani, A. Hanson, G. Smith, P. Funk, H. Yu, J. Longworth., "Anaerobic digestion of municipal solid waste and agricultural waste and the effect of co-digestion with dairy cow manure," *Bioresour. Technol.*, vol. 99, no. 17, pp. 8288–8293, 2008, doi: 10.1016/J.BIORTECH.2008.03.057.

[5] "International Trade Administration | Trade.gov. 2022. South Africa - Agricultural Sector. [online] Available at: <https://www.trade.gov/country-commercial-guides/south-africa-agricultural-sector#:~:text=South%20Africa%20has%20a%20market,%2C%20wine%2C%20and%20most%20vegetables.> [Accessed 18 March 2022]." .

[6] A. Mtibe, T. H. Mokhothu, and L. Z. Linganiso, "Maize stalk (corn stover) to valuable products in "Waste-to-Profit" (W-t-P): Value added Products to Generate Wealth for a Sustainable Economy". *Volume 1*, vol. 1, 2018, pp. 107–133.

[7] N. Berkhout, "South Africa: Produces 2nd highest corn crop," 2020. https://www.allaboutfeed.net/animal-feed/raw-materials/south-africa-produces-2nd-highest-corn-crop/#:~:text=Junior Aklei Chaky-,South Africa produced its second highest corn crop on record,crop of 11.3 million tonnes.&text=The expected commercial yellow c (accessed Mar. 14, 2021).

[8] L. M. Mohlala, M. O. Bodunrin, A. A. Awosusi, M. O. Daramola, N. P. Cele, and P. A. Olubambi, "Beneficiation of corncob and sugarcane bagasse for energy generation and materials development in Nigeria and South Africa: A short overview," *Alexandria Engineering Journal*, vol. 55, no. 3. Elsevier B.V., pp. 3025–3036, 2016, doi: 10.1016/j.aej.2016.05.014.

[9] M. Smyth, A. García, C. Rader, E. J. Foster, and J. Bras, “Extraction and process analysis of high aspect ratio cellulose nanocrystals from corn (Zea mays) agricultural residue,” *Ind. Crops Prod.*, vol. 108, pp. 257–266, 2017, doi: 10.1016/j.indcrop.2017.06.006.

[10] C. Zhang, Z. Geng,M. Cai, J. Zhang, X. Liu, H. Xin, and J. Ma, “Microstructure regulation of super activated carbon from biomass source corncob with enhanced hydrogen uptake,” *Int. J. Hydrogen Energy*, vol. 38, no. 22, pp. 9243–9250, 2013, doi: 10.1016/J.IJHYDENE.2013.04.163.

[11] H. A. Silvério, W. P. Flauzino Neto, N. O. Dantas, and D. Pasquini, “Extraction and characterization of cellulose nanocrystals from corncob for application as reinforcing agent in nanocomposites,” *Ind. Crops Prod.*, vol. 44, pp. 427–436, 2013, doi: 10.1016/j.indcrop.2012.10.014.

[12] A. Mtibe, L. Z. Linganiso, A. P. Mathew, K. Oksman, M. J. John, and R. D. Anandjiwala, “A comparative study on properties of micro and nanopapers produced from cellulose and cellulose nanofibres,” *Carbohydr. Polym.*, vol. 118, pp. 1–8, 2015, doi: 10.1016/J.CARBPOL.2014.10.007.

[13] R. M. dos Santos, W. P. Flauzino Neto, H. A. Silvério, D. F. Martins, N. O. Dantas, and D. Pasquini, “Cellulose nanocrystals from pineapple leaf, a new approach for the reuse of this agro-waste,” *Ind. Crops Prod.*, vol. 50, pp. 707–714, 2013, doi: 10.1016/J.INDCROP.2013.08.049.

[14] S. Thambiraj and D. Ravi Shankaran, “Preparation and physicochemical characterization of cellulose nanocrystals from industrial waste cotton,” *Appl. Surf. Sci.*, vol. 412, pp. 405–416, 2017, doi: 10.1016/J.APSUSC.2017.03.272.

[15] R. Leyva-Ramos, L. A. Bernal-Jacome, and I. Acosta-Rodriguez, “Adsorption of cadmium(II) from aqueous solution on natural and oxidized corncob,” *Sep. Purif. Technol.*, vol. 45, no. 1, pp. 41–49, 2005, doi: 10.1016/J.SEPPUR.2005.02.005.

[16] L. Zhang, L. Tian, R. Sun, C. Liu, Q. Kou, and H. Zuo, “Transformation of corncob into furfural by a bifunctional solid acid catalyst,” *Bioresour. Technol.*, vol. 276, pp. 60–64, 2019, doi: 10.1016/j.biortech.2018.12.094.

[17] C. Duan *et al.*, “Carbohydrates-rich corncobs supported metal-organic frameworks as versatile biosorbents for dye removal and microbial inactivation,” *Carbohydr. Polym.*, vol. 222, p. 115042, 2019, doi: 10.1016/j.carbpol.2019.115042.

[18] W. H. Qu, Y. Y. Xu, A. H. Lu, X. Q. Zhang, and W. C. Li, “Converting biowaste corncob residue into high value added porous carbon for supercapacitor electrodes,” *Bioresour. Technol.*, vol. 189, pp. 285–291, 2015, doi: 10.1016/j.biortech.2015.04.005.

[19] A. M. Das, M. P. Hazarika, M. Goswami, A. Yadav, and P. Khound, “Extraction of cellulose from agricultural waste using Montmorillonite K-10/LiOH and its conversion to renewable energy: Biofuel by using Myrothecium gramineum,” *Carbohydr. Polym.*, vol. 141, pp. 20–27, 2016, doi: 10.1016/j.carbpol.2015.12.070.

[20] R. Wang, L. Jiao, X. Zhou, Z. Guo, H. Bian, and H. Dai, “Highly fluorescent graphene quantum dots from biorefinery waste for tri-channel sensitive detection of Fe3+ ions,” *J. Hazard. Mater.*, vol. 412, p. 125096, 2021, doi: 10.1016/J.JHAZMAT.2021.125096.

[21] S. Jayaweera, K. Yin, X. Hu, and W. J. Ng, “Facile preparation of fluorescent carbon dots for label-free detection of Fe3+,” *J. Photochem. Photobiol. A Chem.*, vol. 370, pp. 156–163, 2019, doi: 10.1016/J.JPHOTOCHEM.2018.10.052.

[22] A. Abbas, T. A. Tabish, S. J. Bull, T. Mariana Lim, and A. N. Phan, “High yield synthesis of graphene quantum dots from biomass waste as a highly selective probe for Fe 3+ sensing,” *Sci Rep.*, vol. 10, pp. 21262 ,2020, doi: 10.1038/s41598-020-78070-2.

[23] P. Wu, Y. Li, and X.-P. Yan, “CdTe Quantum Dots (QDs) Based Kinetic Discrimination of Fe 2+ and Fe 3+ , and CdTe QDs-Fenton Hybrid System for Sensitive Photoluminescent Detection of Fe 2+,” *Proc. Natl. Acad. Sci. U. S. A*, vol. 22, pp. 6252–6257, 2004, doi: 10.1021/ac900788w.

[24] P. Krishnaiah, R. Atchudan, S. Perumal, E. S. Salama, Y. R. Lee, and B. H. Jeon, “Utilization of waste biomass of Poa pratensis for green synthesis of n-doped carbon dots and its application in detection of Mn2+ and Fe3+,” *Chemosphere*, vol. 286, p. 131764, 2022, doi: 10.1016/J.CHEMOSPHERE.2021.131764.

Chapter 2: Literature review

2.1 Introduction: Corncob

The increasing demand for food due to population growth has resulted to an increased agricultural/industrial production which has consequently lead to the acceleration of agricultural waste generation [1]. Maize (*Zea mays*), also knowns as corn is a widely distributed crop in the world, with a global corn production of approximately 10.99×10^{8} tons in the 2018-2019 period [2-4]. In South Africa, corn is the staple food item with over 16 million tons produced in the 2019-2020 period, which is 38% higher than the 2018/19 corn crop production of 11.3 million tons [5, 6]. In South Africa, the corn farming sector consists of both commercial and non-commercial farmers in various provinces such as Free State (34%), North West (32%), Mpumalanga Highveld (24%) and KwaZulu-Natal Midlands (3%) [6,7]. The corn crop is comprised of the stalk, leaf, corn grain, husk, and the corncob [9]. The corn grain, which is the edible part of the plant, used for the production of maize meal, corn flakes, corn flour, and glucose, is 20% of the plant's mass and the remaining parts are agricultural waste [7,8].

The corncob is the central part of the ear maize in which the corn grain are stuck , and is commonly thought of as a residue of the corn after the grains are removed [8,9]. The corn to corncob residue ratio is about 100:18, with approximately 19.782×10^{7} tons of corncob generated annually [3,9,10]. Majority of the corncob waste is used for low value-added applications such as food for livestock, fertilizers, and bedding for small animals, with the remaining portion ending up in dumping sites due to limited space. Some of the corncob residues are burnt directly increasing environmental pollution [6,9]. Several methods have been developed to transform the corncob residue as a feedstock for the production of value added products such as extraction of hemi- celluloses to produce xylitol, furfural, ethanol, and so on [11]. In spite of this, unfortunately, a large amount of corncob still end up in landfills as agricultural waste after the grains are harvested [12]. This has led to the 'use of biomass waste to fabricate novel materials for different applications' becoming a promising concept of waste to wealth in the modern world [13].

Growing research interest has emerged concerning the use of biomass material such as corncob to produce value-added products due to its potential to form inexpensive and environmentally friendly materials without colliding with the food stock, while reducing the pollution caused by biomass waste [14,15]. Researchers have reported several studies on the use of corncob residue, including its use as a feedstock for furfural production[16], biobased rigid polyurethane foam [17], production of ethanol and

xylitol [18,19], production of phenolic compounds [20], and use as a bio-adsorbent [21]. Several studies based on the use of corncob for the fabrication of carbon based materials have also been conducted, such as the use of corncob residue for the fabrication of porous carbon for supercapacitor electrodes [22], hollow spherical carbon [23], carbon nanosheets for lithium–sulfur batteries [24], carbon nanospheres for use as a high-capacity anode for reversible Li-ion battery [25], and carbon quantum for application in detection of metal ions [30]. With global warming and other environmental issues such as pollution, a great deal of attention has been paid to the conversion of agricultural waste (instead of burning) to value added products such as biofuels, preparation of carbon materials, and polymeric materials production such as cellulose [26, 27]. The more agricultural waste is used the less waste that is sent to landfills.

2.2 Cellulose from biomass

Cellulose is the most abundant, renewable natural biopolymer on Earth, made of the D-glucose units linked together via the β-1,4-glycosidic and has a general formular of $(C_6H_{10}O_5)_n$, where n is the number of repeated monomeric β-d-glycopyranose units which varies with the source of the cellulose [26–28]. Cellulose is a colourless, odourless, nontoxic solid polymer found in most plant-based materials, serving as a dominant reinforcing phase in the plant cell wall structures, however cellulose is also synthesized by algae, turnicates, and some bacteria [29–31]. Naturally occurring cellulose does not occur as isolated molecules, but rather it is found as assemblies of individual cellulose chain-forming fibres. These fibrils pack into larger units called microfibrils, which are in turn assembled into fibre. Cellulose have both crystalline (highly ordered) and amorphous (disordered) regions, in the crystalline region the molecular orientations and hydrogen bonding network vary, giving rise to cellulose polymorphs [32]. There are several polymorphs of cellulose namely cellulose I, cellulose II, cellulose III, and cellulose IV [32–35]. Cellulose I and cellulose II are the most common polymorphs of cellulose, cellulose I is the native cellulose while cellulose II is obtained by chemical regeneration of nature cellulose [32,33]. The different polymorphs have different properties such as hydrophilicity, oil/water interface, mechanical properties, thermal stability, and the morphology of the particles, which qualify them for different applications [34,35]. Due to its crystallinity, cellulose I has been used in the synthesis of hydrogels and reinforcement to improve mechanical properties, while Cellulose II has been used as a bioethanol feedstock due to its amorphous nature [35]. Fig. 2.1 shows the basic structural organization of cellulose at the molecular level.

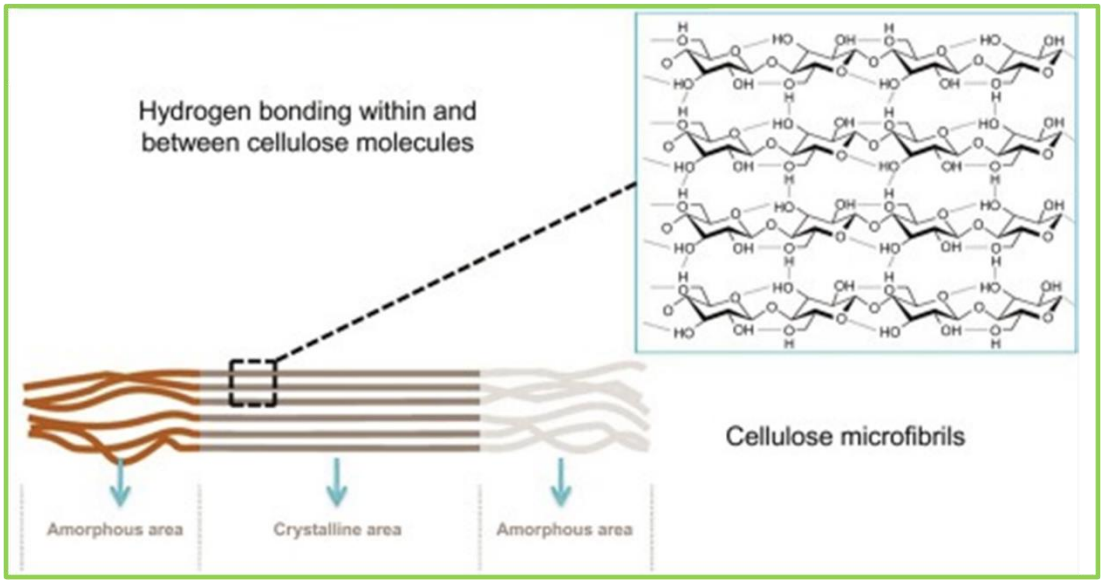

Figure 2.1: Amorphous and crystalline regions of the cellulose polymer [36]

Isolation of cellulose from different lignocellulosic materials such agricultural waste has recently sparked interest due to the growing concern of developing environmentally friendly, biodegradable materials from waste [36,37]. Cellulose has found uses in a wide variety of applications, such as food, construction materials, paper production, biomaterials, and pharmaceuticals [38]. In recent years, it has attracted a great deal of attention and growing research interest owing to its low cost, biodegradability, high surface-to-volume ratio, good mechanical strength, low environment impact, abundancy, easy functionalization, and versatility in nanoscale processing to form cellulose nanomaterial (Nanocellulose) [29, 39–41]. With the nanometre diameter, nanocellulose has drawn a great deal of research interest due to its high strength, excellent stiffness, chemical, large surface area, chemical and physical stability [42]. Nanocellulose can be further classified into three main groups depending on their size and preparation methods, the three groups of nanocellulose are cellulose nanocrystals (CNCs), cellulose nanofibrils (CNFs) and bacterial nanocellulose (BNCs) [43]. Both CNCs and CNFs originated from lignocellulosic wastes while BNCs can be produced from micro-organism such as Gluconacetobacter xylinus [44]. In recent years, the nanocellulose field has undergone major developments with reference to its preparation, functionalization and interesting applications in various fields such as nanocomposites membranes, textiles, reinforcing agent, biomedical application, wood adhesives, as adsorbent, and so on [29,42,45,46]. Fig. 2.2 depicts the evolution process of the extraction CNCs from agricultural waste.

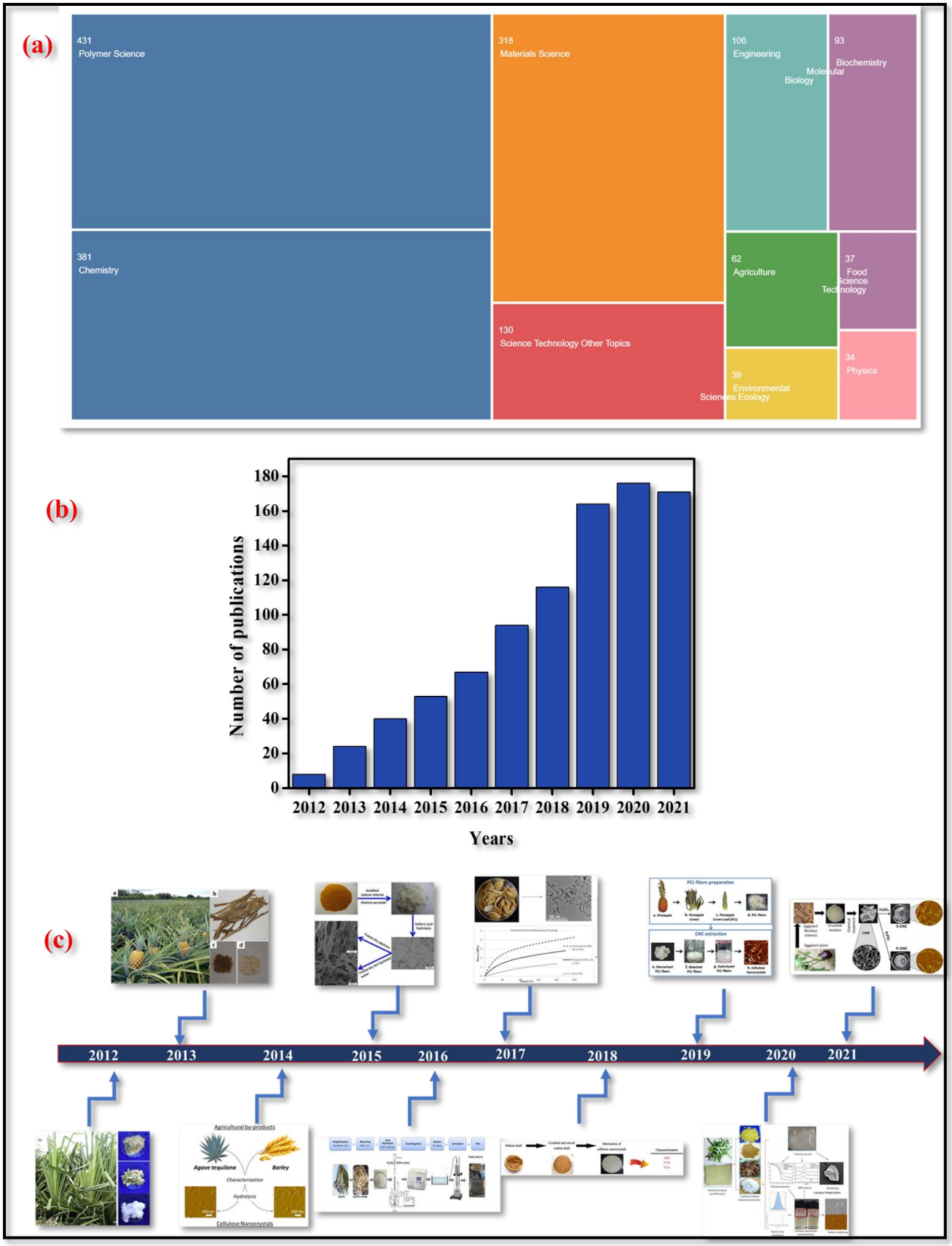

Figure 2.2: The evolution process of CNCs prepared from agricultural waste. (a) A schematic depicting the proportion of publications on extraction of CNCs in from different research fields from 2012 to 2021

obtained from the Web of Science in January 2022. (b) The histogram depicts the number of publications on the extraction of CNCs from 2012 to 2021 obtained from the Web of Science in January 2022. (c) The timeline shows progress on the fabrication of CNCs from agricultural waste from 2012 to 2021 [48–57].

2.3 Cellulose Nanocrystals

Cellulose has both highly ordered crystalline and amorphous regions in varying proportions, depending on its source. Removing the amorphous region influences the structure and crystallinity of the cellulose, resulting in the formation of cellulose nanocrystals (CNCs) [31, 32, 47]. CNCs are needle-like particles made up of cellulose chain segments that have been organized in an almost defect free crystalline structure with at least one dimension of less than or equal to 100 nm [31,48]. CNCs are also known as cellulose nanowhiskers, cellulose whiskers, nanocrystalline cellulose, etc. but CNCs is the most used term [31, 42, 48]. CNCs have a high thermal stability, surface area, and crystallinity compared to bulk cellulose, which has more amorphous fractions [47]. Different types of biomass waste have been used to extract CNCs such as cotton [49], sugarcane bagasse [50], walnut shell [51], soy hulls [48], bamboo fibre [52], and many more. Despite comprehensive research into a variety of biomass wastes, the use of corncob as a natural source for the development of cellulose nanocrystals has yet to be widely explored.

Various techniques have been employed to prepare CNCs from lignocellulosic materials, which include chemical and mechanical techniques [52]. The two classical chemical treatments are acid hydrolysis and enzymatic hydrolysis [53], while the mechanical techniques include ultrasonication, high-pressure homogenization, microfluidization, high-speed blending, grinding, and cryocrushing [52, 54–56]. Chemical methods are currently the most commonly used, owing to their ease of use, short preparation time, and relatively high yield, whereas mechanical methods require a lot of energy and produce nanocrystal products with a wide range of particle sizes [56, 57]. Among the chemical techniques, acid hydrolysis is the most common method for the extraction of cellulose nanocrystals [58]. The following section focuses on the different extraction techniques to extract CNCs from different parts of the agricultural waste.

2.3.1 Pre-treatment of agricultural waste

Since lignocellulosic biomass does not only consist of cellulose (30–50%), but also hemicellulose (19–45%), and lignin (15–35%) by weight, with the other components including chlorophyll, waxes, ash, and resins [39, 40]. Xu *et al*., [41] reported that raw corn

stover consist of cellulose (44.4 ± 0.4 %), hemicellulose (27.8 ± 0.3 %) and lignin (19.6 ± 0.2 %). While Slavutsky [42] reported that sugarcane bagasse consists of cellulose (40.3 ± 1.6 %), hemicellulose (21.4 ± 1.6 %), and lignin (23.84 ± 0.9 %). Hence, the extraction of CNCs from biomass require effort, to overcome this crucial stage in the extraction process, it is important to select adequate pre-treatment methods to remove the non-cellulosic material (hemicellulose, lignin, ash, etc.). The recently reported pre-treatment methods for the extraction of CNCs are summarized in figure 2.3, these methods are determined by the type of feedstock. For instance, Santos *et al*., [59] prepared CNCs from pineapple leaves, which contained several non-cellulosic materials, the pre-treatment was conducted with a sodium hydroxide aqueous solution of 2% (w/w) to disrupt the hemicellulose and lignin bonds, and a bleaching step with an acetate buffer solution of (27 g NaOH and 75 ml glacial acetic acid, diluted to 1 L of distilled water, and 1.7 wt% $NaClO_2$ in water) to remove excess non-cellulosic residue. While Jieng and Hsieh [60] used two methods to pre-treat tomato peels before the extraction of CNCs, the first method involved the use of acidified sodium chlorite delignification, followed by highly effective alkali treatment(KOH). An alternative chlorine-free route involving alkaline hydrolysis and peroxide bleaching was also developed for comparison using NaOH and 4% H_2O_2 under basic condition. In general, several steps are involved in the pre-treatment stages, including the washing, and cutting of the raw materials the raw materials into small pieces [61]. To cleave the ester linkages, and glycosidic side chains of the lignin leading to disruption the source is then subjected to alkali pre-treatments at specific conditions, different alkali solutions have been employed for this process such as KOH, and NaOH [62, 63]. This is followed by bleaching (delignification), in this stage excess non-cellulosic components are eliminated in this stage using sodium chlorite and hydrogen peroxide [64, 65]. Extra steps are usually required to dewax the source and clean up the chemical residues after pre-treatments [43].

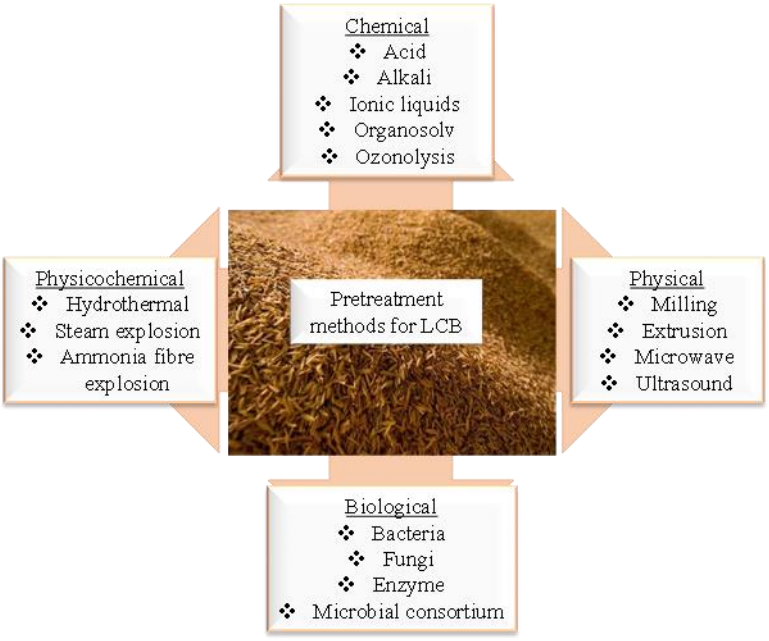

Figure 2.3: Typical and recently reported pre-treatment methods for the extraction of CNCs.

2.3.2 Extraction of CNCs

2.3.2.1 Acid hydrolysis

The extraction of CNCs from cellulosic fibers usually consists of an acid-induced disruption process, during which the glycosidic bonds in the amorphous region are cleaved, under controlled reaction conditions as shown in figure 2.4 (a) [66]. Various strong acids have been employed to degrade bulk cellulose effectively to release crystalline cellulosic CNCs, such as sulphuric acid (H_2SO_4), phosphoric acid (H_3PO_4), hydrochloric acid (HCl), nitric acid (HNO_3), and a mixture of mineral and organic acids [67]. Kassab *et al*., [68] compared the effects of three different acids on the extraction of CNCs from tomato plant residue (H_2SO_4, H_3PO_4, and HCOOH/HCl) to form sulfated CNCs (S-CNC), phosphorylated CNCs (P-CNC) and carboxylated CNCs (C-CNC). The as-produced CNCs exhibited high aspect ratio (up to 98), high crystallinity (up to 89%), and formed stable suspensions in organic solvents compared to previously reported CNCs from other sources. While Wang and colleagues [69] attempted to add phosphate groups on CNCs by phosphoric acid hydrolysis to improve their thermal stability and synthesis conditions, the results showed that the use of phosphoric acid medium to obtain CNCs decrease the degradation temperatures, however, the thermal stability is still comparable to that of other biomasses using H_3PO_4 and H_2SO_4. Nevertheless, the acid hydrolysis treatment with H_2SO_4 to prepare CNCs have widely investigated and appears to be the

most extensively used method, because it has been proven effective in the elimination of amorphous components and resulting in stable CNCs suspensions, detailed mechanism shown in figure 2.4 (b) [86]. H_2SO_4 hydrolysis introduces sulfate groups to the surface of the extracted CNCs, due to the reaction with surface hydroxyl groups of the cellulose through an esterification process, allowing for the formation of anionic sulfate groups [67]. These anionic sulfate groups induce electrostatic repulsion between CNCs molecules and promotes their dispersion in water [59]. However, the sulfate groups compromise the thermal stability of the nanoparticles, which could lead to lower CNCs yields [59,67]. The thermal stability of the sulfuric acid prepared CNCs can be increased by neutralizing the CNCs dialysis [9]. Overall, the acid hydrolysis method is simple, and can be used to extract CNCs from several agricultural residues. Figure 2.5 illustrates the acid hydrolysis mechanism and the process flow diagram for the extraction of CNCs using conventional acid hydrolysis method.

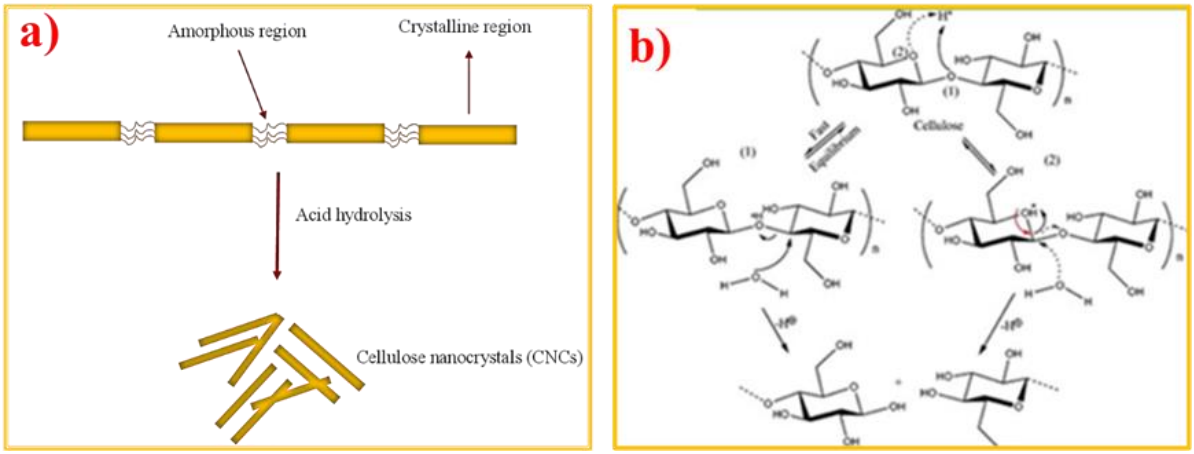

Figure 2.4: Illustrates process of CNCs extraction using the conventional acid hydrolysis method. (a) representation of acid hydrolysis method to extract CNCs. (b) Typical H2SO4 hydrolysis mechanism [82].

2.3.2.2 Oxidation

Oxidation is useful in introducing anionic groups to the cellulose molecules, it is briefly separated into two steps. The first step is the oxidation of the surface hydroxyl group (-OH) of the pre-treated source and removal the amorphous regions [66]. This results in a structure with negatively charged carboxyl groups (-COOH), which could facilitate the dispersion of CNCs in aqueous solutions and further modifications on the surface of

CNCs [71]. The most common type of oxidation is TEMPO-oxidation, TEMPO (1-oxo-2,2,6,6-tétraméthylpipyridine 1-oxyle) is a stable radical that selectively mediates the oxidation of primary alcohols into carboxylic acids through an aldehyde intermediate [72]. Usually, TEMPO mediated oxidation is cooperative with mechanical disintegration, which selectively oxidize C6-primary hydroxyl groups of cellulose to sodium C6-carboxylate groups [73]. A general reaction scheme of the oxidation of C6 hydroxyl to the carboxyl group by the TEMPO treatment is shown in figure 2.5. Zhang *et al*., [74] used TEMPO oxidation to prepare carboxylated CNCs from sugarcane bagasse pulp with the further assistance of ultrasound. Previous studies have used TEMPO mediated oxidation to prepare carboxylated CNCs, however, this method consists of several step processes as well as multiple radical generating chemicals (sodium hypochlorite (NaClO), sodium bromide (NaBr), and TEMPO reagents), therefore limiting the sustainability of the approach [75].

Other oxidation agents such as ammonium persulfate (APS), H_2O_2, and nitro-oxidation (using HNO_3 and $NaNO_2$) have also used to prepare CNCs [76–78]. Zhang *et al.*, [76] compared the effects of the preparation methods using TEMPO and acid hydrolysis, lemon seeds were utilized to extract CNCs by H_2SO_4 (S-LSCNC), APS (A-LSCNC), and TEMPO oxidation (T-LSCNC). The results demonstrated that all CNCs maintained cellulose Iβ structure and had a good dispersion regardless of extraction methods, but the T-LSCNC had a higher yield. This is because TEMPO-oxidation method is also advantageous due to its ability to produce high oxidized yields of up to 90% [86]. Khoshani *et al*., [79] prepared carboxylated CNCs through a one-step catalyst-assisted H_2O_2 oxidation. Similar to TEMPO, these two methods require several pre-treatment steps before the extraction of CNCs, while nitro-oxidation reduce the need to consume multiple chemicals, greatly improving the recyclability of the used chemicals [75]. Sharma *et al*., [80] used a one-step nitro-oxidation to prepare carboxylated CNCs from jute fibers, while Zhan *et al.*, [29] compared the extraction of CNCs using both nitro-oxidation and TEMPO-oxidation from jute fibers. TEMPO-oxidation was performed on pre-treated jute while the nitro-oxidation was performed on the untreated jute. Both oxidation methods were effective and resulted to carboxylated CNCs with good dispersion and high transparency. Figure 2.5. (c) demonstrate the nitro-oxidation mechanism.

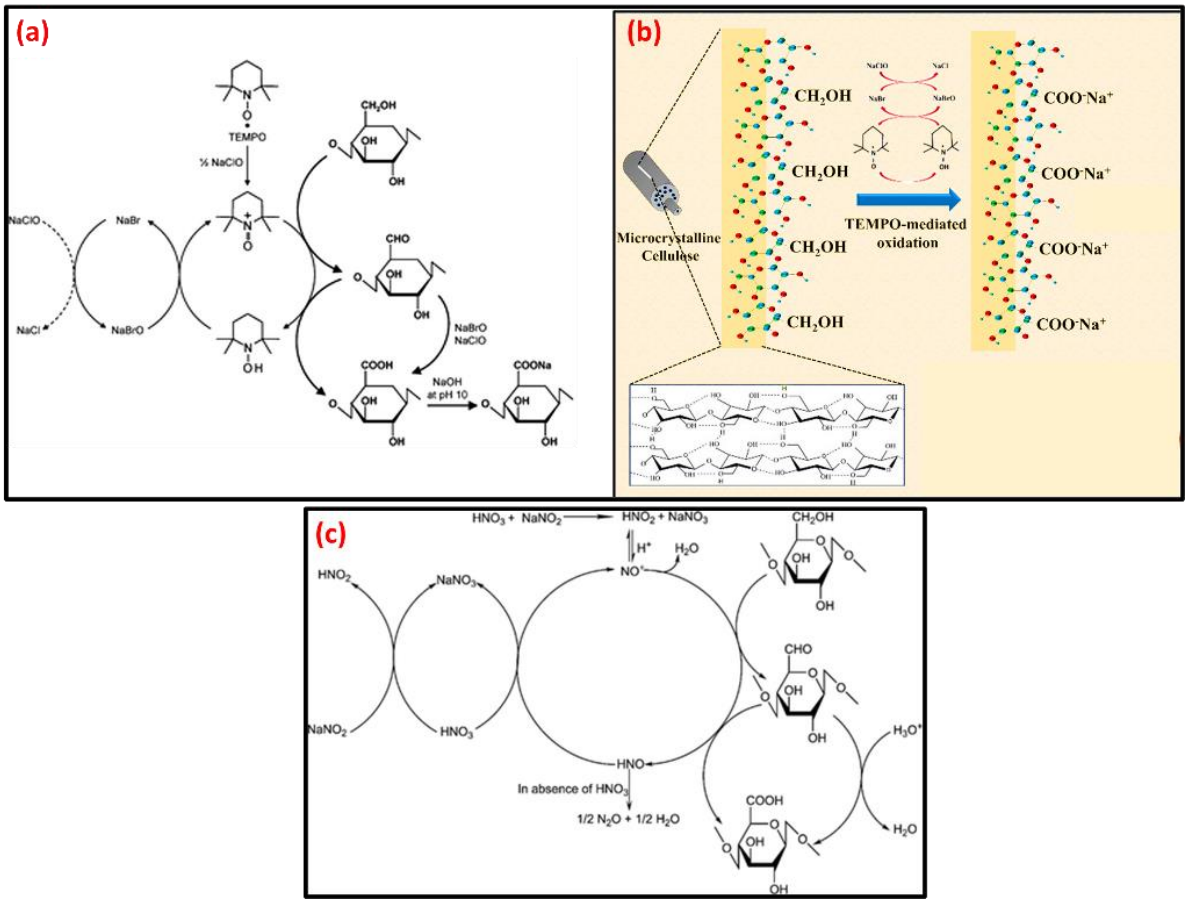

Figure 2.5: A general reaction scheme of the oxidation by the TEMPO and nitro-oxidation treatments. (a) Regioselective oxidation of cellulose by TEMPO-mediated oxidation [81]. (b) Schematic representation showing preparation of CNCs using TEMPO oxidation [71]. (c) Nitro-oxidation mechanism using nitric acid and sodium nitrite [80].

2.3.2.3 Other methods

Other extraction methods such as ionic liquids hydrolysis (ILs) and enzymatic hydrolysis have been utilized to extract CNCs from agricultural waste [66]. ILs hydrolysis has attracted considerable attention in the field of biomass processing due to its low vapor pressure, low energy consuming, and sustainable process since it allows the recycling of reagents and emit the use of hazardous chemicals [82]. This hydrolysis involves two main steps, firstly the pre-treated cellulose is immersed in an IL for a period to allow swelling and water is added to initiate the hydrolysis stage [66]. During the reaction, the hydrogen and oxygen atoms of amorphous cellulose are easily accessible by the dissociated IL to form the electron donor-electron acceptor, the -OH groups break leading to the selective removal of the amorphous region [83]. The above-mentioned extraction methods require

the use of chemicals, while enzymatic hydrolysis use cellulolytic enzymes known as cellulases (mixtures of endoglucanases, exoglucanases, and cellobiohydrolases), these are an interesting class of enzymes possessing the ability to act as a catalyst for the hydrolysis of the cellulose [84]. These enzymes have specific functionalities which can selectively depolymerize the amorphous region of cellulose to prepare CNCs with high crystallinity. Endoglucanase attacks and hydrolyzes the amorphous domains, exoglucanase reacts with the cellulosic chain from either the reducing or nonreducing ends, while cellobiohydrolases hydrolyze cellulose from either the C1 or the C4 ends employing a protein in each case, into cellobiose sub-units [84, 85].

2.3.3 Application of CNCs

Due to the abundant biomass waste, various pre-treatment and extraction methods, outstanding unique nanoscale structure, excellent mechanical properties, thermal stability, biocompatibility, biodegradability, and easy surface modifications, CNCs have attracted rapidly growing scientific and technological interest, and have found application in many fields, such as health care, environmental protection, chemical engineering, and manufacture [86]. Grishkewich *et al*., [87] summarized the recent applications of CNCs in biomedical engineering (tissue engineering, drug delivery, biosensors, and biocatalysts), wastewater treatment (adsorbents), energy and electronics sector (supercapacitors, conductive films, substrates, sensors, and separator for energy storage). Figure 2.6 demonstrates the summarized recent applications of CNCs. CNCs has also found applications in the monitoring and improvement of food quality, Dhar *et al*., [88] fabrication a poly (3-hydroxybutyrate) (PHB)/ CNCs based nanocomposite films with improved gas barrier and migration properties for food packaging applications. Peng *et al*., [89] incorporated CNCs into different food based systems containing polymers as a thickening agent, the CNCs improved the viscosity enhancement at lower particle loading. Besides these promising applications, CNC-based materials have also been applied in the fabrication of carbon-based nanomaterials, Dhar *et al*., used CNCs to prepare graphene with tunable dimensions, while Souza *et al*., [90] prepared luminescent nanocarbon structures. In this study, prepared CNCs were used to fabricate carbon quantum dots (CQDs), which were used for the detection of Fe^{3+} in aqueous solutions.

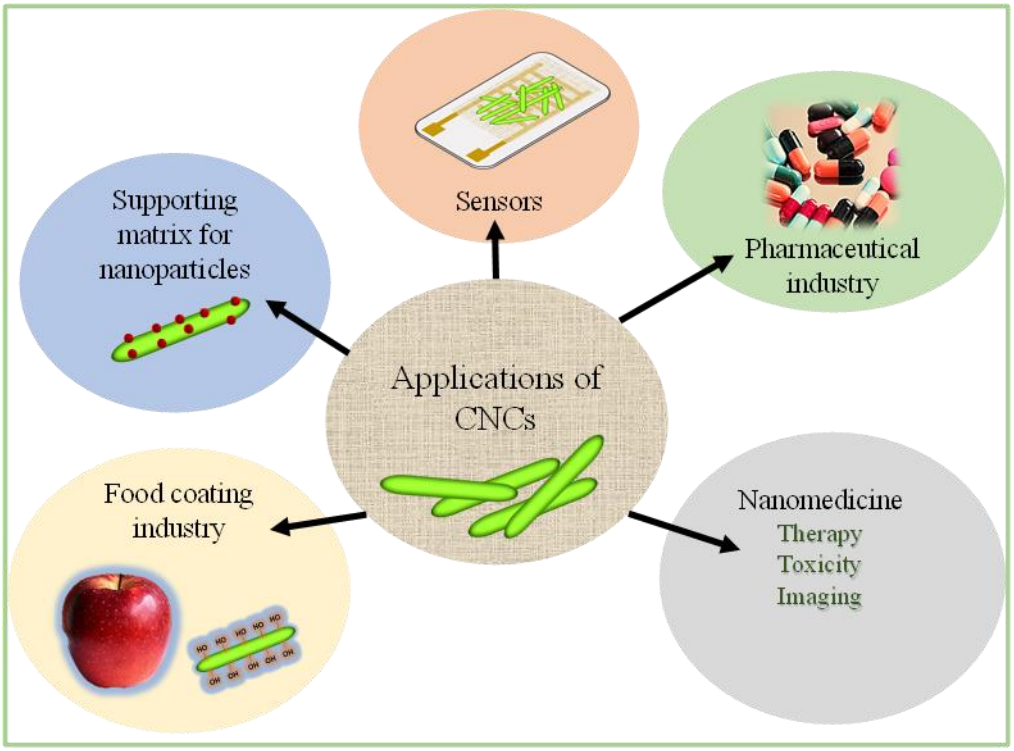

Figure 2.6: Summarized recent applications of CNCs.

2.4 Carbon quantum dots (CQDs)

Since their discovery in 2004 by Xu *et al*., [91] during the purification of single-walled carbon nanotube (SWCNT) through preparative electrophoresis, and then via laser ablation of graphite powder and cement in 2006 by Sun *et al*., [92], carbon quantum dots (CQDs) have gradually become a rising star in the carbon nanomaterials family. They are an emerging subclass of zero dimensional nanoparticles that consists of a carbon core, constituting of different functional groups at the surface [93]. CQDs are characterised by quasi-spherical morphology composed mainly of amorphous carbon with sp^2 hybridised structure and size less than 10 nm [94]. They exhibit attractive properties such as tunable photoluminescence, functionalizability, dispersibility, multicolour emission associated with excitation, biocompatibility, size-dependent optical properties, facile synthesis, and low toxicity as compared to their counterparts, the semiconductor quantum dots (QDs) [95]. These extraordinary features make them suitable for applications in sensors, catalysis , healthcare, and energy storage devices [96].

Over the past decade extensive research has been conducted to explore the synthesis of CQDs, their methods of preparation can be categorised in two main approaches known as the top-down and the bottom-up (shown in figure 2.7 d) [95]. The top-down method involves breaking down large carbon structures such as coal, activated carbon, graphite, and carbon nanotubes into the desired carbon nanostructures through electrochemical oxidation, acidic oxidation, arc discharge, and laser ablation

[97]. The bottom-up route includes the polymerization and carbonization of small molecule precursors, such as citric acid, phenylenediamines, glucose, and aldehyde under a range of different reaction conditions through microwave and hydrothermal methods [98]. Despite the development of various fabrication strategies, the production of CQDs still require complicated instrumentation, expensive precursors, and rigorous experimental conditions that present risks to the natural environment and human health. These have also led to high production costs and constrained the commercialization of CQDs [99]. At present the development of various green fabrication strategies and mass production of CQDs at low costs from natural precursors are of great interest.

The usage of agricultural waste as precursors for the synthesis of CQDs are receiving a great deal of attention since they are rich in elements such as nitrogen (N), hydrogen (H), and oxygen (O), in addition to carbon (C). They are renewable, cost-effective, and environmentally benign compared to other carbon sources [100]. In addition, the production of CQDs from agricultural wastes converts low-value biomass waste into valuable and useful materials. The histograms in figure 2.7 (a and b) depicts the number of publications on CQDs from 2004 to 2021 and the number of publications on agricultural waste based CQDs from 2012 to 202. Zhou *et al*., [101] proposed a green synthesis method by utilizing watermelon peel as carbon precursors for the first time, starting a new trend towards using agricultural waste materials for CQDs preparation. Following this, researchers have utilized different types of agricultural wastes; animal waste (prawn shell [102], manure [103], denatured milk [104], etc.), fruits waste (orange peel [105], sugarcane bagasse pulp [106], walnut shells [107], etc.), and vegetable waste (corncob [108], rice straw [109], wheat straw [110], and more). Figure 2.7 c shows the progress on the fabrication strategies of CQDs from 2012 to 2021 using agricultural waste.

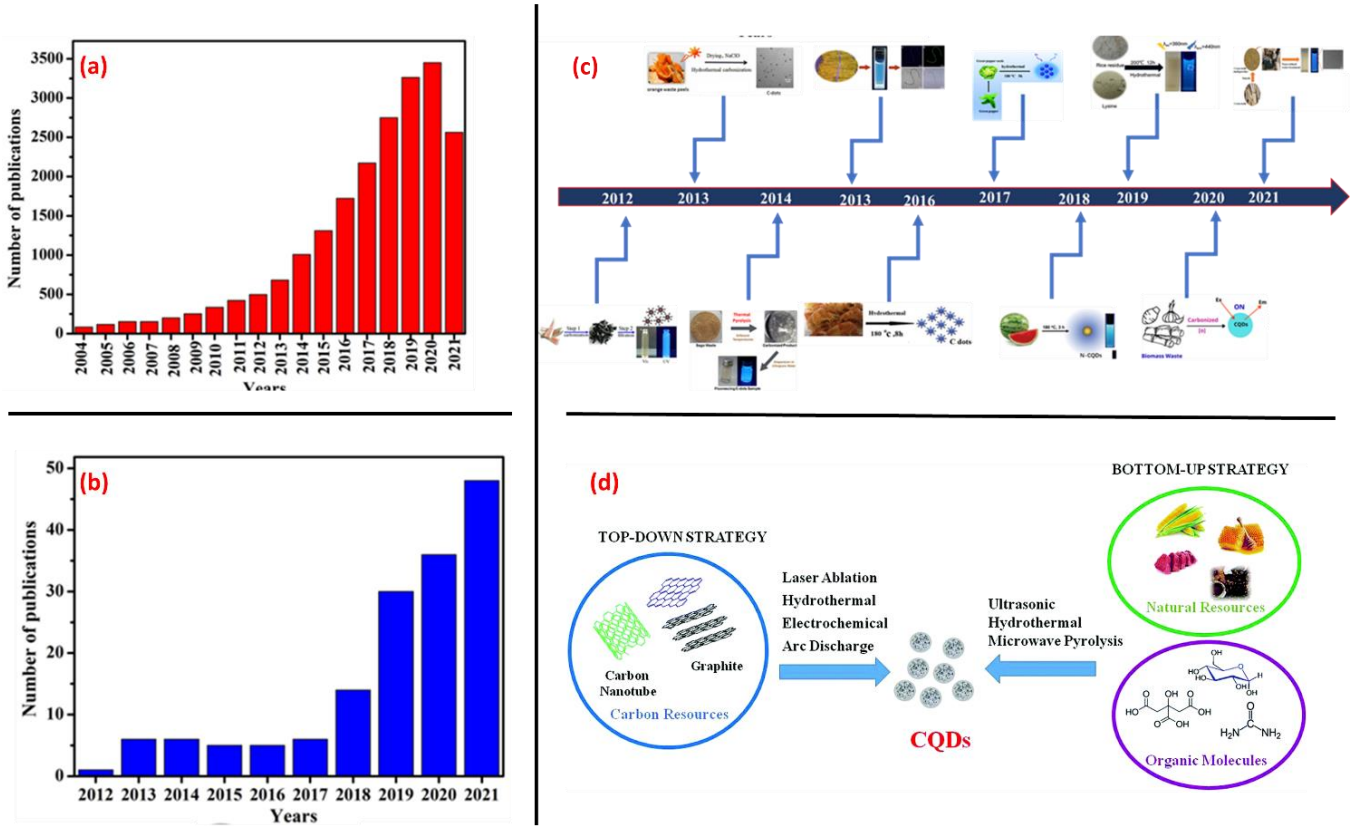

Figure 2.7: The evolution of CQDs. (a) The histogram depicts the number of publications on C-dots from 2004 to 2021 obtained from the Web of Science in October 2021. (b) The histogram depicts the number of publications on agricultural waste based CQDs from 2012 to 2021 obtained from Web of Science in October 2021. (c) shows the progress on the fabrication strategies of CQDs from 2012 to 2021 using agricultural waste [95, 101, 102, 107, 110–114] . (d) Schematic representation of the "top-down" and "bottom-up" approaches for the synthesis of CQDs [115]

Due to differences in biomass surface heteroatoms, particle size, and passivation, CQDs derived from different agricultural residues and synthesis techniques show different luminescent properties, size distribution, and quantum yield (QY) [116]. Conventional methods involved in preparation of agricultural waste based CQDs require complicated equipment, catalysts, several post synthesis purification steps, longer synthesis time, and harsh experimental conditions which results in expensive production costs [95]. Therefore, exploration of green synthesis methods with few synthesis steps to minimize the use of toxic chemicals and reduce synthesis time is still necessary. At present microwave-assisted synthesis is highly desirable due to its simplicity, short synthesis time, low synthesis cost, and results in fast homogeneous rection that is beneficial to the synthesis [117].

2.4.1 Microwave synthesis

Microwave synthesis make use of microwave heating to carbonize organic substances mixed with solvents at a certain microwave power or temperature to break the chemical bonds of the precursors followed by the growth of CQDs [118]. Microwave heating is proving to be a transformational technique in preparative chemistry, unlike conventional methods which conduct heat from the outer boundary of raw materials to the inner through heat conduction, microwave synthesis results in direct penetration of microwaves into precursors, generating the access of uniform elevated heating in an easy, safe, and reproducible way [119], illustrated in figure 2.8. Microwave heating also results to short reaction times, improved product yields, less by-products, easy control of particle sizes, and enhanced purity, thus regarded as an environmentally friendly synthesis method [120]. The properties of CQDs could be regulated by changing the experimental conditions such as the microwave power, reaction time, the proportion of solvents and carbon precursors. Jusuf *et al.*, [121] proposed a waste-reused and eco-friendly microwave-assisted approach for preparing CQDs from eggshell membrane peeled off from the eggshell waste. The prepared CQDs possessed good water solubility, pH dependent fluorescent behaviour with an average size distribution of 3.88±0.56 nm. Palm kernel shell biomass waste were used to prepare photoluminescent CQDs through microwave with an average size distribution of 7.0 nm [122]. Raji *et al*., [123] used a one-step microwave synthesis to prepare photoluminescence CQDs from jackfruit seeds, the CQDs displayed excellent solubility in water, high photoluminescence, high photostability, longer storage stability, and low cytotoxicity. Yao *et al.*, [124] developed multifunctional hybrid composed of CQDs derived from waste crab shell using microwave assisted synthesis, wherein waste crab shell acted not only as a cheap source of carbon but also as a chelating agent to form complexes with metal ions.

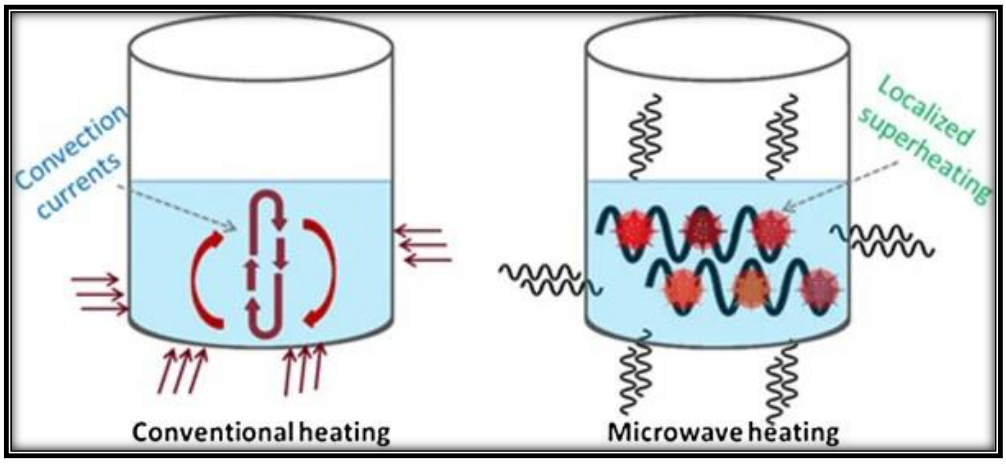

Figure 2.8: Schematic representation of the Conventional and microwave heating mechanisms [125]

2.5 Properties of CQDs

CQDs are the most desired alternative to toxic heavy metal based QDS for fluorescence related applications, due to their high fluorescence stability, environmental friendliness, good biocompatibility, facile synthesis, and low toxicity [93]. These properties strongly depend on several factors including the synthesis technique, the chosen precursors, post-synthesis treatments, time and temperature of the synthesis, pH, surface passivation or functionalization, heteroatom doping, and so on [96]. Not only do these factors affect the microstructure of CQDs, but also the optical properties, and quantum yield (QY). In this section, the physical, chemical, and optical properties of CQDs are discussed in greater detail.

2.5.1 Structural properties

CQDs are typically nanoparticles less than 10 nm, composed of a core-shell structure with sp^2/sp^3 carbon cores functionalized with polar oxygen groups [94]. The existence of the surface groups of CQDs depend mainly on the type of precursor used in the synthesis, when the used precursor is heteroatom-rich, the surface tend to have modified functional groups such as carboxyl, amine, carbonyl, and ether groups [126]. The surface functional groups impart them with excellent water solubility but also ease further surface functionalization with various molecules [127]. In addition, the precursor and synthesis method also determine the composition, morphology, and size distribution of the synthesized CQDs. Various characterization techniques are applied to determine the physical properties and the crystalline structure of the CQDs. These techniques consist of atomic force microscopy (AFM), high-resolution transmission electron microscopy (HRTEM), X-ray diffraction (XRD) and Raman spectroscopy [93]. To investigate their chemical structure, X-ray photoelectron spectroscopy (XPS), element analysis, Fourier transform infrared (FTIR), and nuclear magnetic resonance (NMR) are used [128]. Characterization of CQDs is essential for attaining a better understanding of the mechanisms associated with the unique structural properties of the nanoparticles.

TEM and AFM are used to determine the morphology, the size distribution of CQDs could be measured from TEM images, while AFM is used to measure the height information of C-dots. At present, most biomass-based CQDs are usually spherical with the average particle size less than 10 nm in a state of uniform dispersion [129], although smaller sized CQDs have been obtained from eggshell membrane peel [130] , pomelo peels [131], and garlic husk [132].

There are also some biomass-based CQDs with large size distribution obtained from spent tea [133] and from goose feather with an average size distribution of 21 ± 5 nm for the latter [134]. The crystalline properties are determined using HRTEM, XRD, and Raman spectroscopy. HRTEM is used to determine the lattice fringe spacing of the carbon materials which largely correspond to the different diffraction planes, Atchudan *et al*., showed an HRTEM image of C-dots prepared from banana peel waste with a lattice spacing of 0.21 nm [135]. The XRD spectra of CQDs generally have spectrum broad diffraction peak between 2θ values of 20° to 25° and lattice spacing between 0.31 and 0.38 nm [136]. Zhang *et al.*, showed 3D morphology images of pine wood derived CQDS, with an average height of 2.8 nm, corresponding to 5–7 layers of graphene [137].

The graphitization/crystallization of CQDs are examined by Raman spectroscopy, Raman spectra of biomass-based CQDs (similar to common CQDs synthesized using commercial precursors) exhibit two broad peaks at around 1300 cm^{-1} and 1580 cm^{-1} as shown in figure 2.10 e, which are attributed to the D (sp^3-hybridized) and G (sp^2-hybridized) bands, respectively [138]. The D band is associated with the vibrations of carbon atoms with dangling bonds in the termination plane of disordered graphite and the G-band is related to the in-plane vibrations of sp^2 carbons. Hence, the intensity ratio of the D to G bands (I_D/I_G) is the measure of the defects present on the graphitic structure, a low I_D/I_G ratio represent that the integrity of the graphitic shells is sufficiently high to protect the core material well from corrosion and oxidation [135]. The surface functional groups and elemental composition of CQDs are examined by XPS and FTIR. FTIR spectrum (figure 2.10 f) is used to understand the surface functional groups contained on the CQDs, agricultural waste-based CQDs usually exhibit main characteristic absorption bands of O–H, C–H, C═C, and (C═O), other agricultural waste-based CQDs may contain C-N and C-S bonds [104]. XPS analysis is carried out to delineate the chemical composition and nature of bonding in CQD. Agricultural waste based CQDs generally contain carbon, oxygen, nitrogen, and sulfur, which can be reflected in XPS. XPS can be used to determine the elements and the bonding modes between the contained elements. CQDs usually show three apparent peaks centred around 283, 400, and 530 eV which are attributed to C_{1s}, N_{1s}, and O_{1s}, respectively [139].

2.5.2 Optical properties

Due to the quantum-confinement effect, the optical properties are the most notable feature of CQDs irrespective of their microstructure. CQDs possess excellent optical properties such as wavelength tuned

emission which may be affected by surface state, surface passivation, heteroatom doping, surface defects, etc. This section presents and discus the common optical properties of agricultural waste based CQDs.

2.5.2.1 UV-absorption properties

CQDs usually show absorption in UV region and lower absorption intensity in the visible and near infrared region (NIR) [136]. Biomass C-dots typically show two strong absorptions in the near ultraviolet region around 230–270 nm induced by the π -π* transition of C=C and C=N bonds, whereas lower absorption intensity peak in the visible and NIR region is located around 300–330 nm is ascribed to n–π* transition of C=C or C=O bonds [116]. The UV-vis spectra of dwarf banana peel CQDs [140] show two absorption peaks, one at 272 nm and one at 320 nm, which are due to a π−π* transition of C=C bonds and the n−π* transition of C=O bonds in biomass based carbon dots (BCDs), respectively. Moreover, the nature of the CQDs precursor and surface functional groups can affect the position and intensity of the absorption peaks. Liu *et al*., [141] prepared CQDs from different agricultural waste materials C-CDs (cellulose-based CDs), P-CDs (protein-based CDs), PS-CDs (peanut shell-based CDs), CS-CDs (cotton stalk-based CDs), and S-CDs (soymeal-based CDs)). Two absorption peaks at 273 nm and 322 nm were observed for the P-CDs, while only one absorption peak was observed for the rest of the samples at 281 nm for C-CDs, 278 nm for PS-CDs, 299 nm for CS-CDs, and 328 nm for S-CDs.

2.5.2.2 Fluorescence properties

The fluorescence properties of CQDs are one of the most fascinating features since they can affect the application of CQDs in different fields. CQDs possess excellent fluorescence properties, including excitation wavelength dependent fluorescence, size dependent fluorescence emission, up-conversion luminescence, strong resistance to photobleaching, and good fluorescence stability [142]. The photoluminescence spectroscopy (PL) emission of CQDs occurs when trap states are present in the bandgap (caused by impurities, surface defects, functional groups, and adsorbed molecules). In these cases the photoexcited electron or hole can be trapped and their following recombination leads to a radiative emission of energy [143]. The observed PL is due to the combination of different mechanisms from different sources, the surface state, quantum confinement effect, and molecular state

mechanisms [136]. Most of the CQDs reported so far have a common feature of presenting excitation-dependent emission, giving a decrease in the emission signal which is systematically displaced toward longer wavelengths as the excitation wavelength increases [127]. Figure 2.9 demonstrates a photoluminescence mechanism of CQDs which occur when trap states are present in the bandgap of CQDs. Surface state mechanism is mainly induced by heteroatom doping, surface functionalization and surface passivation. Heteroatom doping is a common method in the preparation of CQDs and allows their intrinsic properties to be tunable and exploited for their desired potential applications. Elements such as N, B, S, and P are used as dopants to replace carbon atoms in the sp^2/sp^3 network [144]. Surface functionalization is related to the introduction of functional groups via covalently bonding on the carbon edge planes [145]. Surface passivation involve the coating of passivating regents (polyethylene glycol (PEG), amine terminated polyethylene glycols (PEG-1500N), poly(ethylenimide)-co-poly(ethyleneglycol)-co-poly(ethyl-enimide) (PPEI), 4,7,10-trioxa-1,13-tridecanediamine (TTDDA), and polyethyleneimine (PEI)) on the surface of the carbon core of CQDs to regulate their surface state [146]. In general, the surface state of CQDs results to a variety of energy levels and lead to various emissive traps [136]. Newman Monday *et al*., [147] prepared nitrogen doped CQDs (N-CQDs) from palm kernel shells obtained using both ethylenediamine and L-phenylalanine. The as-prepared N-CQDs showed fascinating photoluminescence (PL) property with a quantum yield (QY) of 13.7% for ethylenediamine doped N-CQDs and 8.6% for L-phenylalanine doped N-CQDs with an excitation dependent emission wavelength. Chen *et al*., [163] prepared N, S co-doped NQDs from used garlic displaying strong fluorescence with QY of 13%. Nitrogen, phosphorus co-doped CQDs with a QY as high as 76.5% were synthesized by Dong and colleagues [149].

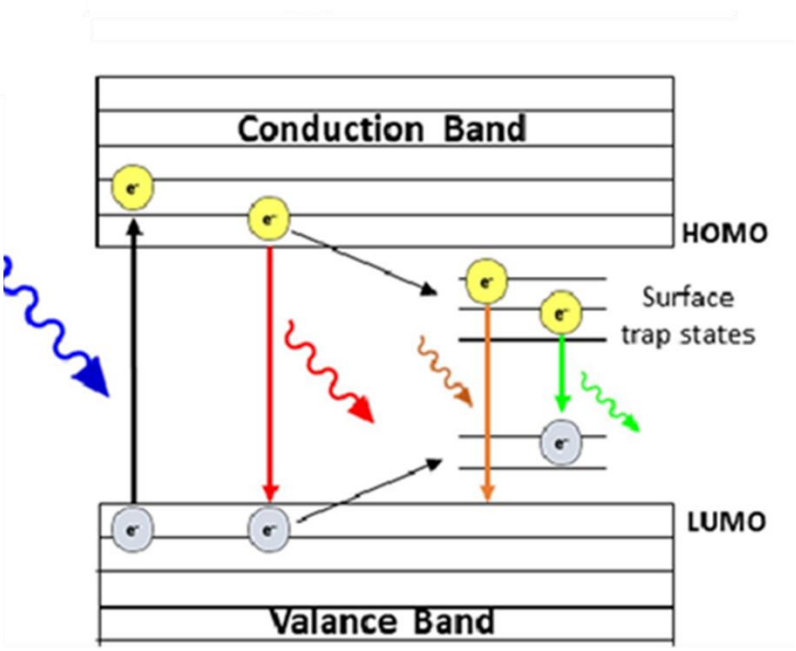

Figure 2.9: Photoluminescence mechanisms of CQDs [147]

2.6 Application of CQDs

CQDs have attracted rapidly growing scientific interest, and have found application in bioimaging, biosensing, fuel cells, supercapacitors, catalysis, solar cells, lithium-ion batteries, drug delivery and light emitting diodes, owing to their outstanding chemical, physical and optical properties [96]. According to a Web of Science search done by Li *et al*., [144] in March 2021, showed that 41 % of CQDs are used in the sensor field, this is due to their strong luminescence properties. CQDs-based sensors give rise to a low limit of detection (LOD), high sensitivity and selectivity [150]. Wang *et al*., [151] proposed a CQDs based PL sensor for the first time and demonstrated that the luminescence of CQDs can be quenched selectively by Fe^{3+} ion through charge transfer mechanism, starting a new trend towards using CQDs for the detection of heavy metal ions. Since the CQDs with different surface states have been utilized for the detection of Fe^{3+}, Zhao *et al*., [152] prepared water soluble, luminescent N-CQDs from chitosan and utilized them for the sensing of Fe^{3+} in aqueous solutions. The N-CQDs presented outstanding selectivity and sensitivity and were successfully applied for the quantitative detection of Fe^{3+} with a linear detection range of 0–500 μM and an LOD of 0.15 μM. N, P co-doped CQDs were adopted as a fluorescent sensor for the effective detection of Fe^{3+} ions in water, with an LOD of 0.1 μM and showed a better linear relationship in the range of 0.1 ~ 50 μM [149]. High luminescence S-CQDs were synthesized from cellulose fibers with a QY of 32%, the as-prepared S-CQDs were utilized to detect Fe^{3+} in pH 0 solutions and showed excellent

selectivity and sensitivity, with a LOD as low as 0.96 μM [168]. PEI functionalized CQDs from coffee grounds have also been utilized to detect Fe^{3+} [154].

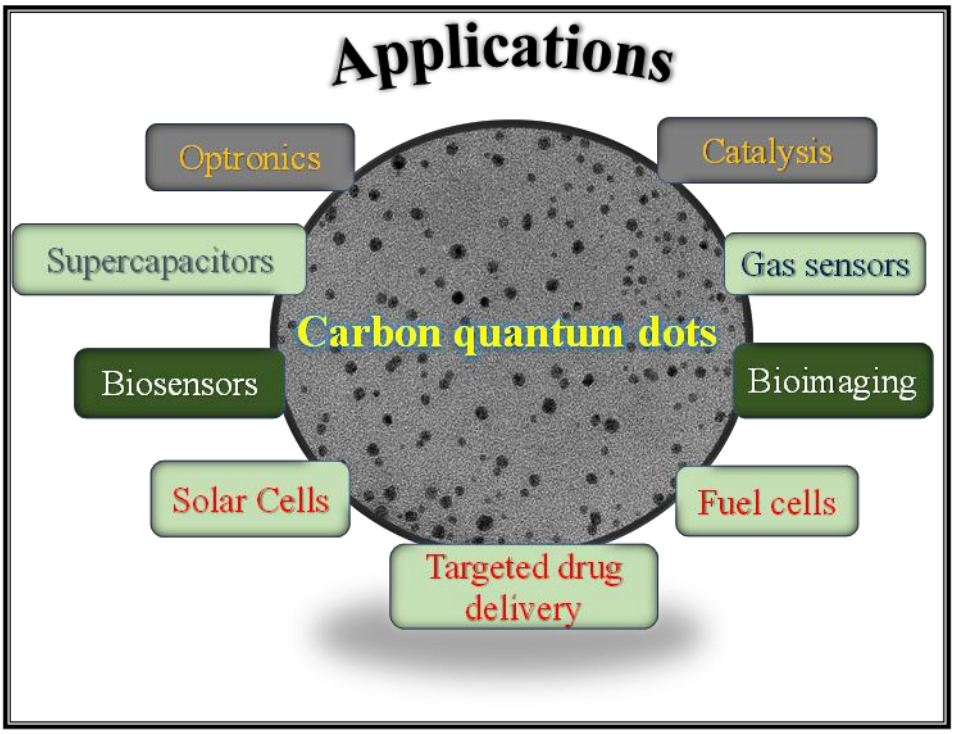

Figure 2.11: Common application for carbon quantum dots

2.7 Activated carbon

Activated carbon (AC) is a promising class of carbon-rich materials containing well-built internal pore structure, with high surface area, well-organized macro, meso, and micro-pores, and high mechanical strength [155]. The surface of the AC is usually rich in heteroatoms such as oxygen, sulfur, hydrogen, nitrogen, halogens, and other elements, in the forms of functional groups or chemically bonded to the structure [156]. Making it versatile for numerous applications in different fields such as pharmaceuticals, food processing, vacuum manufacturing, waste water management, and air pollution [157]. Although the production of global AC has increased by an average annual growth of 5.5 % since the last decade, the production of most commercially available AC still require the use of expensive, non-renewable precursors such as coal and some high-value agroforestry materials, such as bamboo, wood, and coconut [157, 158]. Due to the high cost associated with AC production, the development of cost-effective strategies for AC preparation, such as the use of low-cost, environmentally friendly, and renewable agricultural wastes are of great interest [159]. The production of AC from agricultural is usually justified

by the unique properties of these precursors, the possibility of mass production at low costs, and the conversion of low value agricultural wastes to value-added products and limiting of the environmental pollution and resource consumption.

At present, chemical activation and physical activation are the two methods that have been used to activate carbonaceous materials [160]. In physical activation, precursors are first carbonized followed by activation step by steam or carbon dioxide. During chemical activation, the precursors are impregnated by an activating reagent and followed by a heating process under an inert atmosphere shown in figure 2.10 [161]. Chemical activation of has been reported to be more advantageous over physical activation due to low energy requirements, higher yields, larger surface areas, low activation time, and development of better porous structures [162]. In addition, chemical activation can be considered as an economical and environmentally friendly process since the chemical reagents can be recovered and reused [155]. The most commonly used activating reagents are KOH, $ZnCl_2$, H_3PO_4, K_2CO_3, and NaOH [163]. Several parameters play a role on the properties of the AC, these include activating agent selection, activation temperature and time, the impregnation ratio of activation reagents to precursor, impregnation method, and gas flow during carbonization [157]. Köseoɨlu and Akmil-Başar [162] reported that K_2CO_3 was found to be more effective than the $ZnCl_2$ as a chemical reagent in terms of high surface area, porosity development, and well developed surface morphology, whereas $ZnCl_2$ was effective in producing high yields. Borhan *et al*. [164] investigated the preparation of AC from an agriculture residue through chemical activation using different impregnation ratios of KOH to the precursor from 1:1 to 1:3 precursor: KOH ratios. They found that impregnation ratio had a strong effect on the surface area, pore volume, and the yield decreases with the increase of the variable. The effect of temperature has also been investigated, Sreńscek-Nazzal and colleagues [165] studied the effect of carbonization from 400 to 800 °C and they found that the higher temperature produced better activation with a high surface area. The optimal activation conditions were found at 780 °C with a surface area of 2202 m^2/g.

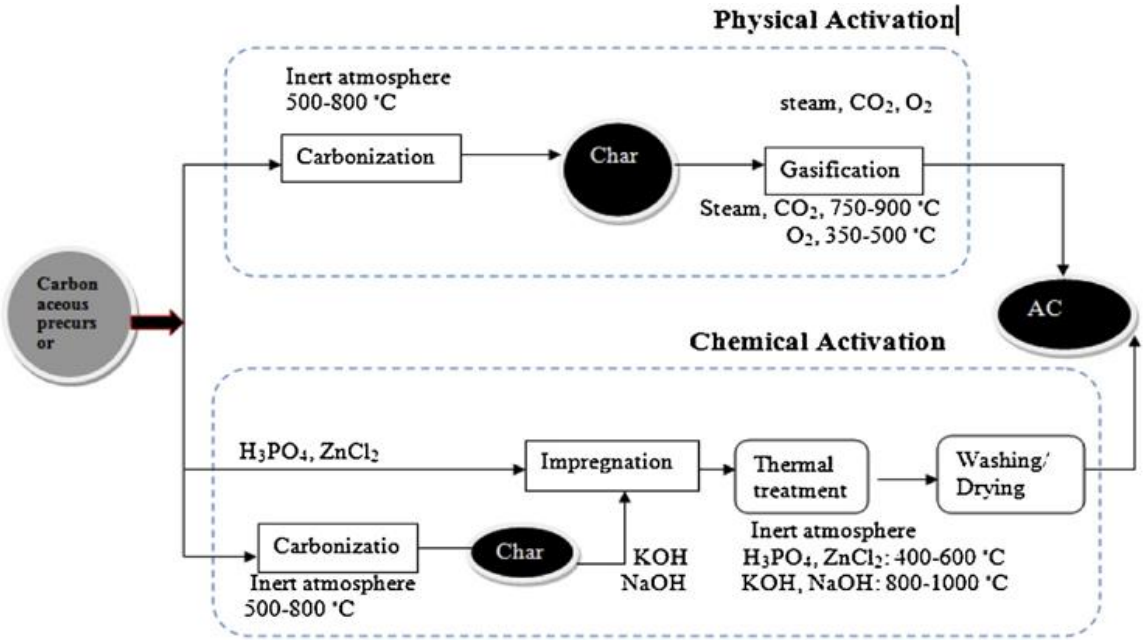

Fig. 2.10: Procedures in physical and chemical methods of AC synthesis [166]

2.7.1 Applications of Activated carbon

AC has found many applications in different fields including water treatment, chemical and petroleum industries, separation, purification, catalysis, energy storage, batteries, fuel cells, nuclear power stations, electrodes for electric double layer capacitors, pharmaceutical, etc. due to their unique high surface area, high mechanical strength, and high adsorptive capacity [156]. For example, Redondo *et al*., [167] used olive pits derived AC to prepare microporous carbon electrodes with an optimized microporosity, enabling a gravimetric and volumetric capacitance in basic aqueous medium up to 260 F g^{-1} and 140 F cm^{-3}, respectively, with good rate capability. Mopoung and collegues [168] prepared AC from tamarind seeds for the adsorption of iodine, methylene blue and Fe (III). It was shown that Fe(III) was adsorbed in alkaline conditions and adsorption increased with increasing Fe(III) initial concentration from 5 to 20 ppm with capacity adsorption of 0.0069–0.019 mg/g. The physical adsorption on AC has been widely explored for the application in separation and purification gas systems and adsorption based gas storage systems [169]. Zhang *et al.* [170] performed a comparative study of CO_2 adsorption isotherms on AC and zeolite, they observed higher CO_2 adsorption capacity of AC compared to that of zeolite at pressures above 1.7 bar. Among the other types of gases are the volatile organic compounds (VOCs), their detection technologies are based on a transducer and an active layer, which converts a desired chemical reaction into a measurable electronic signal such as change in the resistance, frequency, current, or voltage [171]. The detection characteristics of a material are not only dependent on its porous nature but it is also strongly influenced by the chemical property of its surface [172]. As a nonpolar adsorbent, AC

itself has low chemical adsorption and selectivity due to its less surface adsorption active sites, therefore, efforts have been made to improve its affinity, alter the electronic structure of porous carbons, manipulate their surface chemistry, and insert local changes to their matrices by introducing surface functional groups such as carboxyl, carbonyl, hydroxyl, and phenols, or active substances such as metal oxides on their surface [173, 174]. Kim *et al*., [175] fabricated a rapid, repetitive, and selective NO_2 gas sensor from activated carbon fibers (ACFs) containing enriched boron moieties, the boron moieties induced high selectivity toward NO_2 over other VOCs via the strong binding energy.

2.8 Conclusion

With the continuous exploitation of fossil fuels such as coal and oil, the global climate crisis is becoming more and more serious. The growing environmental awareness has resulted in growing research interest in the use of renewable and green resources for sustainable economies. One of them is the usage of agricultural waste for value added product, developing countries specifically experience significant negative impacts associated with poor agricultural waste management. Increasing urbanisation globally has revealed the high demand for alternative energy sources and smart materials. In recent years, agricultural waste has been utilized to prepare different types of carbon materials, a promising class of material for potential application in energy storage, catalysis and chemical sensors due to their unique electrical, optical, and mechanical properties. This can potentially, lead to the replacement of the currently commercialized heavy metal-based devices with cost-effective and eco-friendly carbon-based materials.

2.9 References

[1] W.-J. Liu, K. Tian, Y.-R. He, H. Jiang, and H.-Q. Yu, "High-Yield Harvest of Nanofibers/Mesoporous Carbon Composite by Pyrolysis of Waste Biomass and Its Application for High Durability Electrochemical Energy Storage," *Environ. Sci. Technol*, vol. 48, pp. 13951–13959, 2014, doi: 10.1021/es504184c.

[2] P. Ranum, J. P. Peña-Rosas, and M. N. Garcia-Casal, "Global maize production, utilization, and consumption," *Ann. N. Y. Acad. Sci.*, vol. 1312, pp. 105–112, 2014, doi: 10.1111/nyas.12396.

[3] X. Shao, J. Wang, Z. Liu, N. Hu, M. Liu, and Y. Xu, "Preparation and Characterization of Porous Microcrystalline Cellulose from Corncob," *Ind. Crops Prod.*, vol. 151, pp. 112457, 2020, doi: 10.1016/j.indcrop.2020.112457.

[4] W. Liu, R. Wu, B. Wang, Y. Hu, Q. Hou, P. Zhang, and R. Wu, "Comparative study on different pretreatment on enzymatic hydrolysis of corncob residues," *Bioresour. Technol.*, vol. 295, pp. 122244, 2020, doi: 10.1016/j.biortech.2019.122244.

[5] N. Berkhout, "South Africa: Produces 2nd highest corn crop," 2020. https://www.allaboutfeed.net/animal-feed/raw-materials/south-africa-produces-2nd-highest-corn-crop/#:~:text=Junior Aklei Chaky-,South Africa produced its second highest corn crop on record,crop of 11.3 million tonnes.&text=The expected commercial yellow c (accessed Mar. 14, 2021).

[6] A. Mtibe, T. H. Mokhothu, and L. Z. Linganiso, "Maize stark (corn stover) to valusble products, in Waste-to-Profit (W-t-P): Value added Products to Generate Wealth for a Sustainable Economy", vol. 1, pp. 107–133, 2018.

[7] L. M. Mohlala, M. O. Bodunrin, A. A. Awosusi, M. O. Daramola, N. P. Cele, and P. A. Olubambi, "Beneficiation of corncob and sugarcane bagasse for energy generation and materials development in Nigeria and South Africa: A short overview," *Alexandria Engineering Journal*, vol. 55, no. 3. Elsevier B.V., pp. 3025–3036, 2016, doi: 10.1016/j.aej.2016.05.014.

[8] M. Smyth, A. García, C. Rader, E. J. Foster, and J. Bras, "Extraction and process analysis of high aspect ratio cellulose nanocrystals from corn (Zea mays) agricultural residue," *Ind. Crops Prod.*, vol. 108, pp. 257–266, 2017, doi: 10.1016/j.indcrop.2017.06.006.

[9] H. A. Silvério, W. P. Flauzino Neto, N. O. Dantas, and D. Pasquini, "Extraction and characterization of cellulose nanocrystals from corncob for application as reinforcing agent in

nanocomposites," *Ind. Crops Prod.*, vol. 44, pp. 427–436, 2013, doi: 10.1016/j.indcrop.2012.10.014.

[10] Q. Cao, K. C. Xie, W. R. Bao, and S. G. Shen, "Pyrolytic behavior of waste corn cob," *Bioresour. Technol.*, vol. 94, pp. 83–89, 2004, doi: 10.1016/j.biortech.2003.10.031.

[11] L. Zhang, Y. Wang, W. Liu, Y. Ni, and Q. Hou, "Corncob residues as carbon quantum dots sources and their application in detection of metal ions," *Ind. Crops Prod.*, vol. 133, pp. 18–25, 2019, doi: 10.1016/j.indcrop.2019.03.019.

[12] X. Shao, J. Wang, Z. Liu, N. Hu, M. Liu, and Y. Xu, "Preparation and Characterization of Porous Microcrystalline Cellulose from Corncob," *Ind. Crops Prod.*, vol. 151, pp. 112457, 2020, doi: 10.1016/j.indcrop.2020.112457.

[13] A. Boruah, M. Saikia, T. Das, R. L. Goswamee, and B. K. Saikia, "Blue-emitting fluorescent carbon quantum dots from waste biomass sources and their application in fluoride ion detection in water," *J. Photochem. Photobiol. B Biol.*, vol. 209, pp. 111940, 2020, doi: 10.1016/j.jphotobiol.2020.111940.

[14] H. Wang, W. Zhao, Y. Chen, X. Yang, and X. Meng, "Efficient removal of crystal violet dye using EDTA/ graphene oxide functionalized corncob: a novel low cost adsorbent †," *RSC Adv.*, vol. 9, pp. 21996-22003, 2019, doi: 10.1039/c9ra04003j.

[15] A. Paiva, S. Pereira, A. Sá, D. Cruz, H. Varum, and J. Pinto, "A contribution to the thermal insulation performance characterization of corn cob particleboards," *Energy Build.*, vol. 45, pp. 274–279, 2012, doi: 10.1016/j.enbuild.2011.11.019.

[16] L. Zhang, L. Tian, R. Sun, C. Liu, Q. Kou, and H. Zuo, "Transformation of corncob into furfural by a bifunctional solid acid catalyst," *Bioresour. Technol.*, vol. 276, pp. 60–64, 2019, doi: 10.1016/j.biortech.2018.12.094.

[17] B.-L. Xue, P.-L. Huang, Y.-C. Sun, X.-P. Li, and R.-C. Sun, "Hydrolytic depolymerization of corncob lignin in the view of a bio-based rigid polyurethane foam synthesis †," *RSC Adv.*, vol. 7, pp. 6123-6130, 2017, doi: 10.1039/c6ra26318f.

[18] K.-K. Cheng, J.-A. Zhang, E. Chavez, and J.-P. Li, "Integrated production of xylitol and ethanol using corncob," *Appl. Microbiol. Biotechnol.*, vol. 87, pp. 411–417, 2010, doi: 10.1007/s00253-010-2612-5.

[19] B. Rekha and R. Saravanathamizhan, "Catalytic conversion of corncob biomass into bioethanol," *Int. J. Energy Res.*, vol. 45, no. 3, pp. 4508–4518, 2021, doi: 10.1002/er.6119.

[20] J. Dong, X. Zhu, X. Huang, T. Yin, H. Fang, and Z. Ding, "Antioxidant Activities and Phenolic Compounds of Cornhusk, Corncob and Stigma Maydis," *J. Braz. Chem. Soc.*, vol. 25, no. 11, pp. 1956–1964, 2014, doi: 10.5935/0103-5053.20140177.

[21] C. Duan, X. Meng, C. Liu, W. Lu, J. Liu, W. Wang, W. Zhao, C. Xiong, Y. Ni, and J. Dong, "Carbohydrates-rich corncobs supported metal-organic frameworks as versatile biosorbents for dye removal and microbial inactivation," *Carbohydr. Polym.*, vol. 222, pp. 115042, 2019, doi: 10.1016/j.carbpol.2019.115042.

[22] W. H. Qu, Y. Y. Xu, A. H. Lu, X. Q. Zhang, and W. C. Li, "Converting biowaste corncob residue into high value added porous carbon for supercapacitor electrodes," *Bioresour. Technol.*, vol. 189, pp. 285–291, 2015, doi: 10.1016/j.biortech.2015.04.005.

[23] Z.-Z. Pan, L. Dong, W. Lv, D. Zheng, Z. Li, C. Luo, C. Zheng, Q. Yang, and F. Kang, "A Hollow Spherical Carbon Derived from the Spray Drying of Corncob Lignin for High-Rate-Performance Supercapacitors." *Chemasianj.*, vol. 12, pp.503-506, 2017, doi: 1002/asia.201601724

[24] J. Guo, J. Zhang, F. Jiang, S. Zhao, Q. Su, and G. Du, "Microporous carbon nanosheets derived from corncobs for lithium-sulfur batteries," *Electrochim. Acta*, vol. 176, pp. 853–860, 2015, doi: 10.1016/j.electacta.2015.07.077.

[25] X. Luo, N. Li, X. Guo, and K. Wu, "One-pot hydrothermal synthesis of MoS2 anchored corncob-derived carbon nanospheres for use as a high-capacity anode for reversible Li-ion battery," *J. Solid State Chem.*, vol. 296, p. 122020, 2021, doi: 10.1016/j.jssc.2021.122020.

[26] A. M. Das, M. P. Hazarika, M. Goswami, A. Yadav, and P. Khound, "Extraction of cellulose from agricultural waste using Montmorillonite K-10/LiOH and its conversion to renewable energy: Biofuel by using Myrothecium gramineum," *Carbohydr. Polym.*, vol. 141, pp. 20–27, 2016, doi: 10.1016/j.carbpol.2015.12.070.

[27] L. K. Kian, M. Jawaid, H. Ariffin, and O. Y. Alothman, "Isolation and characterization of microcrystalline cellulose from roselle fibers," *Int. J. Biol. Macromol.*, vol. 103, pp. 931–940, 2017, doi: 10.1016/j.ijbiomac.2017.05.135.

[28] E. Galiwango, N. S. Abdel Rahman, A. H. Al-Marzouqi, M. M. Abu-Omar, and A. A. Khaleel, "Isolation and characterization of cellulose and α-cellulose from date palm biomass waste," *Heliyon*, vol. 5, pp. e02937, 2019, doi: 10.1016/j.heliyon.2019.e02937.

[29] C. B. Zhan, P. R. Sharma, L. H. Geng, S. K. Sharma, R. F. Wang, R. Joshi, and B. S. Hsiao,

"Special Topic: Smart and Functional Fiber Materials Structural characterization of carboxyl cellulose

nanofibers extracted from underutilized sources," S*cience China Technological* Sciences, vol. 6, pp. 971-981, 2019, doi: 10.1007/s11431-018-9441-1.

[30] I. Siró and D. Plackett, "Microfibrillated cellulose and new nanocomposite materials: a review," *Cellulose,* vol. 17, pp. 459–494, 2010, doi: 10.1007/s10570-010-9405-y.

[31] J. George and S. N. Sabapathi, "Cellulose nanocrystals: synthesis, functional properties, and applications," *Nanotechnol. Sci. Appl.,* vol. 8, pp. 45–54, 2015, doi: 10.2147/NSA.S64386.

[32] J. Gong, J. Li, J. Xu, Z. Xiang, and L. Mo, "Research on cellulose nanocrystals produced from cellulose sources with various polymorphs," *RSC Adv.,* vol. 7, pp. 33486-33493, 2017, doi: 10.1039/c7ra06222b.

[33] M. M. Mahmud, A. Perveen, R. A.Jahan, M. A. Matin, S. Y. Wong, X. Li, and M. T. Arafat, "Preparation of different polymorphs of cellulose from different acid hydrolysis medium," *Int. J. Biol. Macromol.,* vol. 130, pp. 969–976, Jun. 2019, doi: 10.1016/j.ijbiomac.2019.03.027.

[34] A. Mandal and D. Chakrabarty, "Isolation of nanocellulose from waste sugarcane bagasse (SCB) and its characterization," *Carbohydr. Polym.*, vol. 86, pp. 1291–1299, 2011, doi: 10.1016/j.carbpol.2011.06.030.

[35] A. G. De Souza, M. T. Junqueira, G. F. De Lima, V. K. Rangari, · Derval, and S. Rosa, "A New Proposal of Preparation of Different Polymorphs of Nanocellulose from Eucalyptus citriodora," *J. Polym. Environ.,* vol. 28, pp. 1150–1159, 2014, doi: 10.1007/s10924-020-01672-4.

[36] S. Singh, K. K. Gaikwad, S. Il Park, and Y. S. Lee, "Microwave-assisted step reduced extraction of seaweed (Gelidiella aceroso) cellulose nanocrystals," *Int. J. Biol. Macromol.,* vol. 99, pp. 506–510, 2017, doi: 10.1016/j.ijbiomac.2017.03.004.

[37] F. Bettaieb, R. Khiaria, M. L.Hassan, M. N. Belgacem, J. Bras, A. Dufresne, and M. F. Mhenni, "Preparation and characterization of new cellulose nanocrystals from marine biomass Posidonia oceanica," *Ind. Crops Prod.,* vol. 72, pp. 175–182, 2015, doi: 10.1016/j.indcrop.2014.12.038.

[38] D. A. Gopakumar, S. Manna, D. Pasquini, S. Thomas, and Y. Grohens, "Nanocellulose: Extraction and application as a sustainable material for wastewater purification,"*New Polymer Nanocomposites for Environmental Remediation, Elsevier Inc*., pp. 469–486, 2018, doi: https://doi.org/10.1016/B978-0-12-811033-1.00019-6.

[39] H. Doh, M. H. Lee, and W. S. Whiteside, "Physicochemical characteristics of cellulose nanocrystals isolated from seaweed biomass," *Food Hydrocoll.,* vol. 102, pp. 105542, 2020, doi: 10.1016/j.foodhyd.2019.105542.

[40] G. Zhao, J. Du,W. Chen, M. Pan, D. Chen, G. J. Zhao, W. Chen, M. Pan, and. D. Chen, "Preparation and thermostability of cellulose nanocrystals and nanofibrils from two sources of biomass: rice straw and poplar wood," *Cellulose*, vol. 26, pp. 8625–8643, 2019, doi: 10.1007/s10570-019-02683-8.

[41] I. B. González, A. L. Rubio, R. Gavara, M. Martínez-Sanz, and I. A. Benito-González, "Cellulose nanocrystal-based films produced by more sustainable extraction protocols from Posidonia oceanica waste biomass," *Cellulose*, vol. 26, pp. 8007–8024, 2019, doi: 10.1007/s10570-019-02641-4.

[42] P. Phanthong, P. Reubroycharoen, X. Hao, G. Xu, A. Abudula, and G. Guan, "Nanocellulose: Extraction and application," *Carbon Resour. Convers.*, vol. 1, pp. 32–43, 2018, doi: 10.1016/j.crcon.2018.05.004.

[43] S. Mishra, P. S. Kharkar, and A. M. Pethe, "Biomass and waste materials as potential sources of nanocrystalline cellulose: Comparative review of preparation methods (2016 – Till date)," *Carbohydr. Polym.*, vol. 207, pp. 418–427, 2019, doi: 10.1016/J.CARBPOL.2018.12.004.

[44] R. Z. Khoo W S Chow H Ismail, "Sugarcane bagasse fiber and its cellulose nanocrystals for polymer reinforcement and heavy metal adsorbent: a review," *Cellulose*, vol. 25, pp.4303–4330, 2018, doi: 10.1007/s10570-018-1879-z.

[45] C. K. Weiss, A. Isogai, and R. Konwarh, "Nanocellulose: From Fundamentals to Advanced Applications," *Front. Chem. | www.frontiersin.org*, vol. 1, p. 392, 2020, doi: 10.3389/fchem.2020.00392.

[46] A. Dufresne, "Nanocellulose: A new ageless bionanomaterial," *Materials Today*, vol. 16, pp. 220–227, 2013, doi: 10.1016/j.mattod.2013.06.004.

[47] R. M. Sheltami, I. Abdullah, I. Ahmad, A. Dufresne, and H. Kargarzadeh, "Extraction of cellulose nanocrystals from mengkuang leaves (Pandanus tectorius)," *Carbohydr. Polym.*, vol. 88, no. 2, pp. 772–779, 2012, doi: 10.1016/j.carbpol.2012.01.062.

[48] W. P. Flauzino Neto, H. A. Silvério, N. O. Dantas, and D. Pasquini, "Extraction and characterization of cellulose nanocrystals from agro-industrial residue - Soy hulls," *Ind. Crops Prod.*, vol. 42, no. 1, pp. 480–488, 2013, doi: 10.1016/j.indcrop.2012.06.041.

[49] Z. Wang, Z. J. Yao, J. Zhou, and Y. Zhang, "Reuse of waste cotton cloth for the extraction of cellulose nanocrystals," *Carbohydr. Polym.*, vol. 157, pp. 945–952, 2017, doi: 10.1016/j.carbpol.2016.10.044.

[50] S. K. Evans, O. N. Wesley, O. Nathan, and M. J. Moloto, “Chemically purified cellulose and its nanocrystals from sugarcane baggase: isolation and characterization,” *Heliyon*, vol. 5, no. 10, p. e02635, 2019, doi: 10.1016/j.heliyon.2019.e02635.

[51] D. Zheng, Y. Zhang, Y. Guo, and J. Yue, “Isolation and Characterization of Nanocellulose with a Novel Shape from Walnut (Juglans Regia L.) Shell Agricultural Waste,” *Polymers*, vol. 11, pp. 1130, 2019, doi: 10.3390/polym11071130.

[52] M. Rasheed, M. Jawaid, B. Parveez, A. Zuriyati, and A. Khan, “Morphological, chemical and thermal analysis of cellulose nanocrystals extracted from bamboo fibre,” *Int. J. Biol. Macromol.*, vol. 160, pp. 183–191, 2020, doi: 10.1016/j.ijbiomac.2020.05.170.

[53] D. Victor Mashego, “Preparation,isolation and characterization of nanocellulose from sugarcane bagasse,” MSc Thesis, 2016, Durban University of Technology.

[54] H. Gu, X. Gao, H. Zhang, K. Chen, and L. Peng, “Fabrication and characterization of cellulose nanoparticles from maize stalk pith via ultrasonic-mediated cationic etherification,” *Ultrason. Sonochem.*, vol. 66, pp. 104932, 2020, doi: 10.1016/j.ultsonch.2019.104932.

[55] J. Li, X. Wei, Q. Wang, J. Chen, G. Chang, L. Kong, J. Su, and Y. Liu, “Homogeneous isolation of nanocellulose from sugarcane bagasse by high pressure homogenization,” *Carbohydr. Polym.*, vol. 90, no. 4, pp. 1609–1613, 2012, doi: 10.1016/j.carbpol.2012.07.038.

[56] C. Liu, B. Li, H. Du, D. Lv, Y. Zhang, G. Yu, X. Mu, and H. Peng, “Properties of nanocellulose isolated from corncob residue using sulfuric acid, formic acid, oxidative and mechanical methods,” *Carbohydr. Polym.*, vol. 151, pp. 716–724, 2016, doi: 10.1016/j.carbpol.2016.06.025.

[57] Q. Jiang, X. Xing, Y. Jing, and Y. Han, “Preparation of cellulose nanocrystals based on waste paper via different systems,” *Int. J. Biol. Macromol.*, vol. 149, pp. 1318–1322, 2020, doi: 10.1016/j.ijbiomac.2020.02.110.

[58] J. Guo, X. Guo, S. Wang, and Y. Yin, “Effects of ultrasonic treatment during acid hydrolysis on the yield, particle size and structure of cellulose nanocrystals,” *Carbohydr. Polym.*, vol. 135, pp. 248–255, 2016, doi: 10.1016/j.carbpol.2015.08.068.

[59] R. M. dos Santos, W. P. Flauzino Neto, H. A. Silvério, D. F. Martins, N. O. Dantas, and D. Pasquini, “Cellulose nanocrystals from pineapple leaf, a new approach for the reuse of this agro-waste,” *Ind. Crops Prod.*, vol. 50, pp. 707–714, 2013, doi: 10.1016/j.indcrop.2013.08.049.

[60] F. Jiang and Y. Lo Hsieh, “Cellulose nanocrystal isolation from tomato peels and assembled nanofibers,” *Carbohydr. Polym.*, vol. 122, pp. 60–68, 2015, doi:

10.1016/J.CARBPOL.2014.12.064.

[61] N. Sai Prasanna and J. Mitra, “Isolation and characterization of cellulose nanocrystals from Cucumis sativus peels,” *Carbohydr. Polym.*, vol. 247, pp. 116706, 2020, doi: 10.1016/J.CARBPOL.2020.116706.

[62] E. Espino, M. Cakir, S. Domenek, A. D. Román-Gutiérrez, N. Belgacem, and J. Bras, “Isolation and characterization of cellulose nanocrystals from industrial by-products of Agave tequilana and barley,” *Ind. Crops Prod.*, vol. 62, pp. 552–559, 2014, doi: 10.1016/J.INDCROP.2014.09.017.

[63] Y. Mazlita, H.V. Lee, and S.B.A. Hamid, “Preparation of Cellulose Nanocrystals Bio-Polymer From Agro-Industrial Wastes: Separation and Characterization,” *Polymers & Polymer Comp.*, vol. 24, pp. 2016, doi: 10.1177/096739111602400907

[64] C. Trilokesh, and B. Uppuluri, “isolation and characterization of cellulose nanocrystals from jackfruit peel,” *Scientific Reports*, vol. 9, pp. 16709, 2019, doi: 10.1038/s41598-019-53412-x.

[65] E. Hafemann, R. Battisti, D. Bresolin, C. Marangoni, R. Antonio, and F. Machado, “Enhancing Chlorine-Free Purification Routes of Rice Husk Biomass Waste to Obtain Cellulose Nanocrystals Statement of Novelty,” *Waste and Biomass Valorization*, vol. 11, pp. 6595–6611, 2020, doi: 10.1007/s12649-020-00937-2.

[66] S. Huang, X. Liu, C. Chang, and Y. Wang, “Recent developments and prospective food-related applications of cellulose nanocrystals: a review,” *Cellulose*, vol. 27, pp. 2991–3011, 2020, doi: 10.1007/s10570-020-02984-3.

[67] M. Mariano, N. El Kissi, and A. Dufresne, “Cellulose Nanocrystals and Related Nanocomposites: Review of some Properties and Challenges,” *J. Polym. Sci., Part B Polym. Phys*, vol. 52, pp. 791–806, 2014, doi: 10.1002/polb.23490.

[68] Z. Kassab, I. Kassem, H. Hannache, R. Bouhfid, A. E. Kacem, and Q. M. Achaby, “Tomato plant residue as new renewable source for cellulose production: extraction of cellulose nanocrystals with different surface functionalities,” *Cellulose*, vol. 27, doi: 10.1007/s10570-020-03097-7.

[69] Z. Wang, Z. Yao, J. Zhao, M. He, Q. Jiang, S. Li, Y. Ma, M. Liu, and S. Luo, “Isolation and characterization of cellulose nanocrystals from pueraria root residue,” *Int. J. Biol. Macromol.*, vol. 129, pp. 1081–1089, 2019, doi: 10.1016/j.ijbiomac.2018.07.055.

[70] Kusmono, R. F. Listyanda, M. W. Wildan, and M. N. Ilman, “Preparation and characterization of cellulose nanocrystal extracted from ramie fibers by sulfuric acid hydrolysis,” *Heliyon*, vol. 6, pp.

e05486, 2020, doi: 10.1016/J.HELIYON.2020.E05486.

[71] N. Pal, S. Banerjee, P. Roy, and K. Pal, "Reduced graphene oxide and PEG-grafted TEMPO-oxidized cellulose nanocrystal reinforced poly-lactic acid nanocomposite film for biomedical application," *Mater. Sci. Eng. C*, vol. 104, pp. 109956, 2019, doi: 10.1016/J.MSEC.2019.109956.

[72] B. Li *et al.*, "Cellulose nanocrystals prepared via formic acid hydrolysis followed by TEMPO-mediated oxidation," *Carbohydr. Polym.*, vol. 133, pp. 605–612, 2015, doi: 10.1016/J.CARBPOL.2015.07.033.

[73] R. Rohaizu and W. D. Wanrosli, "Sono-assisted TEMPO oxidation of oil palm lignocellulosic biomass for isolation of nanocrystalline cellulose," *Ultrason. Sonochem.*, vol. 34, pp. 631–639, 2017, doi: 10.1016/J.ULTSONCH.2016.06.040.

[74] K. Zhang, P. Sun, H. Liu, S. Shang, J. Song, and D. Wang, "Extraction and comparison of carboxylated cellulose nanocrystals from bleached sugarcane bagasse pulp using two different oxidation methods," *Carbohydr. Polym.*, vol. 138, pp. 237–243, 2016, doi: 10.1016/J.CARBPOL.2015.11.038.

[75] P. R. Sharma, R. Joshi, S. K. Sharma, and B. S. Hsiao, "A Simple Approach to Prepare Carboxycellulose Nanofibers from Untreated Biomass," *Biomacromolecules*, vol. 18, pp. 2333–2342, 2017, doi: 10.1021/acs.biomac.7b00544.

[76] H. Zhang, Y. Chen, S. Wang, L. Ma, Y. Yu, H. Dai, and Y. Zhang, "Extraction and comparison of cellulose nanocrystals from lemon (Citrus limon) seeds using sulfuric acid hydrolysis and oxidation methods," *Carbohydr. Polym.*, vol. 238, p. 116180, 2020, doi: 10.1016/J.CARBPOL.2020.116180.

[77] A. Isogai, T. Hänninen, S. Fujisawa, and T. Saito, "Review: Catalytic oxidation of cellulose with nitroxyl radicals under aqueous conditions," *Prog. Polym. Sci.*, vol. 86, pp. 122–148, 2018, doi: 10.1016/J.PROGPOLYMSCI.2018.07.007.

[78] P. R. Sharma, A. Chattopadhyay, C. Zhan, S. K. Sharma, and B. S. Hsiao, "Lead removal from water using carboxycellulose nanofibers prepared by nitro-oxidation method," *Cellulose*, vol. 25, doi: 10.1007/s10570-018-1659-9.

[79] R. Koshani, T. G. M. Van De Ven, and A. Madadlou, "Characterization of Carboxylated Cellulose Nanocrytals Isolated through Catalyst-Assisted H 2 O 2 Oxidation in a One-Step Procedure," *J. Agric. Food Chem.*, vol. 66, pp, 7692–7700, 2018, doi: 10.1021/acs.jafc.8b00080.

[80] P. R. Sharma, B. Zheng, S. K. Sharma, C. Zhan, R. Wang, S. R. Bhatia, and B. S. Hsiao "High

Aspect Ratio Carboxycellulose Nanofibers Prepared by Nitro-Oxidation Method and Their Nanopaper Properties," A*CS Appl. Nano Mater.*, vol. 1, pp. 3969–3980, 2018, doi: 10.1021/acsanm.8b00744.

[81] A. Isogai, T. Saito, and H. Fukuzumi, "TEMPO-oxidized cellulose nanofibers," *Nanoscale*, vol. 3, pp. 71-85, 2011, doi: 10.1039/c0nr00583e.

[82] X. Song, L. Zhou, B. Ding, X. Cui, Y. Duan, and J. Zhang, "Simultaneous improvement of thermal stability and redispersibility of cellulose nanocrystals by using ionic liquids," *Carbohydr. Polym.*, vol. 186, pp. 252–259, 2018, doi: 10.1016/J.CARBPOL.2018.01.055.

[83] G. Abdalla, S. Haron, H. Mahmood, M. Hilmi Noh, M. Z. Alam, and M. Moniruzzaman, "Ionic Liquids as a Sustainable Platform for Nanocellulose Processing from Bioresources: Overview and Current Status," *ACS Sustainable Chem. Eng.*, vol. 9, pp. 1008–1034, 2021, doi: 10.1021/acssuschemeng.0c06409.

[84] D. Trache, M. H. Hussin, M. K. M. Haafiz, and V. K. Thakur, "Recent progress in cellulose nanocrystals: sources and production," *Nanoscale*, vol. 9, pp. 1763, 2017, doi: 10.1039/c6nr09494e.

[85] C. Rovera, M. Ghaani, N. Santo, S. Trabattoni, R. T. Olsson, D. Romano, and S. Farris, "Enzymatic Hydrolysis in the Green Production of Bacterial Cellulose Nanocrystals," *ACS Sustainable Chem. Eng.*, vol. 6, pp. 7725–7734, 2018, doi: 10.1021/acssuschemeng.8b00600.

[86] H. Du, W. Liu, M. Zhang, C. Si, X. Zhang, and B. Li, "Cellulose nanocrystals and cellulose nanofibrils based hydrogels for biomedical applications," *Carbohydr. Polym.*, vol. 209, pp. 130–144, 2019, doi: 10.1016/J.CARBPOL.2019.01.020.

[87] N. Grishkewich, N. Mohammed, J. Tang, and K. C. Tam, "Recent advances in the application of cellulose nanocrystals," *Curr. Opin. Colloid Interface Sci.*, vol. 29, pp. 32–45, 2017, doi: 10.1016/J.COCIS.2017.01.005.

[88] P. Dhar, U. Bhardwaj, A. Kumar, and V. Katiyar, "Poly (3-hydroxybutyrate)/Cellulose Nanocrystal Films for Food Packaging Applications: Barrier and Migration Studies," *Polymer Engineering & Science,* vol. 55, pp. 2388-2395, 2015, doi: 10.1002/pen.24127.

[89] B. Peng Juntao Tang Pingmei Wang Jianhui Luo Peiwen Xiao Yuanping Lin Kam Chiu Tam, B. Peng, Á. P. Wang Á J Luo Á P Xiao, J. Tang, J. K. Tang Á C Tam, and Y. Lin, "Rheological properties of cellulose nanocrystal-polymeric systems," *Cellulose*, vol. 25, pp. 3229–3240, 2018, doi: 10.1007/s10570-018-1775-6.

[90] D. R. da S. Souza, J. P. de Mesquita, R. M. Lago, L. D. Caminhas, and F. V. Pereira, “Cellulose nanocrystals: A versatile precursor for the preparation of different carbon structures and luminescent carbon dots,” *Ind. Crops Prod.*, vol. 93, pp. 121–128, 2016, doi: 10.1016/J.INDCROP.2016.04.073.

[91] X. Xu, R. Ray, Y. Gu, H. J. Ploehn, L. Gearheart, K. Raker, and W. A. Scrivens, “Electrophoretic Analysis and Purification of Fluorescent Single-Walled Carbon Nanotube Fragments,” *J. AM. CHEM. SOC*, vol. 126, pp. 12736–12737, 2004, doi: 10.1021/ja040082h.

[92] Y.-P. Sun, B. Zhou, Y. Lin, W. Wang, K. A. S. Fernando, P. Pathak, M. J. Meziani, B. A. Harruff, X.Wang, H. Wang, P. G. Luo, H. Yang, M. E. Kose, B. Chen, L. M. Veca, and S. Y. Xie “Quantum-Sized Carbon Dots for Bright and Colorful Photoluminescence,” *J. Am. Chem. Soc.*, vol. 128, pp. 7756–7757, 2006, doi: 10.1021/ja062677d.

[93] Y. Zhuo, H. Miao, D. Zhong, S. Zhu, and X. Yang, “One-step synthesis of high quantum-yield and excitation-independent emission carbon dots for cell imaging,” *Mater. Lett.*, vol. 139, pp. 197–200, 2015, doi: 10.1016/J.MATLET.2014.10.048.

[94] M. Kurian and A. Paul, “Recent trends in the use of green sources for carbon dot synthesis–A short review,” *Carbon Trends*, vol. 3, pp. 100032, 2021, doi: 10.1016/J.CARTRE.2021.100032.

[95] X. W. Tan, A. N. B. Romainor, S. F. Chin, and S. M. Ng, “Carbon dots production via pyrolysis of sago waste as potential probe for metal ions sensing,” *J. Anal. Appl. Pyrolysis*, vol. 105, pp. 157–165, 2014, doi: 10.1016/J.JAAP.2013.11.001.

[96] C. Kang, Y. Huang, H. Yang, X. F. Yan, and Z. P. Chen, “A Review of Carbon Dots Produced from Biomass Wastes,” *Nanomaterials*, vol. 10, pp. 2316, 2020, doi: 10.3390/nano10112316.

[97] A. Sharma and J. Das, “Small molecules derived carbon dots: Synthesis and applications in sensing, catalysis, imaging, and biomedicine,” *J. of Nanobiotechnology*, vol. 17, 2019, doi: 10.1186/s12951-019-0525-8.

[98] H. G. Ye, X. Lu, R. Cheng, J. Guo, H. Li, C. F. Wang, and S. Chen, “Mild bottom-up synthesis of carbon dots with temperature-dependent fluorescence,” *J. Lumin.*, vol. 238, pp. 118311, 2021, doi: 10.1016/J.JLUMIN.2021.118311.

[99] A. Abbas, T. A. Tabish, S. J. Bull, T. Mariana Lim, and A. N. Phan, “High yield synthesis of graphene quantum dots from biomass waste as a highly selective probe for Fe 3+ sensing,” *Sci Rep.*, vol. 10, pp. 21262, 2020, doi: 10.1038/s41598-020-78070-2.

[100] M. Ge, X. Huang, J. Ni, Y. Han, C. Zhang, S. Li, J. Cao, J. Li, Z. Chen, and S. Han,“One-step

synthesis of self-quenching-resistant biomass-based solid-state fluorescent carbon dots with high yield for white lighting emitting diodes," *Dye. Pigment.*, vol. 185, pp. 108953, 2021, doi: 10.1016/J.DYEPIG.2020.108953.

[101] J. Zhou, Z. Sheng, H. Han, M. Zou, and C. Li, "Facile synthesis of fluorescent carbon dots using watermelon peel as a carbon source," *Mater. Lett.*, vol. 66, no. 1, pp. 222–224, 2012, doi: 10.1016/J.MATLET.2011.08.081.

[102] G. Gedda, C. Y. Lee, Y. C. Lin, and H. F. Wu, "Green synthesis of carbon dots from prawn shells for highly selective and sensitive detection of copper ions," *Sensors Actuators B Chem.*, vol. 224, pp. 396–403, 2016, doi: 10.1016/J.SNB.2015.09.065.

[103] C. D. A. D. E. S. Barbosa, ,J. R. Corrêa,G. A. Medeiros,G. Barreto, K. G. Magalhães, A. L. de Oliveira, J. Spencer, M. O. Rodrigues, and B. A. D. Neto, "Carbon Dots (C-dots) from Cow Manure with Impressive Subcellular Selectivity Tuned by Simple Chemical Modification," *Chem. - A Eur. J.*, vol. 21, pp. 5055–5060, 2015, doi: 10.1002/chem.201406330.

[104] A. S. Sharma, J. Xuing, A. Viswadevarayalu, Y. Rong, D. Sabarinathan, S. Ali, A. Akomeah, A.A. Agyekum, H. Li, and Q. Chen, "Facile preparation of fluorescent carbon quantum dots from denatured sour milk and its multifunctional applications in the fluorometric determination of gold ions, in vitro bioimaging and fluorescent polymer film," *J. Photochem. Photobiol. A Chem.*, vol. 401, pp. 112788, 2020, doi: 10.1016/J.JPHOTOCHEM.2020.112788.

[105] X. Hu, Y. Li, Y. Xu, Z. Gan, X. Zou, J. Shi, X. Huang, Z. Li, and Y. Li, "Green one-step synthesis of carbon quantum dots from orange peel for fluorescent detection of Escherichia coli in milk," *Food Chem.*, vol. 339, p. 127775, 2021, doi: 10.1016/J.FOODCHEM.2020.127775.

[106] T. S. and R. S. D., "Green synthesis of highly fluorescent carbon quantum dots from sugarcane bagasse pulp," *Appl. Surf. Sci.*, vol. 390, pp. 435–443, 2016, doi: 10.1016/J.APSUSC.2016.08.106.

[107] C. Cheng, Y. Shi, M. Li, M. Xing, and Q. Wu, "Carbon quantum dots from carbonized walnut shells: Structural evolution, fluorescence characteristics, and intracellular bioimaging," *Mater. Sci. Eng. C*, vol. 79, pp. 473–480, 2017, doi: 10.1016/J.MSEC.2017.05.094.

[108] L. Zhang, Y. Wang, W. Liu, Y. Ni, and Q. Hou, "Corncob residues as carbon quantum dots sources and their application in detection of metal ions," *Ind. Crops Prod.*, vol. 133, pp. 18–25, 2019, doi: 10.1016/J.INDCROP.2019.03.019.

[109] T. Jorn-am, J. Praneerad, R. Attajak, N. Sirisit, J. Manyam, and P. Paoprasert, "Quasi-solid, bio-

renewable supercapacitor with high specific capacitance and energy density based on rice electrolytes and rice straw-derived carbon dots as novel electrolyte additives," *Colloids Surfaces A Physicochem. Eng. Asp.*, vol. 628, pp. 127239, 2021, doi: 10.1016/J.COLSURFA.2021.127239.

[110] M. Yuan, R. Zhong, H. Gao, W. Li, X. Yun, J. Liu, X. Zhao, G. Zhao, and F. Zhan, "One-step, green, and economic synthesis of water-soluble photoluminescent carbon dots by hydrothermal treatment of wheat straw, and their bio-applications in labeling, imaging, and sensing," *Appl. Surf. Sci.*, vol. 355, pp. 1136–1144, 2015, doi: 10.1016/J.APSUSC.2015.07.095.

[111] A. Prasannan and T. Imae, "One-pot synthesis of fluorescent carbon dots from orange waste peels," in *Industrial and Engineering Chemistry Research*, vol. 52, no. 44, pp. 15673–15678, 2013, doi: 10.1021/ie402421s.

[112] M. Lu, Y. Duan, Y. Song, J. Tan, and L. Zhou, "Green preparation of versatile nitrogen-doped carbon quantum dots from watermelon juice for cell imaging, detection of Fe3+ ions and cysteine, and optical thermometry," *J. Mol. Liq.*, vol. 269, pp. 766–774, 2018, doi: 10.1016/J.MOLLIQ.2018.08.101.

[113] H. Qi, M. Teng, M. Liu, S. Liu, J. Li, H. Yu, C. Teng, Z. Huang, H. Li, Q. Shao, A. Umar, T. Ding, Q. Gao, and Z. Guo, "Biomass-derived nitrogen-doped carbon quantum dots: highly selective fluorescent probe for detecting Fe3+ ions and tetracyclines," *J. Colloid Interface Sci.*, vol. 539, pp. 332–341, 2019, doi: 10.1016/J.JCIS.2018.12.047.

[114] A. Boruah, M. Saikia, T. Das, R. L. Goswamee, and B. K. Saikia, "Blue-emitting fluorescent carbon quantum dots from waste biomass sources and their application in fluoride ion detection in water," *J. Photochem. Photobiol. B Biol.*, vol. 209, p. 111940, 2020, doi: 10.1016/J.JPHOTOBIOL.2020.111940.

[115] B. De and N. Karak, "Recent progress in carbon dot–metal based nanohybrids for photochemical and electrochemical applications," *J. Mater. Chem. A.*, vol. 5, no. 5, pp. 1826–1859, 2017, doi: 10.1039/C6TA10220D.

[116] X. Lin, M. Xiong, J. Zhang, C. He, X. Ma, H. Zhang, Y. Kuang, M. Yang, and Q. Huang, "Carbon dots based on natural resources: Synthesis and applications in sensors," *Microchem. J.*, vol. 160, pp. 105604, 2021, doi: 10.1016/J.MICROC.2020.105604.

[117] L. P. Magagula, N. Moloto, S. Gqoba, P. J. Kooyman, T. E. Motaung, and E. C. Linganiso, "Synthesis of fluorescent nitrogen-doped carbon spheres from corncob residue for the detection of Fe (III) in aqueous solutions," *2021 IEEE Sensors*, pp. 1–4, 2021, doi:

10.1109/SENSORS47087.2021.9639764.

[118] C. O. Kappe, “Synthetic Methods Controlled Microwave Heating in Modern Organic Synthesis,” *Angew. Chem. Int. Ed*, vol. 43, pp. 6250–6284, 2004, doi: 10.1002/anie.200400655.

[119] Y. Liu, D. Guo, Y. Gao, B. Tong, Y. Li, and Y. Zhu, “Non-thermal effect of microwave on the chemical structure and luminescence properties of biomass-derived carbon dots via hydrothermal method,” *Appl. Surf. Sci.*, vol. 552, 2021, doi: 10.1016/j.apsusc.2021.149503.

[120] Y.-J. Zhu and F. Chen, “Microwave-Assisted Preparation of Inorganic Nanostructures in Liquid Phase,” *Chem. Rev.*, vol. 114, pp. 6462–6555, 2014, doi: 10.1021/cr400366s.

[121] B. N. Jusuf, N. S. Sambudi, I. Isnaeni, and S. Samsuri, “Microwave-assisted synthesis of carbon dots from eggshell membrane ashes by using sodium hydroxide and their usage for degradation of methylene blue,” *J. Environ. Chem. Eng.*, vol. 6, pp. 7426–7433, 2018, doi: 10.1016/J.JECE.2018.10.032.

[122] W. L. Ang, C. A. L. Mee, N. S. Sambudi, A. W. Mohammad, C. P. Leo, E. Mahmoudi, M. Ba-Abbad, and A. Benamor, “Microwave-assisted conversion of palm kernel shell biomass waste to photoluminescent carbon dots,” *Sci. Rep.*, vol. 10, 2020, doi: 10.1038/s41598-020-78322-1.

[123] K. Raji, V. Ramanan, and P. Ramamurthy, “Facile and green synthesis of highly fluorescent nitrogen-doped carbon dots from jackfruit seeds and its applications towards the fluorimetric detection of Au3+ ions in aqueous medium and in: In vitro multicolor cell imaging,” *New J. Chem.*, vol. 43, pp. 11710–11719, 2019, doi: 10.1039/c9nj02590a.

[124] Y. Y. Yao, G. Gedda, W. M. Girma, C. L. Yen, Y. C. Ling, and J. Y. Chang, “Magnetofluorescent Carbon Dots Derived from Crab Shell for Targeted Dual-Modality Bioimaging and Drug Delivery,” *ACS Appl. Mater. Interfaces*, vol. 9, pp. 13887–13899, 2017, doi: 10.1021/acsami.7b01599.

[125] V. Gnaneswar Gude, P. Patil, E. Martinez-Guerra, S. Deng, and N. Nirmalakhandan, “Microwave energy potential for biodiesel production,” *Sustain Chem Process.*, vol. 1, 2013, doi: 10.1186/2043-7129-1-5 2013.

[126] J. Zhang and S. H. Yu, “Carbon dots: large-scale synthesis, sensing and bioimaging,” *Mater. Today*, vol. 19, no. 7, pp. 382–393, 2016, doi: 10.1016/J.MATTOD.2015.11.008.

[127] W. Meng, X. Bai, B. Wang, Z. Liu, S. Lu, and B. Yang, “Biomass-Derived Carbon Dots and Their Applications,” *ENERGY & ENVIRONMENTAL MATER*, vol. 2, pp. 172-192, 2019, doi: 10.1002/eem2.12038.

[128] L. Liang, A. Veksha, M. Z. Bin Mohamed Amrad, S. A. Snyder, and G. Lisak, "Upcycling of exhausted reverse osmosis membranes into value-added pyrolysis products and carbon dots," *J. Hazard. Mater.*, vol. 419, pp. 126472, 2021, doi: 10.1016/J.JHAZMAT.2021.126472.

[129] Q. Ye, F. Yan, Y. Luo, Y. Wang, X. Zhou, and L. Chen, "Formation of N, S-codoped fluorescent carbon dots from biomass and their application for the selective detection of mercury and iron ion," *Spectrochim. Acta Part A Mol. Biomol. Spectrosc.*, vol. 173, pp. 854–862, 2017, doi: 10.1016/J.SAA.2016.10.039.

[130] B. N. Jusuf, N. S. Sambudi, I. Isnaeni, and S. Samsuri, "Microwave-assisted synthesis of carbon dots from eggshell membrane ashes by using sodium hydroxide and their usage for degradation of methylene blue," *J. Environ. Chem. Eng.*, vol. 6, no. 6, pp. 7426–7433, 2018, doi: 10.1016/j.jece.2018.10.032.

[131] J. Li, L. Zhang, P. Li, Y. Zhang, and C. Dong, "One step hydrothermal synthesis of carbon nanodots to realize the fluorescence detection of picric acid in real samples," *Sensors Actuators B Chem.*, vol. 258, pp. 580–588, 2018, doi: 10.1016/J.SNB.2017.11.096.

[132] P. Das, S. Ganguly, P. P. Maity, H. K. Srivastava, M. Bose, S. Dhara, S. Bandyopadhyay, A. K. Das, S. Banerjee, and N. C. Das, "Converting waste Allium sativum peel to nitrogen and sulphur co-doped photoluminescence carbon dots for solar conversion, cell labeling, and photobleaching diligences: A path from discarded waste to value-added products," *J. Photochem. Photobiol. B Biol.*, vol. 197, p. 111545, 2019, doi: 10.1016/J.JPHOTOBIOL.2019.111545.

[133] A. Abbas, T. A. Tabish, S. J. Bull, T. M. Lim, and A. N. Phan, "High yield synthesis of graphene quantum dots from biomass waste as a highly selective probe for Fe3+ sensing," *Sci. Rep.*, vol. 10, 2020, doi: 10.1038/s41598-020-78070-2.

[134] R. Liu, J. Zhanga, M. Gaoa, Z. Lia, J. Chena, D. Wub, and P. Liu, "A facile microwave-hydrothermal approach towards highly photoluminescent carbon dots from goose feathers †," *RSC Adv.*, vol. 5, pp. 4428-4433, 2015, doi: 10.1039/c4ra12077a.

[135] R. Atchudan, T. N. Jebakumar Immanuel Edison, M. Shanmugam, S. Perumal, T. Somanathan, and Y. R. Lee, "Sustainable synthesis of carbon quantum dots from banana peel waste using hydrothermal process for in vivo bioimaging," *Phys. E Low-dimensional Syst. Nanostructures*, vol. 126, p. 114417, 2021, doi: 10.1016/J.PHYSE.2020.114417.

[136] H. Liu, J. Ding, K. Zhang, and L. Ding, "Construction of biomass carbon dots based fluorescence sensors and their applications in chemical and biological analysis," *TrAC Trends Anal. Chem.*,

vol. 118, pp. 315–337, 2019, doi: 10.1016/J.TRAC.2019.05.051.

[137] S. Zhao, X. Song, X. Chai, P. Zhao, H. He, and Z. Liu, "Green production of fluorescent carbon quantum dots based on pine wood and its application in the detection of Fe3+," *J. Clean. Prod.*, vol. 263, pp. 121561, 2020, doi: 10.1016/j.jclepro.2020.121561.

[138] X. Wen, L. Shi, G. Wen, Y. Li, C. Dong, J. Yang, and S. Shuang, "Green and facile synthesis of nitrogen-doped carbon nanodots for multicolor cellular imaging and Co2+ sensing in living cells," *Sensors Actuators B Chem.*, vol. 235, pp. 179–187, Nov. 2016, doi: 10.1016/J.SNB.2016.05.066.

[139] S. Godavarthi, K.M. Kumar, E.V. Vélez, A.Hernandez-Eligio, M.Mahendhir, N.Hernandez-Como, M.Aleman, and L. M. Gomez, "Nitrogen doped carbon dots derived from Sargassum fluitans as fluorophore for DNA detection," *J. Photochem. Photobiol. B Biol.*, vol. 172, pp. 36–41, 2017, doi: 10.1016/J.JPHOTOBIOL.2017.05.014.

[140] R. Atchudan, T. N. J. I. Edison, S. Perumal, N. Muthuchamy, and Y. R. Lee, "Hydrophilic nitrogen-doped carbon dots from biowaste using dwarf banana peel for environmental and biological applications," *Fuel*, vol. 275, pp. 117821, 2020, doi: 10.1016/J.FUEL.2020.117821.

[141] Y. Liu, C. Zhu, Y. Gao, L. Yang, J. Xu, X. Zhang, C. Lu, Y. Wang, and Y. Zhu, "Biomass-derived nitrogen self-doped carbon dots via a simple one-pot method: Physicochemical, structural, and luminescence properties," *Appl. Surf. Sci.*, vol. 510, pp. 145437, 2020, doi: 10.1016/j.apsusc.2020.145437.

[142] Z. Li, Q. Wang, Z. Zhou, S. Zhao, S. Zhong, L. Xu, Y. Gao, and X. Cui, "Green synthesis of carbon quantum dots from corn stalk shell by hydrothermal approach in near-critical water and applications in detecting and bioimaging," *Microchem. J.*, vol. 166, p. 106250, 2021, doi: 10.1016/J.MICROC.2021.106250.

[143] A. Cayuela, M. L. Soriano, C. Carrillo-Carrió, and M. Valcá, "Semiconductor and carbon-based fluorescent nanodots: the need for consistency," *Chem. Commun*, vol. 52, p. 1311, 2016, doi: 10.1039/c5cc07754k.

[144] S. Li, L. Li, H. Tu, H. Zhang, D. S.Silvester, C. E.Banks, G. Zou, H. Hou, and X. Ji, "The development of carbon dots: From the perspective of materials chemistry," *Mater. Today*, vol. 51, pp. 188–207, 2021, doi: 10.1016/J.MATTOD.2021.07.028.

[145] F. Yan, Y. Jiang, & X. Sun, Z. Bai, Y. Zhang, and X. Zhou, "Surface modification and chemical functionalization of carbon dots: a review," *Microchim Acta.*, vol. 185, pp. 424, 2018, doi: 10.1007/s00604-018-2953-9.

[146] A. M. Craciun, A. Diac, M. Focsan, C. Socacib, K. Magyari, D. Maniua, I. Mihalache, L. M. Veca, S. Astilean, and A. Terec, "Surface passivation of carbon nanoparticles with p-phenylenediamine towards photoluminescent carbon dots," *RSC Adv.*, vol. 6, pp. 56944-56951, 2016, doi: 10.1039/c6ra10127e.

[147] Y. Newman Monday, J. Abdullah, N. A. Yusof, S. A. Rashid, and R. H. Shueb, "Facile Hydrothermal and Solvothermal Synthesis and Characterization of Nitrogen-Doped Carbon Dots from Palm Kernel Shell Precursor," *Appl. Sci.*, vol. 11, pp. 1630, doi: 10.3390/app11041630.

[148] Y. Chen, Y. Wu, B. Weng, B. Wang, and C. Li, "Facile synthesis of nitrogen and sulfur co-doped carbon dots and application for Fe(III) ions detection and cell imaging," *Sensors Actuators B Chem.*, vol. 223, pp. 689–696, 2016, doi: 10.1016/J.SNB.2015.09.081.

[149] G. Dong, K. Lang, H. Ouyang, W. Zhang, L. Bai, S. Chen, Z. Zhang, Y. Gao, Z. Mua, and X. Zhao, "Facile synthesis of N, P-doped carbon dots from maize starch via a solvothermal approach for the highly sensitive detection of Fe 3+ †," *RSC Adv.*, vol. 10, pp. 33483-33489, 2020, doi: 10.1039/d0ra06209j.

[150] H. Qi, M. Teng, M. Liu, S. Liu, J. Li, H. Yu, C. Teng, Z. Huang, H. Liu, Q. Shao, A. Umar, T. Ding, Q. Gaog, and Z. Guo, "Biomass-derived nitrogen-doped carbon quantum dots: highly selective fluorescent probe for detecting Fe3+ ions and tetracyclines," *J. Colloid Interface Sci.*, vol. 539, pp. 332–341, 2019, doi: 10.1016/J.JCIS.2018.12.047.

[151] D. Wang, L. Wang, X. Dong, Z. Shi, and J. Jin, "Chemically tailoring graphene oxides into fluorescent nanosheets for Fe3+ ion detection," *Carbon N. Y.*, vol. 50, no. 6, pp. 2147–2154, 2012, doi: 10.1016/J.CARBON.2012.01.021.

[152] L. Zhao, Y. Wang, X. Zhao, Y. Deng, and Y. Xia, "Facile Synthesis of Nitrogen-Doped Carbon Quantum Dots with Chitosan for Fluorescent Detection of Fe 3+," *Polymers.*, vol. 11, pp. 1731, 2019, doi: 10.3390/polym11111731.

[153] G. Yang, X. Wan, Y. Su, X. Zeng, and J. Tang, "Acidophilic S-doped carbon quantum dots derived from cellulose fibers and their fluorescence sensing performance for metal ions in an extremely strong acid environment," *J. Mater. Chem. A*, vol. 4, no. 33, pp. 12841–12849, 2016, doi: 10.1039/C6TA05943K.

[154] L. Wang, W.Lia, B. Wu, Z. Li, S. Wang, Y. Liu, D. Pan, and M. Wu, "Facile synthesis of fluorescent graphene quantum dots from coffee grounds for bioimaging and sensing," *Chem. Eng. J.*, vol. 300, pp. 75–82, 2016, doi: 10.1016/J.CEJ.2016.04.123.

[155] S. Z. Naji and C. T. Tye, “A review of the synthesis of activated carbon for biodiesel production: Precursor, preparation, and modification,” *Energy Convers. Manag. X*, vol. 13, pp. 100152,+ 2022, doi: 10.1016/J.ECMX.2021.100152.

[156] M. A. Yahya, Z. Al-Qodah, and C. W. Z. Ngah, “Agricultural bio-waste materials as potential sustainable precursors used for activated carbon production: A review,” *Renew. Sustain. Energy Rev.*, vol. 46, pp. 218–235, 2015, doi: 10.1016/J.RSER.2015.02.051.

[157] D. Duan *et al.*, “Activated carbon from lignocellulosic biomass as catalyst: A review of the applications in fast pyrolysis process,” *J. Anal. Appl. Pyrolysis*, vol. 158, pp. 105246, 2021, doi: 10.1016/J.JAAP.2021.105246.

[158] Y. Zhang, H. Lei, Z. Yang, K. Qian, and E. Villota, “Renewable High-Purity Mono-Phenol Production from Catalytic Microwave-Induced Pyrolysis of Cellulose over Biomass-Derived Activated Carbon Catalyst,” *ACS Sustainable Chem. Eng.*, vol. 6, pp. 5349–5357, 2018, doi: 10.1021/acssuschemeng.8b00129.

[159] Z. Heidarinejad, M. H. Dehghani, M. Heidari, · Gholamali Javedan, I. Ali, and M. Sillanpää, “Methods for preparation and activation of activated carbon: a review,” *Environ. Chem. Lett.*, vol. 18, pp. 393–415, 2020, doi: 10.1007/s10311-019-00955-0.

[160] P. González-García, “Activated carbon from lignocellulosics precursors: A review of the synthesis methods, characterization techniques and applications,” *Renew. Sustain. Energy Rev.*, vol. 82, pp. 1393–1414, 2018, doi: 10.1016/J.RSER.2017.04.117.

[161] X. L. Duan, C. G. Yuan, T. T. Jing, and X. D. Yuan, “Removal of elemental mercury using large surface area micro-porous corn cob activated carbon by zinc chloride activation,” *Fuel*, vol. 239, pp. 830–840, 2019, doi: 10.1016/J.FUEL.2018.11.017.

[162] E. Köseoğlu and C. Akmil-Başar, “Preparation, structural evaluation and adsorptive properties of activated carbon from agricultural waste biomass,” *Adv. Powder Technol.*, vol. 26, pp. 811–818, 2015, doi: 10.1016/J.APT.2015.02.006.

[163] W. Ao, J. Fu, X. Mao, Q. Kang, C. Ran, Y. Liu, H. Zhang, Z. Gao, J. Li, G. Liu, and J. Dai, “Microwave assisted preparation of activated carbon from biomass: A review,” *Renew. Sustain. Energy Rev.*, vol. 92, pp. 958–979, 2018, doi: 10.1016/J.RSER.2018.04.051.

[164] A. Borhan, S. Yusup, J. W. Lim, and P. L. Show, “Characterization and Modelling Studies of Activated Carbon Produced from Rubber-Seed Shell Using KOH for CO 2 Adsorption,” *Processes*, vol. 7, pp. 855, 2019, doi: 10.3390/pr7110855.

[165] J. Sreńscek-Nazzal, W. Kamińska, B. Michalkiewicz, and Z. C. Koren, "Production, characterization and methane storage potential of KOH-activated carbon from sugarcane molasses," *Ind. Crops Prod.*, vol. 47, pp. 153–159, 2013, doi: 10.1016/J.INDCROP.2013.03.004.

[166] J. Bedia, M. Peñas-Garzón, A. Gómez-Avilés, J. J. Rodriguez, and C. Belver, "A Review on the Synthesis and Characterization of Biomass-Derived Carbons for Adsorption of Emerging Contaminants from Water," *C*, vol. 4, pp. 63, 2018, doi: 10.3390/c4040063.

[167] E. Redondo, J. Carretero-González, E. Goikolea, J. Ségalini, and R. Mysyk, "Effect of pore texture on performance of activated carbon supercapacitor electrodes derived from olive pits," *Electrochim. Acta*, vol. 160, pp. 178–184, 2015, doi: 10.1016/j.electacta.2015.02.006.

[168] S. Mopoung, P. Moonsri, W. Palas, and S. Khumpai, "Characterization and Properties of Activated Carbon Prepared from Tamarind Seeds by KOH Activation for Fe(III) Adsorption from Aqueous Solution," *Sci. World J.*, vol. 2015, pp. 1–9, 2015, doi: 10.1155/2015/415961.

[169] V. K. Singh and E. Anil Kumar, "Measurement and analysis of adsorption isotherms of CO2 on activated carbon," *Appl. Therm. Eng.*, vol. 97, pp. 77–86, 2016, doi: 10.1016/j.applthermaleng.2015.10.052.

[170] Z. Zhang, W. Zhang, X. Chen, Q. Xia, and Z. Li, "Adsorption of CO_2 on Zeolite 13X and Activated Carbon with Higher Surface Area," *Sep. Sci. Technol.*, vol. 45, no. 5, pp. 710–719, 2010, doi: 10.1080/01496390903571192.

[171] H. Nazemi, A. Joseph, J. Park, and A. Emadi, "Advanced Micro-and Nano-Gas Sensor Technology: A Review," *Sensors*, vol. 19, pp. 1285, 2019, doi: 10.3390/s19061285.

[172] K. Zhou, W. Ma, Z. Zeng, X. Ma, X. Xu, Y. Guo, H. Li, and L. Li, "Experimental and DFT study on the adsorption of VOCs on activated carbon/metal oxides composites," *Chem. Eng. J.*, vol. 372, pp. 1122–1133, Sep. 2019, doi: 10.1016/j.cej.2019.04.218.

[173] W. Zheng, J. Hu, S. Rappeport, Z. Zheng, Z. Wang, Z. Han, J. Langer, and J. Economy, "Activated carbon fiber composites for gas phase ammonia adsorption," *Microporous Mesoporous Mater.*, vol. 234, pp. 146–154, 2016, doi: 10.1016/J.MICROMESO.2016.07.011.

[174] N. A. Travlou, C. Ushay, M. Seredych, E. Rodríguez-Castello, and T. J. Bandosz, "Nitrogen-Doped Activated Carbon-Based Ammonia Sensors: Effect of Specific Surface Functional Groups on Carbon Electronic Properties," *ACS Sensors.*, vol. 1, pp. 591–599, 2016, doi: 10.1021/acssensors.6b00093.

[175] D. W. Kim, S. Ha, Y. Ko, J. H. Wee, H. J. Kim, S. Y. Jeong, T. Tojo, C. M Yang, Y. A. Kim,

"Rapid, repetitive and selective NO2 gas sensor based on boron-doped activated carbon fibers," *Appl. Surf. Sci.*, vol. 531, pp. 147395, 2020, doi: 10.1016/J.APSUSC.2020.147395.

Chapter 3: Synthesis and Characterization of cellulose nanocrystals (CNCs)

3.1 Introduction

The increasing environmental crisis caused by non-renewable/non-biodegradable material has motivated the efforts towards the development of new types of green bio-based and degradable materials from natural sources for a variety of applications while minimizing the creation of waste [1]. In this context, the use of agricultural waste as feedstock for the production of value-added materials for sustainable economies has been the object of intensive academic and industrial research [2]. The reuse of these agricultural waste residues results in the reduction of accumulated waste in the environment and in the preparation of novel, low-cost, high-performance materials from renewable and sustainable waste [3]. The utilization of crop residues could result in an additional source of revenue for farmers and contribute to the agro-industry diversification by offering a market for agro-waste that is not centred on food products [1].

Corn is one of the most popular crops in the world, cultivated by the ancient people, hence becoming a culture of extreme economic importance due to its multi-purpose uses for humans and animals [4]. In South Africa, corn is the staple food item with approximately 8 million tons produced yearly, occupying approximately 3.1 million hectares (ha) of land [5]. Corn is comprised of the stalk, leaf, cob, grains, and husk. The corn grains, which is the edible part of the plant is 20% of the plant's mass and the remaining parts are regarded as agricultural waste [6].The corncob (CC) is the central part of the ear of maize in which the grains are stuck, it constitutes 20–30% of the corn crop [7, 8]. So far, CC has been widely used to produce animal bedding, animal feed and industrial products such as xylose, xylo-oligomers, xylitol, and furfural [9]. However, a large amount of corncob still ends up in landfills or burnt directly to recover heat after the grains are harvested, causing air pollution. This is due to the lack of adequate technology and little knowledge about possible value addition on such agricultural wastes, therefore, methods for transforming CC into valuable products are worthy of concern [5].

The use of CC as a source of cellulose nanocrystals (CNCs) provide a natural resource that is renewable and low cost when compared to the main biomass sources of CNCs such as trees and

cotton [10]. CNCs are highly crystalline, needle-like particles with length in the range of 100.0 - 500.0 nm and a diameter between 5–30 nm, that can be inexhaustibly obtained from a variety of highly available and renewable cellulose-rich sources [11]. CNCs have drawn a great deal of attention for applications in the manufacturing of biocomposite packaging materials, biomedical sector, and the energy to the electronics sectors [12]. This is due to their high aspect ratio, high crystallinity, low density, nanoscale dimension and unique morphology [12].

The main process for the isolation of CNCs is based on acid hydrolysis, wherein the amorphous regions of cellulose are degraded to release crystalline cellulose, with higher resistance to acid attack [13]. Sulfuric acid is the most commonly used acid for hydrolysis, because it has been proven effective in the elimination of amorphous components and result in stable CNCs suspensions [14]. The creation of stable suspensions by sulfuric acid has been attributed to a small number of sulfate ester groups introduced to the surface of the CNCs during hydrolysis [14]. Although this method is simple to operate, some disadvantages also need to be noted such as several pre-treatment steps for untreated raw materials [15]. Recently, a one-step method termed 'Nitro-oxidation" have been used to extract cellulose from untreated biomass materials [16]

It is well known that the morphology and chemical properties of CNCs depend on the source and the extraction process. This study explored the extraction of CNCs from corncob using two different methods (i.e., sulfuric acid hydrolysis, and nitro-oxidation). The properties of the obtained CNCs were comparatively investigated. The raw corncob, chemically purified cellulose and the CNCs were characterized for surface morphology using SEM and TEM, the surface functional groups were determined by FTIR, crystallinity analysis using XRD and thermal properties using TGA.

3.2 Materials and methods

3.2.1 Materials

Corncob was obtained from a local pet store (Johannesburg, South Africa). The other reagents: potassium hydroxide (KOH), sodium chlorite ($NaClO_2$), acetic acid, sulphuric acid (H_2SO_4, 98 %), microcrystalline cellulose, nitric acid (55 %), sodium nitrite (≥ 97 wt%), and cellulose membrane (D9402) were all obtained from Sigma Aldrich, South Africa, and they were used without any further modification.

3.2.2 Sample preparation

3.2.2.1 Pre-treatment

Initially the raw corncob (CC) was washed with distilled water to remove any impurities. It was then dried at 100 °C for 6 h before grinding into a fine powder using a blender. The isolation of the cellulose was done according to previously documented methods (Johar *et al.,* [17]) but with some minor modifications. Briefly, the powdered sample was then treated with potassium hydroxide aqueous solution of 7% (w/v) for 4 hours at 80 °C under mechanical stirring and then washed several times with distilled water until a neutral pH (6-7) was maintained, and finally dried at 100 °C for 6 hours in an oven (this sample was the labelled ACC). After this treatment, the sample was subjected to bleaching with aqueous chlorite (1.7 wt, % $NaClO_2$ in distilled water), the bleaching process was completed by adding a buffer solution of acetic acid until a pH value of 4 was maintained. The bleaching treatment was performed at 80 °C for 4 hours, followed by washing repeatedly with distilled water until a neutral pH was reached and the sample was left to dry at 100 °C for 6 hours.

3.2.2.2 Extraction of cellulose nanocrystals using acid hydrolysis

The pre-treated CC was used to prepare CNCs by acid hydrolysis as described in literature (Johar *et al.,* [17]) with slight modifications. The bleached CC (BCC) was hydrolysed with 50 wt% of H_2SO_4 with a 1:10 g/mL ratio of BCC to the dilute acid at 45 °C for 30 min under constant stirring. This reaction was then quenched by addition of 10-fold cold deionized water to the reaction mixture, followed by centrifugation at 10000 rpm for 15 min three times to remove the acidic solution. The supernatant was discarded, and the precipitate re-dispersed in deionized water and dialyzed against deionized water until a neutral pH was maintained. The suspension was then sonicated in an ice bath sonicator for 1 h to homogenize the generated cellulose nanocrystals. The generated nanocrystals were further centrifuged at 6, 000 rpm for 30 min. This sample was labelled CC-CNCs and stored in the refrigerator at for further analysis.

For comparison, CNCs from the commercial microcrystalline cellulose (MCC) were prepared. Briefly, MCC was dispersed in 50 wt% of H_2SO_4 with a 1:10 g/mL ratio of MCC to the dilute acid at 45 °C for 30 min under constant stirring. The washing, neutralization, and storage steps were done following the same procedure used for the CNCs obtained from the corncob.

3.2.2.3 Preparation of CNCs using Nitro-oxidation

Nitro-oxidised cellulose nanocrystals (NOCNCs) were extracted from raw CC powder without any chemical pre-treatment as described in literature by Sharma *et al*., [18]. Typically, 5 g of powdered corncob was nitro-oxidised using 70 mL (22.2 mmol) of nitric acid which was placed in a three-neck round bottom flask. When the samples were completely soaked in the acid 9.80 g (28 mmol) of sodium nitrite was added to the reaction mixture under continuous stirring, upon the addition of sodium nitrite, red fumes were formed inside the flask. To prevent the red fumes from escaping, the round flask mouths were covered with stoppers and the flask was maintained at 50°C for 12 h. The reaction was then quenched by the addition 0f 10-fold cold distilled water, after equilibration, an upper layer containing unreacted reagents was observed. Distilled water was added to the CNCs, where the solution was stirred, settled, and decanted. This step was then repeated 3 times until the CNCs were suspended in water. The suspension was then diluted with distilled water and centrifuged at 10 000 rpm for 15 min, and the supernatant was removed. This step was repeated 3 times until the pH reached above 2.5. The suspension was then dialyzed and equilibrated for 6–7 days until the conductivity of water reached below 5 µS. To improve the dispersion of the CNCs, the suspension was then treated with 4% sodium bicarbonate with a 1:10 g/v until a pH value of 7.5 was reached. Figure 3.1 below illustrate the step-by-step synthesis procedure of the CNCs from corncob.

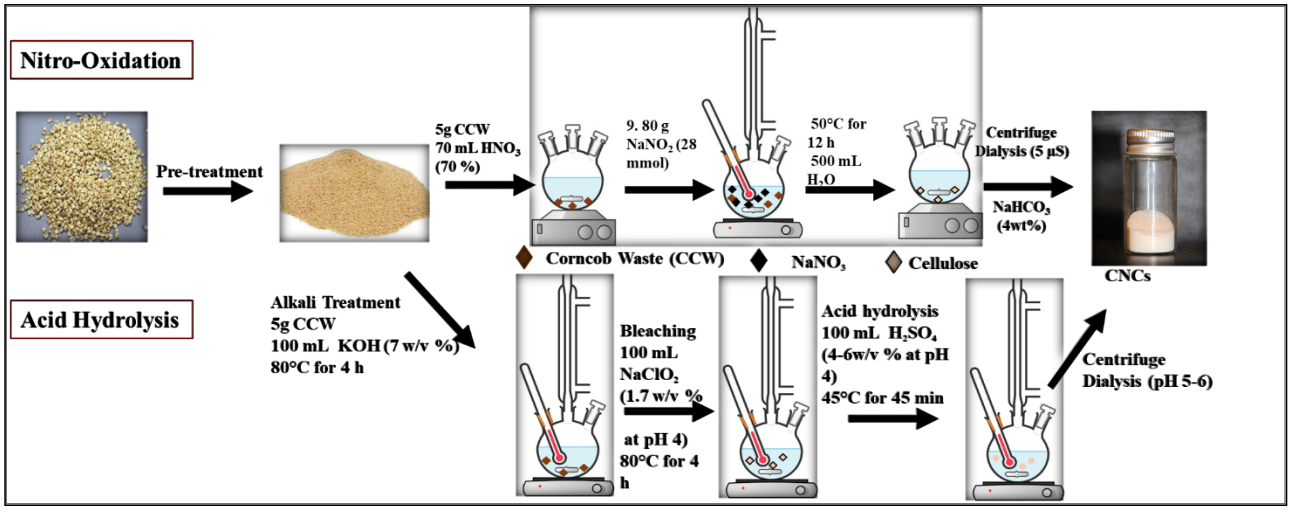

Figure 3.1: Graphical illustration of the synthesis of NOCNCs and CC-CNCs from corncob.

3.3 Characterization techniques

The structural properties of CC-CNCs, MCC-CNCs, and NOCNCs (including their morphology, crystallographic nature, and size) were determined using the listed techniques.

3.3.1 X-ray powder diffraction (XRD)

The PXRD technique was used to identify and determine the crystalline phase of the synthesized materials based on their diffraction patterns. A Bruker D2 phaser equipped with Cu-Kα radiation (λ = 1.5405 Å)), at an operating voltage of 30 kV and current of 10 mA was used. Small amounts of samples were grinded into fine powders and packed into a PXRD zero-background sample holder, the measurements were collected at 2θ = 10-90 °. The crystallinity index was calculated using equation 1 as shown below [17].

$$CrI\ (\%) = \frac{I_{002} - I_{am}}{I_{002}} \times 100 \qquad eqn\ (1)$$

Where, I_{002} denotes the maximum intensity of the 002-lattice diffraction peak at the 2θ value around 22°, while I_{am} is the minimum intensity scattered by the amorphous part of the sample at 2θ value around 16°.

3.3.2 Scanning electron microscopy (SEM)

SEM was used to determine the surface morphology of the CC, A-CC, B-CC, and NOCNCs using the Tescan Vega SEM. For measurements, the powdered samples were placed onto the carbon tape which was mounted on a SEM stub. The stub was coated with carbon, gold, and palladium before analysis.

3.3.3 Transmission electron microscopy (TEM)

Morphological properties and particle sizes of the CC-CNCs and MCC-CNCs were determined using FEI G^2 TECNAI Spirit T12. The samples were dispersed in ethanol and then placed on a copper grid coated with a carbon film. The samples were dried before carrying out TEM analysis at an accelerating voltage of 120 kV.

3.3.4 Fourier transform infrared spectroscopy (FTIR)

FTIR spectroscopy was used to determine structural changes on the samples as a result of chemical modification by the detection of functional groups. The changes in functional groups of the materials; CC, A-CC, B-CC, CC-CNCs, MCC-CNCs, and NOCNCs were analysed using the Brucker TENSOR 27

FTIR. The FTIR spectra of the samples were recorded in the transmittance mode in the range of 4000 cm^{-1} to 800 cm^{-1}.

3.3.5 Thermogravimetric analysis (TGA)

TGA was used to study the thermal stability of CC, A-CC, B-CC, CC-CNCs, MCC-CNCs, and NOCNCs using the TA Q50 instrument. Approximately 10.0 mg of the solid samples was weighed and heated from 35-900 °C at the rate of 20 °C/min in air/ Nitrogen purged at a flow rate of 20 mL/min. Both the derivative thermal gravimetric (DTG) and weight loss (TG) were obtained and analysed.

3.4 Results and discussion

3.4.1 Fourier transform infrared (FTIR) spectroscopy analysis

The functional groups that are present on the surface of the CC before and after chemical treatment, and the obtained CNCs (CC-CNCs, MCC-CNCs, and NOCNCs) were determined using FTIR as shown in figure 3.2. (a) The broad peak observed around 3046-3675 cm^{-1} present in all spectra is a representative of the O-H stretch of hydrogen bonds, while at 2805-2990 cm^{-1} is attributed to the C-H stretching vibrations [19]. The peak around 1642 cm^{-1} is assigned to O-H bending, caused by the hydrophilic nature of cellulose [20]. The peak at 1721 cm^{-1} in untreated CC is due to the acetyl and ester groups of residual hemicelluloses, this peak is absent in the chemically treated samples and the CNCs, due to the dissolution of the hemicellulose component present in the corncob [21]. The strong peaks around 1030 cm^{-1} are attributed to the skeletal vibration of the C-O-C in the pyranose skeletal ring, while the small peaks at 894 cm^{-1} and 1161 cm^{-1} are attributed to the C1 group frequency of the β-glycosidic linkages between sugar units and the CO antisymmetric bridge [22]. The bands between 1320 and 1460 cm^{-1} are attributed to the CH_2 inter-twinned in cellulosic material [23]. The disappearance of the 1240-1511 cm^{-1} peaks present on the corncob after chemical treatment results from the removal of non-cellulosic material [24]. These results depicted that the cellulose molecular structure remains unaffected following chemical treatment of CC and MCC.

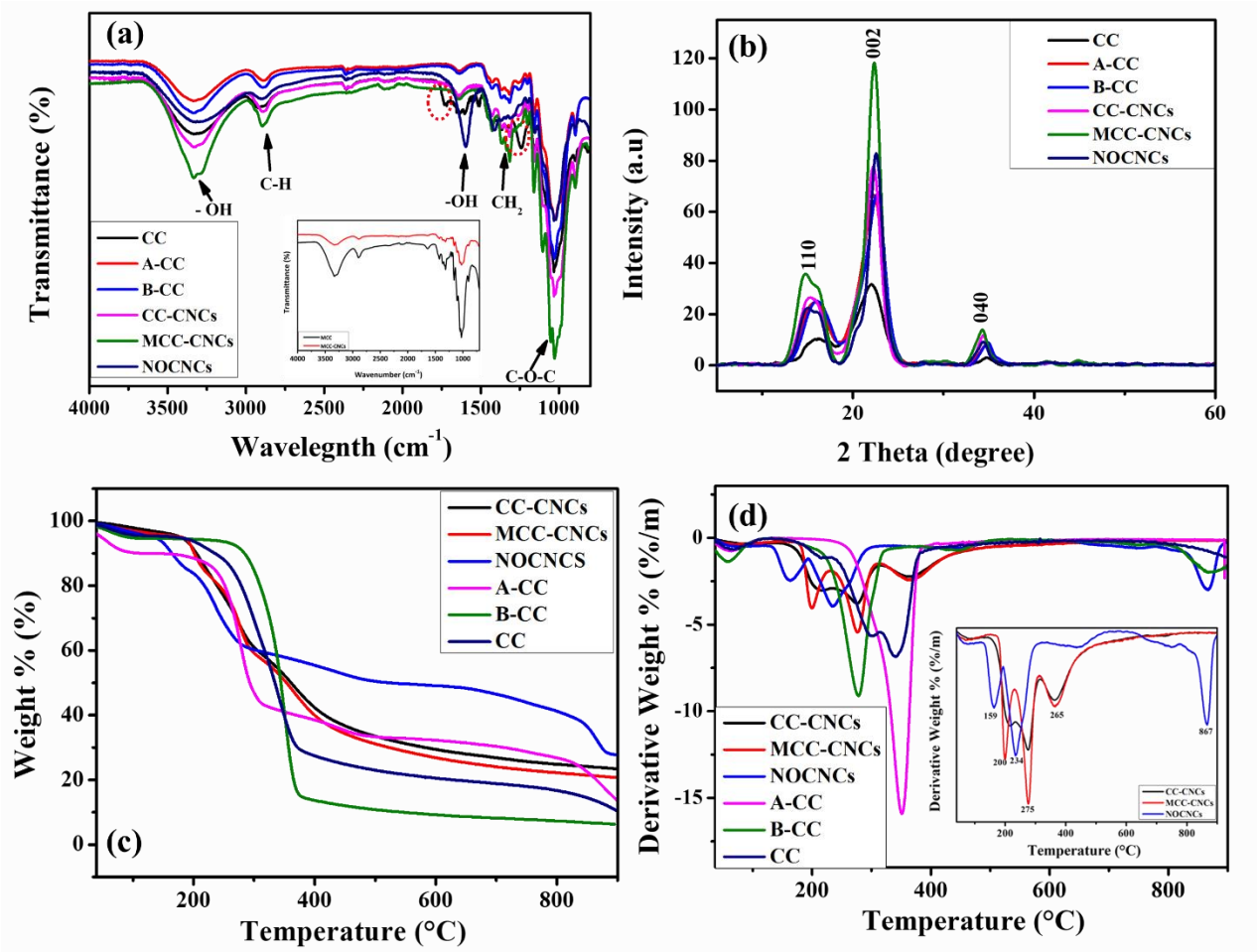

Figure curves 3.2: (a) FTIR spectra and (b) XRD patterns of CC, A-CC, B-CC, CC-CNCs, MCC-CNCs, and NOCNCs. (c) TGA and (d) DTG of CC, A-CC, B-CC, CC-CNCs, MCC-CNCs, and NOCNCs. The inset in figure 3.2 (b and d) shows the FTIR of MCC and MCC-CNCs and the DTG of the extracted cellulose nanocrystals.

3.4.2 X-ray diffraction (XRD) analysis

The XRD patterns of CC, A-CC, B-CC, and the CNCs are represented in figure 3.2 (b) above. The crystallinity index (CrI) of various CNCs was determined and denotes the ratio of the crystalline constituents to the amorphous regions of a material, it also provides information about the thermal and mechanical properties of CNCs [23]. It is apparent from Figure 3.2 (b) that all samples are comprised of three characteristic peaks at around 16°, 22°, and 34°, corresponding to the (101), (002), and (040) crystallographic planes respectively, which are characteristics peaks of cellulose I [15]. The presences of these peaks confirmed that the crystalline structure of cellulose I remain intact after chemical treatment and CNCs extraction using acid hydrolysis and nitro-oxidation. Similar patterns were observed when CNCs were extracted by chemical treatment from biomass waste such as rice husk [17], sugarcane

bagasse [23], pineapple leaf fibres [25], and even from maize stalk pith [26]. The crystallinity indexes of the CNCs (CrI%) were calculated using the XRD patterns, an increase of crystallinity index was observed from the untreated corncob waste to the cellulose nanocrystals. The crystallinity of NOCNCs (74.37 %), MCC-CNCs (70.24 %), and CC-CNCs (69.12 %) showing a slight difference, which may attribute to the fact that both acid hydrolysis and nitro-oxidation treatment can result in the removal of amorphous regions and the formation of higher crystallinity CNCs. However, the crystallinity of the raw corncob increased from CC (52.01 %), ACC (59.28%), to B-CC (62.22 %) which is due to the removal of non- cellulosic materials. The XRD of the residue obtained after alkali treatment when preparing CC-CNCs demonstrates that there are additional peaks which may be due to the presence of KOH (shown in the supplementary information figure S3.1).

3.4.3 Thermogravimetric analysis (TGA)

In order to study the thermal stability and degradation properties of the untreated corncob, treated corncob, and the CNCs, TGA analysis was carried out. Figure 3.2 (c and d) shows the TGA and corresponding derivative curves for the analysed samples. As can be seen from Figure 3.2 (c and d), all samples exhibited weight loss in the region of 35–100 °C of about 10 %, corresponding to the evaporation of the absorbed moisture molecules on the surface of the samples [26]. .All samples showed a large mass loss at 200–360 °C, mainly attributing to the decomposition of cellulose itself [23]. All the decompositions at the temperature range of 360–500 °C, are attributed to the breaking of glycosidic bonds, degradation of carbon-containing skeleton with production of low molecular weight compounds and formation of charred residue [15]. The thermal degradation of acid hydrolysed CNCs proceeded at lower temperatures than the B-CC and has an additional peak. This behaviour was expected given that the introduction of sulfate groups diminishes the thermal stability in the CNCs, because of the dehydration reaction of cellulose [7]. The residue left after complete degradation of the samples were observed to be about 10.99%, 11.85%, 6.06%, 20.40% ,23.36% and 28.05% for the CC, A-CC, B-CC, MCC-CNCs, CC-CNCs, and NOCNCs respectively. The higher residual amounts recorded for the sulphuric acid treated CNCs is attributed to sulfonated crystals, which are thermally more stable than the desulfonated crystals and have a very slow degradation rate which contributes to incomplete thermal degradation [28]. There are three major decomposition stages from the CNCs, the derivative of the NOCNCs show four distinct major peaks. The peak at 159 °C corresponds to anhydroglucoronic units. Another peak adjacent to the anhydroglucoronic unit at 234 °C, resembling noncrystalline cellulose with a small residual peak of crystalline cellulose at around 400 °C. The results obtained here are in

agreement with the results obtained in a previous study where nitro-oxidation was used to extract cellulose [18]. The peak at 867 °C is due to the decomposition of sodium nitrite [29].

3.4.4 Morphological image analysis by SEM and TEM

Morphological properties were investigated by SEM and TEM analysis. The photographs and SEM images of CC, A-CC, and B-CC are shown in figure 3.3 (a -f). In the untreated CC the cellulose fibers are bonded by hemicellulose and lignin which result in a brown colour, but after chemical treatments (alkali and bleaching) the obtained products colour changes to yellowish and a white respectively (figure. 3.3 d-f). The colour change confirms the removal of non-cellulosic components and is a significant sign for morphological change in their structures. During alkali treatment, hemicellulose is solubilized and washed out, resulting in a colour change with cellulose and lignin residue. This step may also result in the breakdown of some alkali-labile bonds such as ether and ester linkages resulting in openings in the fiber matrix leading to easy penetration of bleaching agents during the subsequent bleaching treatment [30]. During the bleaching process, the presence of acidified $NaClO_2$ solution leads to the oxidization of lignin, resulting in the formation of new functional groups such as carbonyl, carboxylic, and hydroxyl while whitening the pulp as shown in figure 3.3 (f) [31]. Throughout the treatments, the cellulose became highly purified and crystalline since after the bleaching process, the cellulose become separated fibers that are not intact on the corncob, which confirmed the removal of hemicellulose, lignin, and other extracts. The SEM images (figure 3.3 (a-c)) show the morphology of the CC at the different treatment stages. It is evident from figure 3.3 (a) that the CC displays a framework with unique integrated porous structures and thin layers stacked together. While the A-CC and B-CC exhibited a fiber-like, and spherical structures with decreasing diameters after the bleaching. On the other hand, the MCC exhibited irregular, flat, and porous rood like aggregates (shown if figure S3.2).

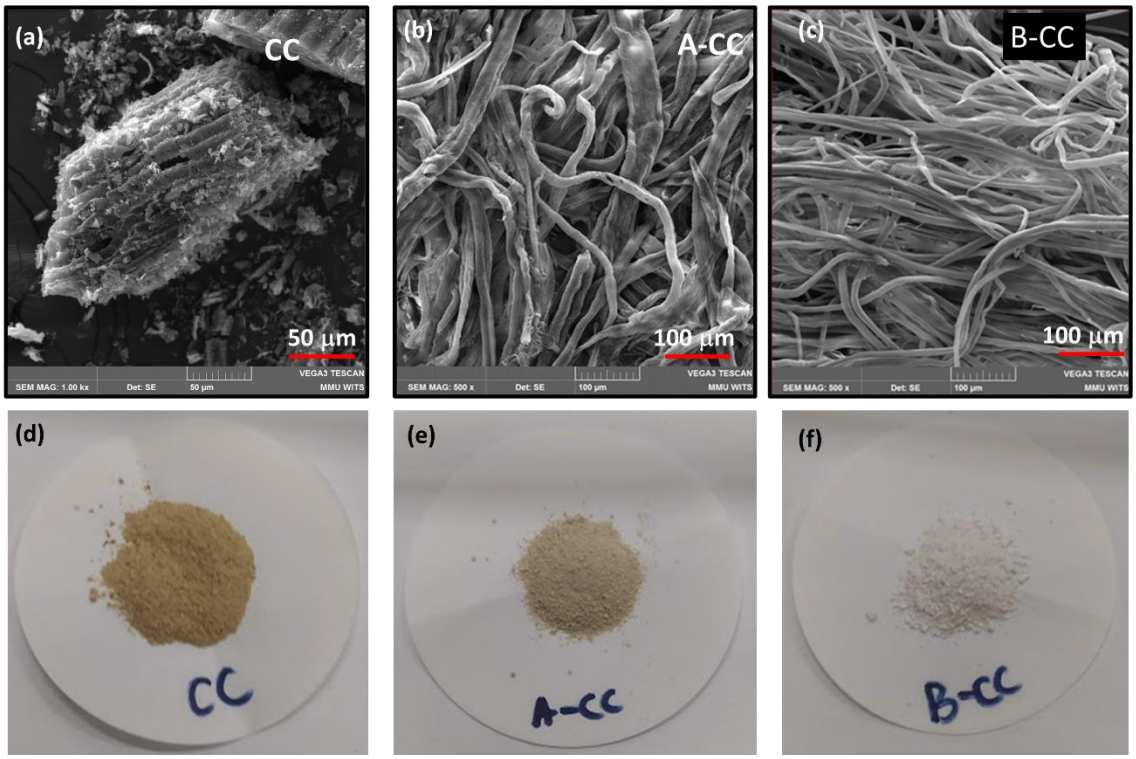

Figure 3.3: (a) SEM images of the CC, A-CC, and B-CC. (b) Photographs of the CC, A-CC, and B-CC.

The prepared cellulose fibers are consisted of both amorphous and crystalline regions. During the acid hydrolysis of B-CC and M-CC, as well as nitro-oxidation of the CC the amorphous regions are destructed and removed by breaking the β-1,4-glucopyranose linkage in cellulose structure [31]. Therefore, the micro-sized fibers are separated into nanosized crystals as shown in figure 3.4 (a-c). According to figure 3.4 (a and b), the CC-CNCs and MCC-CNCs have rod like structure with an interconnected web-like distribution so that each fiber total length is covered by other fibers. As a result, it was difficult to calculate the average size distribution. While the NOCNCs (figure 3.4 c) consisted of both rod like morphology and a sheet like structure. The photographs demonstrated in figure 3.4 (d-f) show the different colours suggesting different properties and morphology.

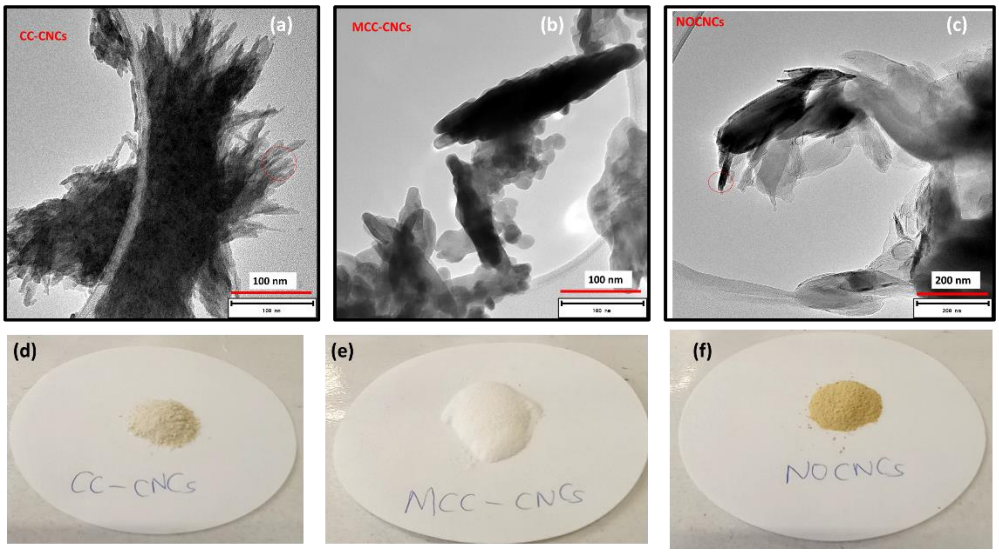

Figure 3.4: (a) TEM images of the CC-CNCs, MCC-CNCs, and NOCNCs. (b) Photographs of the CC-CNCs, MCC-CNCs, and NOCNCs.

3.5 Conclusion

The increasing environmental awareness currently has pushed researchers towards the usage of agricultural waste to prepare large quantities of economic, renewable, and environmentally friendly resources such cellulose. There are several crucial steps to prepare CNCs, including grinding of raw materials, removal of non-cellulosic components such as lignin and hemicellulose, and the extraction of CNCs by chemical treatment. The different conditions used at the different extraction stages affect the crystallinity, surface functionalization, and thermal stability of the final product. In this study, two methods were utilized to prepare CNCs from corncob, these were then compared to CNCs extracted from commercial microcrystalline cellulose. The crystallinity of the NOCNCs was obtained to be 74.37 %, which was significantly higher than that of MCC-CNCs (70.24 %), and CC-CNCs (69.12 %). TEM analysis confirmed that the CNCs have different morphologies. The FT-IR confirmed the presence of -OH, C-H, Skeletal vibration of the C-O-C in pyranose skeletal ring, and β-glycosidic linkages. The results obtained herein suggest that CC, which is regarded as waste, can be effectively utilized for several other purposes since they possess the advantages of being sustainable and biodegradable.

3.6 References

[1] R. M. dos Santos, W. P. Flauzino Neto, H. A. Silvério, D. F. Martins, N. O. Dantas, and D. Pasquini, "Cellulose nanocrystals from pineapple leaf, a new approach for the reuse of this agro-waste," *Ind. Crops Prod.*, vol. 50, pp. 707–714, 2013, doi: 10.1016/J.INDCROP.2013.08.049.

[2] M. A. Henrique, H. A. Silvério, W. P. Flauzino Neto, and D. Pasquini, "Valorization of an agro-industrial waste, mango seed, by the extraction and characterization of its cellulose nanocrystals," *J. Environ. Manage.*, vol. 121, pp. 202–209, 2013, doi: 10.1016/J.JENVMAN.2013.02.054.

[3] S. Thambiraj and D. Ravi Shankaran, "Preparation and physicochemical characterization of cellulose nanocrystals from industrial waste cotton," *Appl. Surf. Sci.*, vol. 412, pp. 405–416, 2017, doi: 10.1016/J.APSUSC.2017.03.272.

[4] R. H. Longaresi, A. J. de Menezes, M. A. Pereira-da-Silva, D. Baron, and S. L. Mathias, "The maize stem as a potential source of cellulose nanocrystal: Cellulose characterization from its phenological growth stage dependence," *Ind. Crops Prod.*, vol. 133, pp. 232–240, 2019, doi: 10.1016/J.INDCROP.2019.02.046.

[5] A. Mtibe, L. Z. Linganiso, A. P. Mathew, K. Oksman, M. J. John, and R. D. Anandjiwala, "A comparative study on properties of micro and nanopapers produced from cellulose and cellulose nanofibres," *Carbohydr. Polym.*, vol. 118, pp. 1–8, 2015, doi: 10.1016/J.CARBPOL.2014.10.007.

[6] M. Smyth, A. García, C. Rader, E. J. Foster, and J. Bras, "Extraction and process analysis of high aspect ratio cellulose nanocrystals from corn (Zea mays) agricultural residue," *Ind. Crops Prod.*, vol. 108, pp. 257–266, 2017, doi: 10.1016/J.INDCROP.2017.06.006.

[7] H. A. Silvério, W. P. Flauzino Neto, N. O. Dantas, and D. Pasquini, "Extraction and characterization of cellulose nanocrystals from corncob for application as reinforcing agent in nanocomposites," *Ind. Crops Prod.*, vol. 44, pp. 427–436, 2013, doi: 10.1016/J.INDCROP.2012.10.014.

[8] C. Liu, B. Li, H. Du, D. Lv, Y. Zhang, G. Yu, X. Mu, and H. Peng, "Properties of nanocellulose isolated from corncob residue using sulfuric acid, formic acid, oxidative and mechanical methods," *Carbohydr. Polym.*, vol. 151, pp. 716–724, 2016, doi: 10.1016/j.carbpol.2016.06.025.

[9] W. Liu, R. Wu, B. Wang, Y. Hu, Q. Hou, P. Zhang, and R. Wu, "Comparative study on different pretreatment on enzymatic hydrolysis of corncob residues," *Bioresour. Technol.*, vol. 295, pp. 122244, 2020, doi: 10.1016/J.BIORTECH.2019.122244.

[10] Z. Wang, Z. J. Yao, J. Zhou, and Y. Zhang, “Reuse of waste cotton cloth for the extraction of cellulose nanocrystals,” *Carbohydr. Polym.*, vol. 157, pp. 945–952, 2017, doi: 10.1016/J.CARBPOL.2016.10.044.

[11] A. Y. Melikoğlu, S. E. Bilek, and S. Cesur, “Optimum alkaline treatment parameters for the extraction of cellulose and production of cellulose nanocrystals from apple pomace,” *Carbohydr. Polym.*, vol. 215, pp. 330–337, 2019, doi: 10.1016/J.CARBPOL.2019.03.103.

[12] H. Du, W. Liu, M. Zhang, C. Si, X. Zhang, and B. Li, “Cellulose nanocrystals and cellulose nanofibrils based hydrogels for biomedical applications,” *Carbohydr. Polym.*, vol. 209, pp. 130–144, 2019, doi: 10.1016/J.CARBPOL.2019.01.020.

[13] F. Luzi et al., “Valorization and extraction of cellulose nanocrystals from North African grass: Ampelodesmos mauritanicus (Diss),” *Carbohydr. Polym.*, vol. 209, pp. 328–337, 2019, doi: 10.1016/J.CARBPOL.2019.01.048.

[14] Kusmono, R. F. Listyanda, M. W. Wildan, and M. N. Ilman, “Preparation and characterization of cellulose nanocrystal extracted from ramie fibers by sulfuric acid hydrolysis,” *Heliyon*, vol. 6, pp. e05486, 2020, doi: 10.1016/J.HELIYON.2020.E05486.

[15] H. Zhang et al., “Extraction and comparison of cellulose nanocrystals from lemon (Citrus limon) seeds using sulfuric acid hydrolysis and oxidation methods,” *Carbohydr. Polym.*, vol. 238, pp. 116180, 2020, doi: 10.1016/J.CARBPOL.2020.116180.

[16] P. R. Sharma Aurnov Chattopadhyay Chengbo Zhan Sunil K Sharma Lihong Geng Benjamin S Hsiao, “Lead removal from water using carboxycellulose nanofibers prepared by nitro-oxidation method,” doi: 10.1007/s10570-018-1659-9.

[17] N. Johar, I. Ahmad, and A. Dufresne, “Extraction, preparation and characterization of cellulose fibres and nanocrystals from rice husk,” *Ind. Crops Prod.*, vol. 37, no. 1, pp. 93–99, 2012, doi: 10.1016/j.indcrop.2011.12.016.

[18] P. R. Sharma, R. Joshi, S. K. Sharma, and B. S. Hsiao, “A Simple Approach to Prepare Carboxycellulose Nanofibers from Untreated Biomass*,” Biomacromolecules*, vol. 18, pp. 2333–2342, 2017, doi: 10.1021/acs.biomac.7b00544.

[19] J. Xu, E. F. Krietemeyer, V. M. Boddu, S. X. Liu, and W. C. Liu, “Production and characterization of cellulose nanofibril (CNF) from agricultural waste corn stover,” *Carbohydr. Polym.*, vol. 192, pp. 202–207, 2018, doi: 10.1016/J.CARBPOL.2018.03.017.

[20] E. Galiwango, N. S. Abdel Rahman, A. H. Al-Marzouqi, M. M. Abu-Omar, and A. A. Khaleel, "Isolation and characterization of cellulose and α-cellulose from date palm biomass waste," *Heliyon*, vol. 5, pp. e02937, 2019, doi: 10.1016/J.HELIYON.2019.E02937.

[21] B. M. Cherian, L. A. Pothan, T. Nguyen-Chung, G. Mennig, M. Kottaisamy, and S. Thomas, "A Novel Method for the Synthesis of Cellulose Nanofibril Whiskers from Banana Fibers and Characterization," *J. Agric. Food Chem.*, vol. 56, pp. 5617–5627, 2008, doi: 10.1021/jf8003674.

[22] A. M. Das, M. P. Hazarika, M. Goswami, A. Yadav, and P. Khound, "Extraction of cellulose from agricultural waste using Montmorillonite K-10/LiOH and its conversion to renewable energy: Biofuel by using Myrothecium gramineum," *Carbohydr. Polym.*, vol. 141, pp. 20–27, 2016, doi: 10.1016/j.carbpol.2015.12.070.

[23] S. K. Evans, O. N. Wesley, O. Nathan, and M. J. Moloto, "Chemically purified cellulose and its nanocrystals from sugarcane baggase: isolation and characterization," *Heliyon*, vol. 5, pp. e02635, 2019, doi: 10.1016/J.HELIYON.2019.E02635.

[24] P. Kampeerapappun, "Extraction and Characterization of Cellulose Nanocrystals Produced by Acid Hydrolysis from Corn Husk," *J. Met. Mater. Miner.*, vol. 25, pp. 19–26, 2015, doi: 10.14456/jmmm.2015.3.

[25] L. Ravindran, M. S. Sreekala, and S. Thomas, "Novel processing parameters for the extraction of cellulose nanofibres (CNF) from environmentally benign pineapple leaf fibres (PALF): Structure-property relationships," *Int. J. Biol. Macromol.*, vol. 131, pp. 858–870, 2019, doi: 10.1016/J.IJBIOMAC.2019.03.134.

[26] H. Gu, X. Gao, H. Zhang, K. Chen, and L. Peng, "Fabrication and characterization of cellulose nanoparticles from maize stalk pith via ultrasonic-mediated cationic etherification*," Ultrason. Sonochem.*, vol. 66, pp. 104932, 2020, doi: 10.1016/J.ULTSONCH.2019.104932.

[27] M. S. Sreekala, and S. Thomas, "Novel processing parameters for the extraction of cellulose nanofibres (CNF) from environmentally benign pineapple leaf fibres (PALF): Structure-property relationships," *Int. J. Biol. Macromol.*, vol. 131, pp. 858–870, 2019, doi: 10.1016/J.IJBIOMAC.2019.03.134.

[28] C. Verma, M. Chhajed, P. Gupta, S. Roy, and P. K. Maji, "Isolation of cellulose nanocrystals from different waste bio-mass collating their liquid crystal ordering with morphological exploration," *Int. J. Biol. Macromol.*, vol. 175, pp. 242–253, 2021, doi: 10.1016/J.IJBIOMAC.2021.02.038.

[29] Q. Guo and T. Wang, “Study on preparation and thermal properties of sodium nitrate/silica composite as shape-stabilized phase change material,” *Thermochim. Acta.*, vol. 613, pp. 66–70, 2015, doi: 10.1016/J.TCA.2015.05.023.

[30] G. Akhlamadi, E. K. Goharshadi, and S. V. Saghir, “Extraction of cellulose nanocrystals and fabrication of high alumina refractory bricks using pencil chips as a waste biomass source,” *Ceram. Int.*, vol. 47, no. 19, pp. 27042–27049, 2021, doi: 10.1016/J.CERAMINT.2021.06.117.

[31] M. A. Mohamed, W. N. W. Salleh, J. Jaafar, S. E. A. M. Asri, and A. F. Ismail, “Physicochemical properties of ‘green’ nanocrystalline cellulose isolated from recycled newspaper,” 2015, doi: 10.1039/c4ra17020b.

CHAPTER 4: PREPARATION OF ACTIVATED CARBON FROM CORNCOB WASTE BIOMASS

4.1 Introduction

The increasing consumption of fossil fuels and intensification of environmental problems has led to the development of efficient, clean and sustainable new materials [1]. As a result, there has been an increase in the production of green and renewable materials from sources such as lignocellulosic materials due to their abundance and availability [2]. In recent years, there has been a growing research interest in the use of agricultural waste materials from the agro-industrial sector for the production of sustainable and green carbon materials such as activated carbon (AC). AC is a carbonaceous material that is predominantly amorphous in nature and has high porous structure with a high surface area and mechanical strength which depends largely on the precursor material and activation process [3].

Most of the commercially available AC is produced from fossil fuel-based precursors such as petroleum and coal, and some high-value agroforestry materials such as bamboo, wood, and coconut. These precursors are expensive and environmentally unfriendly hence the increasing focus on agricultural waste which is cheaper, readily available, renewable, structurally porous, and environmentally friendly [4, 5]. The amount of agricultural waste being generated annually across the globe has intensified due to increase in food demand as a result of population growth [6]. In recent years the use of different agricultural waste biomass, such as pomegranate peel waste [7], rice husk [8], spent coffee grounds [9], sugarcane bagasse waste [10], peanut shells [11], and many more as precursor materials to prepare porous carbons at a low cost.

At present, two methods have been utilized to prepare activated carbonaceous materials, namely, chemical and physical activation methods [2]. Physical activation involves the pyrolysis of precursors at high temperatures (500–1100 °C) followed by activation in the presence of oxidizers such as steam or carbon dioxide. During chemical activation, the raw materials are impregnated with a chemical activating agent and then pyrolyzed at temperatures between 400–900 °C [12]. Chemical activation has been reported to be more advantageous over physical activation due to low energy requirements, higher yields, larger surface areas, low activation time, development of porous structures, and it is considered to be economical and

environmentally friendly since the chemical reagents can be recovered and reused [13]. The most commonly used chemical activating reagents are KOH, $ZnCl_2$, H_3PO_4, K_2CO_3, and NaOH [14]. Different activation reagents, raw materials, ratio between the chemical agent and precursor mass, and pyrolysis temperature result in activated carbon with different properties, table 4.1 is a summary of surface area values (m^2/g) from different biomass waste precursors used for the preparation of AC.

AC is usually rich in heteroatoms such as oxygen, sulphur, hydrogen, nitrogen, halogen and other elements, in the forms of functional groups or atoms which are bonded chemically to the AC structure [15]. This makes it versatile for numerous applications in different fields such as pharmaceuticals, food processing, vacuum manufacturing, wastewater management, and air pollution [4]. Although the use of corncob to produce activated carbon has been reported in literature, the use of K_2CO_3 as an activating agent has yet to be explored. In this work, activated carbon was prepared from corncob waste as a precursor using K_2CO_3 as a chemical activating agent. The effects of the impregnation ratios of the chemical of activating reagent and precursor were investigated.

Table 4.1. Comparison of surface areas of activated carbon prepared from lignocellulosic waste.

Source	**Preparation method and conditions**	**BET surface area (m^2/g)**	**Reference**
Corncob	Pyrolysis, 800 °C for 2 h, K_2CO_3	1508.53	This work
Tomato waste	Pyrolysis, 600 °C for 1 h, $ZnCl_2$	1093	[16]
Orange peel	Pyrolysis, 950 °C for 1 h, K_2CO_3	1352	[2]
Peanut shell	Pyrolysis, 750 °C for 2h, KOH	1523	[17]
Grape bagasse	Pyrolysis, 500 °C for 1h, H_3PO_4	1455	[18]
Coconut shells	Microwave, 1000 °C for 2 h, CO_2	2000	[19]

4.2 Materials and methods

4.2.1 Materials

Corncob was obtained from a local pet store (Johannesburg, South Africa). The other reagents: potassium carbonate (K_2CO_3) and hydrochloric acid (HCl) were all obtained from Sigma Aldrich, South Africa and used without any further purification. Distilled water was used to prepare aqueous solutions.

4.2.2 Preparation and characterization of activated carbon

Initially, the raw corncob (CC) was washed with distilled water to remove any impurities. It was then dried at 100 °C for 6 h before grinding into a fine powder using a home blender. The obtained CC powder was directly mixed with a chemical activator i.e., solid potassium carbonate at the fixed weight ratios from CC /K_2CO_3 = 1:0 to 1:3. The mixtures were placed on a quartz boat inside a tubular furnace that was heated at 800 °C (heating rate: 10 °C/min) under N_2 atmosphere for 2 h. The furnace was then allowed to cool to room temperature and the resulting samples were washed several times with 1M HCl and distilled water. Finally, the samples were dried in an oven at 100 °C for 12 h. Figure 4.1 demonstrates graphical illustration of the AC synthesis. The activated porous carbons synthesized were labelled as ACC 1:0, ACC 1:1, ACC 1:2, and ACC 1:3 where ACC refers to activated corncob and 1:x is the ratio of CC/K_2CO_3.

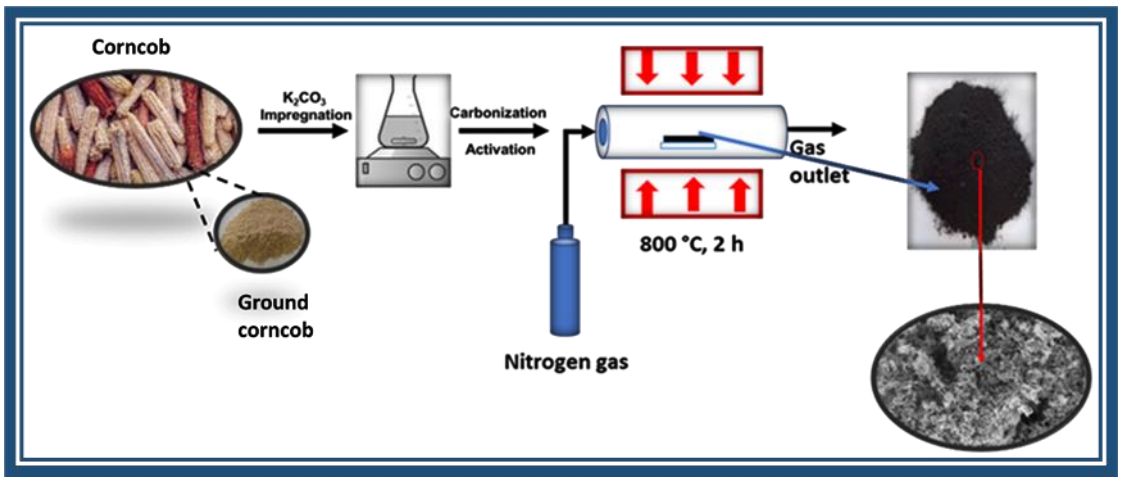

Figure 4. 1: Graphical illustration of activated carbon synthesis

4.3 Characterization

X-ray diffraction (XRD) (Bruker D2 Phaser) with a monochromatic Cu Kα radiation (λ = 0.15405 nm) generated at 30 kV and 10 mA was used to explore the crystalline structure of the activated carbons. A measurement of specific surface areas of the activated carbons and composites was determined using N_2 adsorption (at 77 K), using a surface and porosity analyser (A Micromeritics Tristar 3000). The morphology of the activated carbon and elemental composition were studied by Scanning Electron Microscopy (SEM) with Energy Dispersive X-Ray Analysis (EDX) using a ZEISS Gemini SEM 560 instrument with sub 1 kV. The thermal stability of the materials was monitored using a Perkin Elmer 6000 thermogravimetric analyser (TGA).

4.4 Results and discussion

4.4.1 X-ray diffraction

The X-ray diffraction profile of the raw CC and activated carbon materials (ACC 1:0, ACC 1:1, ACC 1:2, ACC 1:3) are shown in figure 4.2 a. The raw CC comprised of three characteristic peaks at 2θ = 16°, 22°, and 34°, corresponding to the (101), (002), and (040) crystallographic planes [20]. The 101 and 040 peaks disappear when the raw materials are activated with K_2CO_3 and carbonized at all the different ratios. This indicates that the CC was fully carbonized and formed a new carbon structure. All the activated carbon materials had low intensity and broad diffraction peaks at 2θ = 23.8 and 42.5°, representing the (002) and (100) planes of graphite, respectively [21]. The result suggests that the carbon structures have a low graphitization degree and a turbostratic structure of disordered carbon was formed [22]. Similar XRD peaks were reported when Xie et al., prepared AC from CC using KOH as an activating agent at 800°C for 2 h with heating rate of 8 °C/min [23]. The carbonization of the raw material without any chemical activating agent produced AC with similar crystallographic properties to the ACs produced in the presence of K_2CO_3. Kennedy et al., reported that the small peak at 2θ = 42.5° indicates that the formation of pores is due to the decomposition of carbon along the direction of the graphic structures [24].

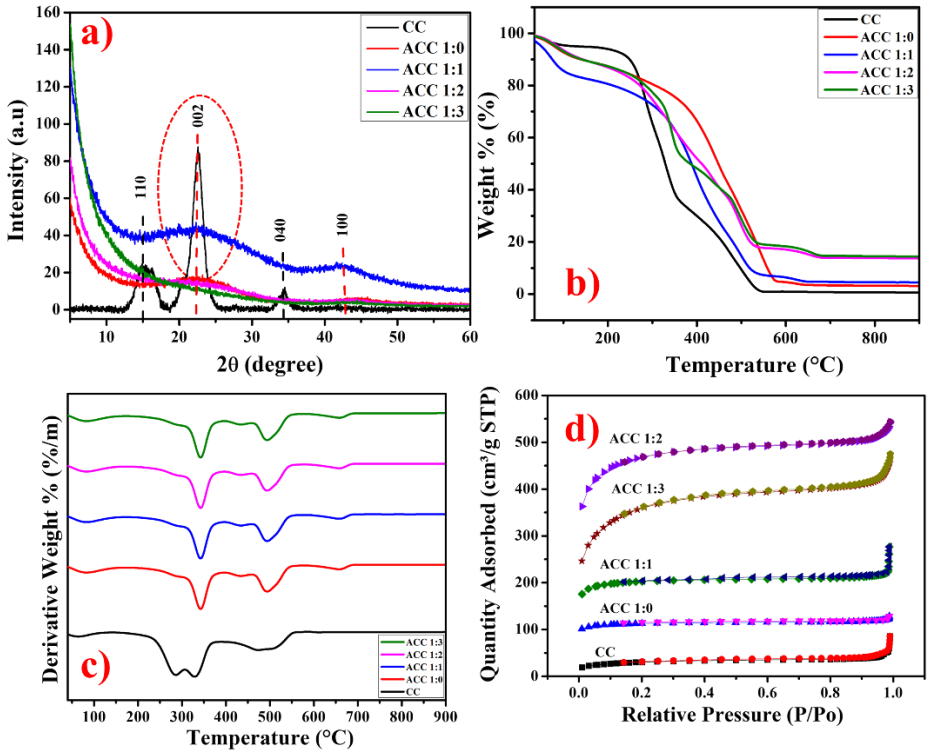

Figure 4.2: (a) XRD patterns, (b) TGA, (c) differential thermal analysis (DTG) and N_2 adsorption–desorption isotherms for corncob and activated carbons prepared using different impregnation ratios.

4.4.2 Thermal stability

The thermal stability of the prepared materials was conducted using the thermogravimetric characterization method. Figure 4.2 (b and c) present the TGA and DTG of the five samples. The thermograms provided in figure 4.2 (c) indicate that all the ACC's samples have similar degradation patterns with five decomposition regions. The weight loss in the first region of all samples at a temperature around 100 ℃ is attributed to the elimination of adsorbed moisture. The decomposition in the second region around 300 ℃ correspond to the loss of hemicellulose, the third decomposition stage of is between 300–450 ℃ and ascribed to the complete decomposition of the samples [25]. In the last region (450–900 ℃), the rate was very slow and almost a constant weight was maintained in all the samples due to other graphitic materials. On the other hand, corncob consist of three decomposition stages, the first stage at the temperature range of 40–135 ℃ is attributed to the elimination of adsorbed moisture. The second decomposition stage at 200 ℃ - 400 ℃ correspond to the loss of hemicelluloses and cellulose [26]. The third stage, is the carbonization of corncob to form solid residue such as chars and organic

residue, which suggests that the minimum temperature required for the carbonization of the corncob is 450 °C [27].The remnant ash content left after the process was 0.22 %, 3.44 %, 4.94%, 13.30%, and 14.84% for the CC, ACC 1:0, ACC 1:1, ACC 1:2, and ACC 1:3 respectively.

4.4.3 Nitrogen adsorption-desorption

The N_2 adsorption-desorption isotherms of activated carbons prepared at different impregnation ratios and the raw CC are shown in figure 4.2 c. The shape of N_2 adsorption–desorption isotherms are different for the different impregnation ratios, these isotherms belong to different types (isotherms II and IV) of IUPAC classification [28]. A type II isotherm indicates an indefinite multi-layer formation after completion of the monolayer and is found in adsorbents with a wide distribution of pore sizes and type IV isotherms indicate a significantly developed meso-structure due to the occurrence of the widening of the existing microspores [29]. The formation of porous structures using K_2CO_3 involves the reduction of K_2CO_3 to form K, K_2O, CO and CO_2 under inert conditions. The potassium compound formed during the activation step diffuses into the internal structure of char matrix [30], widens the existing pores and creates new porosities, consistent with the following reactions [31].

$$K_2CO_3 + 2C \rightarrow 3CO + 2K \qquad \text{eq (1)}$$

$$K_2CO_3 \rightarrow K_2 + CO_2 \qquad \text{eq (2)}$$

$$K_2O + 2C \rightarrow CO + 2K \qquad \text{eq (3)}$$

At relatively low pressures (<0.15 P/P_0), the adsorbed N_2 volume increased steeply, indicating an increase in the number of mesoporous and macro-pores [32]. It is noted that the hysteresis loop evidently increased at about $P/P_0 > 0.9$, which means that the materials consist of macro-pores. For all impregnation ratios a plateau is not apparently reached rather adsorption occurs over the entire pressure interval indicating the presence of a wide range of pore diameters. The specific surface areas (S_{BET}) (shown in table 4.1) are 101.49, 357.57, 642.93, 1508.53, and 1183.46 m^2/g for samples CC, ACC 1:0, ACC 1:1, ACC 1:2, and ACC 1:3 respectively. This demonstrates that the presence of an activating enhances the specific surface area. The surface area increased with increasing impregnation ratios, and maximum surface area and pore volume were obtained at an

impregnation ratio of 1:2 (ACC: K_2CO_3). The decrease in the volume of adsorbed N_2 at the 1:3 impregnation ratio was attributed to a reduction in the materials' porosities at higher pressures due to collapsing pores [12]. The obtained surface areas are comparable to previous studies as shown in table 4.1.

Table 4.2: Textural characteristics of corncob -derived activated carbons using different impregnation ratios.

	BET surface area (m^2/g)	**Pore volume (cm^3/g)**	**Pore size (nm)**
CC	101.49	0.12	3.93
ACC 1:0	357.57	0.19	2.17
ACC 1:1	642.93	0.43	2.5
ACC 1:2	1508.53	0.81	2.17
ACC 1:3	1183.46	0.72	2.41

4.4.4 Scanning electron microscopy

The morphology and chemical composition of all materials was characterized using SEM-EDX analysis. The scanning electron micrographs are shown in figure 4.3. The figures indicate that the ACC obtained in this study consist of irregular and heterogeneous surface morphologies, with well-developed pores of various sizes and shapes that tend to change with different impregnation ratios. Important differences between the surface of the raw CC and the activated carbons were observed, the raw corncob consisted smooth surface with minor pores, while a gradual improvement on the porosity was observed with increase in the impregnation ratios. The image of the sample carbonized at the impregnation ratio of 1:0 demonstrates porous but less regular surface morphology (figure 4.3 b), whereas remarkably regular surface morphologies are observed for the other samples carbonized at the impregnation ratios of 1:1 to 1:2 (figure 4.3 c-e). ACC 1:3 demonstrated a spongy like morphology confirming the collapse of the pore structure.

The observation clearly confirmed that K_2CO_3 activation of corncob results in the formation of porous structures.

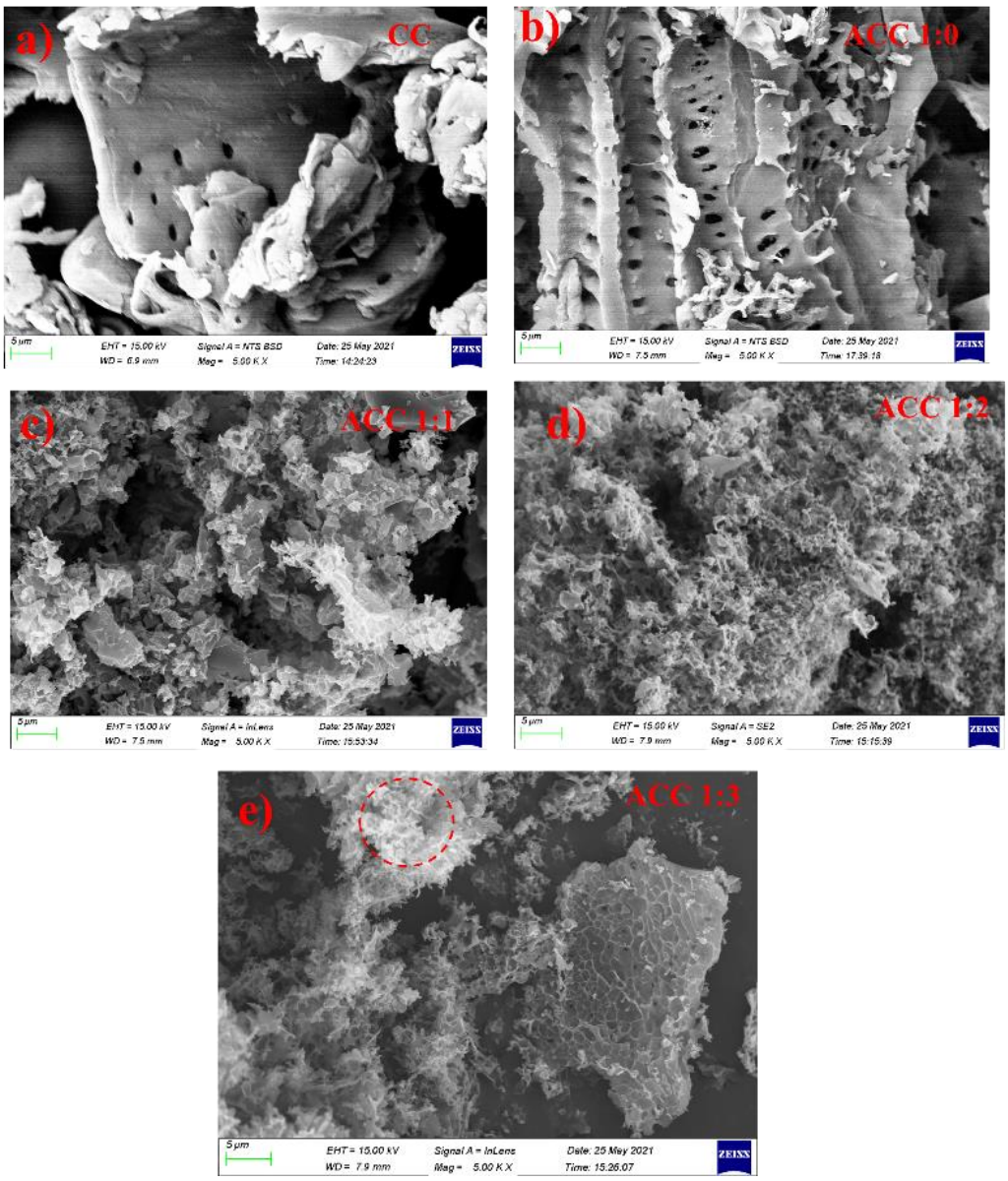

Figure 4.3: SEM images of (a) CC, (b)ACC 1:0, (c) ACC 1:1, (d) ACC 1:2, and (e) ACC 1:3.

The elemental analysis was conducted using X-ray dispersive energy (EDX) method. The results of EDX characterization for raw CC and the activated carbons are shown in figure 4.4. The results of the EDX analysis revealed that the materials consisted of carbon (C), oxygen (O), silica (Si), magnessium (Mg), and calcium (Ca) which are usaully present in activated carbon [33]. The highest peak was recorded for the carbon element compared to the other elements indicating that carbon is the highest elemental content of the materials. The carbon contents of

activated carbons (≥60.48%) are considerably higher than the carbon content of raw corncob (56.7%). This is because the volatile molecules, such as hydrogen and oxygen, leave from activated carbons during carbonization process; resulting in AC rich in carbon contents [34]. The effects of impregnation ratios on the elemental composition of activated carbons, demonstrates that with increasing impregnation ratio, the carbon content of ACs is increased, which is in agreement with results reported by Kumar *et al*., [35]. The impurity peaks are due to the gold and palladium coating material.

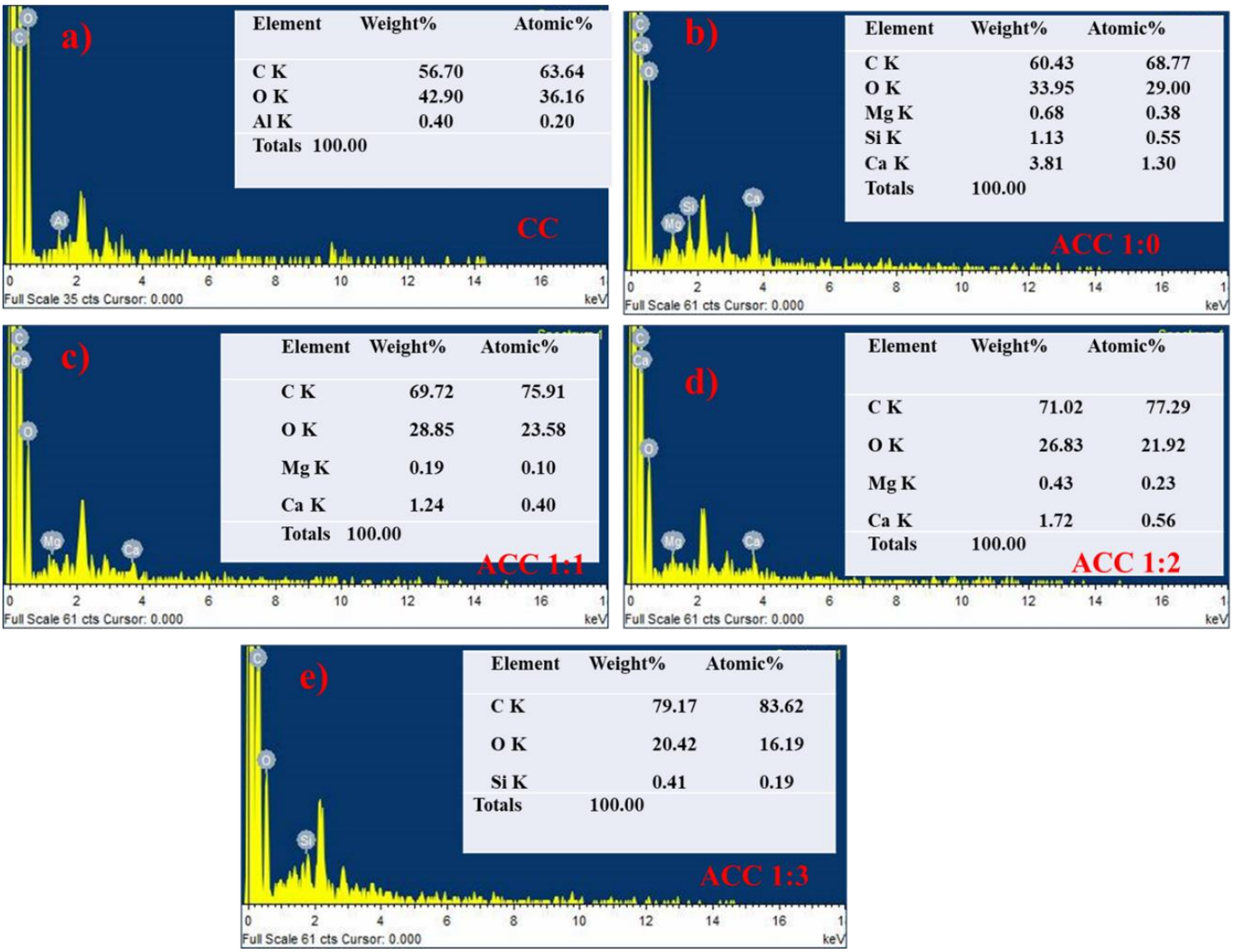

Figure 4.4: EDX analysis of (a) CC, (b) ACC 1:0, (c) ACC 1:1, (d) ACC 1:2, and (e) ACC 1:3.

4.5 Conclusion

This study examined synthesis and characterization of activated carbon from corncob residue using potassium carbonate as a chemical activation agent. Herein, the activated carbon samples were prepared at 800 °C for 2h with impregnation weight ratios of corncob to K_2CO_3 ranging from 1:0 to 1:3. The characteristics of the prepared ACC's were examined using scanning electron microscopy, X-ray dispersive energy, thermogravimetric analysis, N_2 adsorption-desorption and X-ray powder diffraction. The experimental results illustrated significant improvements in the BET surface area as the impregnation ratio increased from 1:0 to 1:2 (CC/ K_2CO_3), however, decreasing BET surface area at the ratio of 1:3 was attributed to collapsing pores. The best activated carbon sample ($S_{BET} = 1523.2$ m^2/g with a pore volume $= 0.81$ cm^3/g) was obtained at an impregnation ratio of 1:2. The SEM micrographs showed a high porosity development on AC as a result of the activation treatment while EDX confirmed the presence the presence of carbon, oxygen, silica, magnessium, and calcium.

4.6 References

[1] F. Ma, S. Ding, H. Ren, and Y. Liu, “Sakura-based activated carbon preparation and its performance in supercapacitor applications,” *RSC Advances*., vol. 9, pp.2474-2483, 2019, doi: 10.1039/c8ra09685f.

[2] E. Köseoğlu and C. Akmil-Başar, “Preparation, structural evaluation and adsorptive properties of activated carbon from agricultural waste biomass,” *Adv. Powder Technol*., vol. 26, pp. 811–818, 2015, doi: 10.1016/J.APT.2015.02.006.

[3] S. Z. Naji and C. T. Tye, “A review of the synthesis of activated carbon for biodiesel production: Precursor, preparation, and modification,” *Energy Convers. Manag. X*, vol. 13, pp. 100152, 2022, doi: 10.1016/J.ECMX.2021.100152.

[4] D. Duan, “Activated carbon from lignocellulosic biomass as catalyst: A review of the applications in fast pyrolysis process,” *J. Anal. Appl. Pyrolysis*, vol. 158, pp. 105246, 2021, doi: 10.1016/J.JAAP.2021.105246.

[5] Y. Zhang, H. Lei, Z. Yang, K. Qian, and E. Villota, “Renewable High-Purity Mono-Phenol Production from Catalytic Microwave-Induced Pyrolysis of Cellulose over Biomass-Derived Activated Carbon Catalyst,” *ACS Sustainable Chem. Eng.*, vol. 6, pp. 5349–5357, 2018, doi: 10.1021/acssuschemeng.8b00129.

[6] W.-J. Liu, K. Tian, Y.R. He, H. Jiang, and H.-Q. Yu, “High-Yield Harvest of Nanofibers/Mesoporous Carbon Composite by Pyrolysis of Waste Biomass and Its Application for High Durability Electrochemical Energy Storage,” *Environ. Sci. Technol*., vol. 48, pp. 13951–13959, 2014, doi: 10.1021/es504184c.

[7] I. Ali et al., “Green preparation of activated carbon from pomegranate peel coated with zero-valent iron nanoparticles (nZVI) and isotherm and kinetic studies of amoxicillin removal in water,” Environmental Science and Pollution Research, vol 27, pp. 1-12, 2020, doi: 10.1007/s11356-020-09310-1/Published.

[8] D. Liu, W. Zhang, and W. Huang, “Effect of removing silica in rice husk for the preparation of activated carbon for supercapacitor applications,” *Chinese Chem. Lett*., vol. 30, pp. 1315–1319, 2019, doi: 10.1016/J.CCLET.2019.02.031.

[9] G. A. Figueroa Campos et al., “Preparation of Activated Carbons from Spent Coffee Grounds and Coffee Parchment and Assessment of Their Adsorbent Efficiency,” *Processes*, vol. 9, pp. 1396, 2021, doi: 10.3390/pr9081396.

[10] Y. Guo, C. Tan, J. Sun, W. Li, J. Zhang, and C. Zhao, “Porous activated carbons derived from waste sugarcane bagasse for CO2 adsorption,” *Chem. Eng. J.*, vol. 381, pp. 122736, 2020, doi: 10.1016/J.CEJ.2019.122736.

[11] W. Xu, Q. Zhao, R. Wang, Z. Jiang, Z. Zhang, X. Gao, and Z. Ye, “Optimization of organic pollutants removal from soil eluent by activated carbon derived from peanut shells using response surface methodology,” *Vacuum*, vol. 141, pp. 307–315, 2017, doi: 10.1016/J.VACUUM.2017.04.031.

[12] A. E. Ogungbenro, D. V. Quang, K. A. Al-Ali, L. F. Vega, and M. R. M. Abu-Zahra, “Synthesis and characterization of activated carbon from biomass date seeds for carbon dioxide adsorption,” J. *Environ. Chem. Eng.*, vol. 8, pp. 104257, 2020, doi: 10.1016/J.JECE.2020.104257.

[13] J. Wang and S. Kaskel, “KOH activation of carbon-based materials for energy storage,” *J. Mater. Chem*, vol. 22, pp. 23710-23725, 2012, doi: 10.1039/c2jm34066f.

[14] W. Ao, J. Fu, X. Mao, Q. Kang, C. Ran, Y. Liu, H. Zhang, Z. Gao, J. Lia, G. Liu, and J. Dai, “Microwave assisted preparation of activated carbon from biomass: A review,” *Renew. Sustain. Energy Rev.*, vol. 92, pp. 958–979, 2018, doi: 10.1016/J.RSER.2018.04.051.

[15] M. A. Yahya, Z. Al-Qodah, and C. W. Z. Ngah, “Agricultural bio-waste materials as potential sustainable precursors used for activated carbon production: A review,” *Renew. Sustain. Energy Rev.*, vol. 46, pp. 218–235, 2015, doi: 10.1016/J.RSER.2015.02.051.

[16] H. Sayğili and F. Güzel, “High surface area mesoporous activated carbon from tomato processing solid waste by zinc chloride activation: process optimization, characterization and dyes adsorption,” *J. Clean. Prod.*, vol. 113, pp. 995–1004, 2016, doi: 10.1016/J.JCLEPRO.2015.12.055.

[17] S. Wang, H. Nam, and H. Nam, “Preparation of activated carbon from peanut shell with KOH activation and its application for H2S adsorption in confined space,” *J. Environ. Chem. Eng.*, vol. 8, pp. 103683, 2020, doi: 10.1016/J.JECE.2020.103683.

[18] H. Demiral and C. Güngör, “Adsorption of copper (II) from aqueous solutions on activated carbon prepared from grape bagasse,” *J. Clean. Prod.*, vol. 124, pp. 103–113, 2016, doi: 10.1016/J.JCLEPRO.2016.02.084.

[19] K. Yang, J. Peng, C. Srinivasakannan, L. Zhang, H. Xia, and X. Duan, “Preparation of high surface area activated carbon from coconut shells using microwave heating,” *Bioresour. Technol.*, vol. 101, pp. 6163–6169, 2010, doi: 10.1016/j.biortech.2010.03.001.

[20] H. Zhang, Y. Chen, S. Wang, L. Ma, Y. Yu, H. Dai, and Y. Zhang, “Extraction and comparison of cellulose nanocrystals from lemon (Citrus limon) seeds using sulfuric acid hydrolysis and oxidation methods,” *Carbohydr. Polym.*, vol. 238, pp. 116180, 2020, doi: 10.1016/J.CARBPOL.2020.116180.

[21] J. Singh, H. Bhunia, and S. Basu, “Adsorption of CO2 on KOH activated carbon adsorbents: Effect of different mass ratios,” *J. Environ. Manage.*, vol. 250, pp. 109457, 2019, doi: 10.1016/J.JENVMAN.2019.109457.

[22] Y. Luo, D. Li, Y. Chen, X. Sun, Q. Cao, and X. Liu, “The performance of phosphoric acid in the preparation of activated carbon-containing phosphorus species from rice husk residue,”,*Journal of Materials Science,* vol. 54, pp.5008-5021,2018, doi: 10.1007/s10853-018-03220-x.

[23] X. Xie, D. Wu, H. Hou, X. Sun, Y. Zhang, R. Yu, S. Zhang, B. Wang, and W. Du, “Dielectric parameters of activated carbon derived from rosewood and corncob*,” Journal of Materials Science: Materials in Electronics*, vol. 31, pp. 18077–18084, 2020, doi: 10.1007/s10854-020-04358-8.

[24] L. J. Kennedy, J. J. Vijaya, and G. Sekaran, “Effect of Two-Stage Process on the Preparation and Characterization of Porous Carbon Composite from Rice Husk by Phosphoric Acid Activation*,” Ind. Eng. Chem. Res.*, vol. 43, pp. 1832–1838, 2004, doi: 10.1021/ie034093f.

[25] T. B. Gebreegziabher, S. Wang, and H. Nam, “Adsorption of H2S, NH3 and TMA from indoor air using porous corncob activated carbon: Isotherm and kinetics study,” *J. Environ. Chem. Eng.*, vol. 7, pp. 103234, 2019, doi: 10.1016/J.JECE.2019.103234.

[26] G. Kishore Gupta, M. Ram, R. Bala, M. Kapur, and M. Kumar Mondal, “Pyrolysis of Chemically Treated Corncob for Biochar Production and Its Application in Cr(VI) Removal*,” Environmental Progress & Sustainable Energy*, vol. 37, pp.1606-1617, 2017, doi: 10.1002/ep.12838.

[27] K. Sonu, M. Sogani, Z. Syed, A. Dongre, and G. Sharma, “Enhanced Decolorization and Treatment of Textile Dye Wastewater Through Adsorption on Acid Modified Corncob Derived Biochar,” *ChemistrySelect*, vol. 5, pp. 12287–12297, 2020, doi: 10.1002/SLCT.202003156.

[28] M. N. Kajama, “Hydrogen permeation using nanostructured silica membranes,” *WIT Transactions on Ecology and the Environment*, pp. 447–456,2015, doi: 10.2495/SDP150381.

[29] D. Liu, W. Zhang, H. Lin, Y. Li, H. Lu, and Y. Wang, “A green technology for the preparation of high capacitance rice husk-based activated carbon,” *J. Clean. Prod.*, vol. 112, pp. 1190–1198, 2016, doi: 10.1016/J.JCLEPRO.2015.07.005.

[30] K. Y. Foo and B. H. Hameed, “Utilization of rice husks as a feedstock for preparation of activated carbon by microwave induced KOH and K2CO3 activation,” *Bioresour. Technol.*, vol. 102, no. 20, pp. 9814–9817, 2011, doi: 10.1016/J.BIORTECH.2011.07.102.

[31] D. W. McKee, “Mechanisms of the alkali metal catalysed gasification of carbon,” *Fuel*, vol. 62, pp. 170–175, 1983, doi: 10.1016/0016-2361(83)90192-8.

[32] H. Li, F. Zheng, J. Wang, J. Zhou, X. Huang, L. Chen, P. Hu, J. Gao, Q. Zhen, S. Bashire, J. L. Liu, “Facile preparation of zeolite-activated carbon composite from coal gangue with enhanced adsorption performance,” *Chem. Eng. J.*, vol. 390, pp. 124513, 2020, doi: 10.1016/J.CEJ.2020.124513.

[33] S. Alam, M. S. Khan, W. Bibi, I. Zekker, J. Burlakovs, M. M. Ghangrekar, G. D. Bhowmick, A. Kallistova, N. Pimenov, and M. Zahoor, “Preparation of Activated Carbon from the Wood of Paulownia tomentosa as an Efficient Adsorbent for the Removal of Acid Red 4 and Methylene Blue Present in Wastewater,” *Water*, vol. 13, pp. 1453, 2021, https://doi.org/10.3390/w13111453.

[34] O. Üner and Y. Bayrak, “The effect of carbonization temperature, carbonization time and impregnation ratio on the properties of activated carbon produced from Arundo donax,” *Microporous Mesoporous Mater.*, vol. 268, pp. 225–234, 2018, doi: 10.1016/J.MICROMESO.2018.04.037.

[35] A. Kumar and H. M. Jena, “Preparation and characterization of high surface area activated carbon from Fox nut (Euryale ferox) shell by chemical activation with H3PO4,” *Results Phys.*, vol. 6, pp. 651–658, 2016, doi: 10.1016/J.RINP.2016.09.012.

Chapter 5: Preparation of activated carbon, copper oxide and polyvinyl alcohol composites for potential application in chemical sensors

5.1 Introduction

In recent years, the urgency in monitoring air pollution using eco-friendly high-performance materials has motivated researchers to explore prospective and cost-effective materials. This is because of the high demand for simple, responsive and stable electronic sensors suitable for environmental monitoring in different fields such as safety in mining, air pollution control, and firefighting [1]. A variety of materials including metal/metal oxide nanoparticles, inorganic semiconductors, carbon nanomaterials, and conjugated polymers have been explored as potential materials for resistive gas sensing applications [2]. Carbon-based materials have large surface area, low power consumptions, and good thermal and chemical stability, which are desirable properties in gas sensing [1, 3].

Among carbon-based materials, activated carbon (AC) has been considered to be the most promising sensing material because of its inner porous structure, large specific surface area, rich surface chemistry, chemical stability, the possibility of moulding its structure for specific applications, and most importantly, it is a low-cost material when compared to other forms of carbon such as carbon nanotubes (CNTs) [4]. Due to its low sensitivity and conductivity at room temperature, its application in operable sensors is restricted. Modification of AC surface is necessary to improve interaction between the sensing material and target gases in order to achieve high gas adsorption at low gas concentrations. Many efforts have been made in order to improve the sensing performance of AC by introducing surface functional groups such as carboxyl, carbonyl, hydroxyl, and phenols, or active substances such as metal oxides on the AC surface [5, 6]. For example, Huang et al., synthesized a metal oxide (MnO_2)/AC composite and reported that the composite exhibited better electrochemical performance compared to pristine AC [7]. Khaleed et al., prepared a NiO/AC composite and reported that the composite had better conductivity compared to both the pristine NiO and AC [1].

The field of nanotechnology has drawn much interdisciplinary effort in the development of nanomaterials which has been providing promising innovative technologies due to their distinct physical features, electrical conductivity, chemical resistivity, and chemical characteristics, compared to those materials in bulk state [8]. Nanomaterials are being introduced into all aspects of life such as the advanced nano-substances in energy, biomedical and environment fields [9]. Copper oxide nanoparticles (CuO NPs) have gained significant importance due to their distinctive electrical and thermal conductivity, relatively high melting point, great solder ability, low electrochemical migration behaviour, and low cytotoxicity [10]. CuO NPs are widely used in the field of catalysis, gas sensors, waste treatment, batteries, food preservation, high temperature superconductors, solar energy conversion, and dye removal [9, 11]. There have been reports demonstrating that different morphologies of CuO NPs are suitable for the detection of various gases such as ethanol and acetone [12]. However, metal oxide-based gas sensors require high operating temperature to achieve excellent sensing performance which could lead to high power consumption and drift problems caused by sintering and diffusion process [13, 14]. Therefore, new methods should be explored to minimize these challenges.

In this work, we report room temperature synthesis of CuO NPs and oil bath preparation of ACC/PVA/CuO composite using the ACC 1:2 sample (reported in chapter 4) and study the VOC gas sensing properties of the composite. The aim of this work was to investigate the role of CuO on the sensing properties of AC when exposed to different VOCs and evaluate which composite shows the highest response.

5.2 Materials and methods

5.2.1 Materials

Copper nitrate hexahydrate (Cu $(NO_3)_2 \cdot 6H_2O$), sodium hydroxide (NaOH), and ethanol absolute (99.9% purity) was purchased from Sigma-Aldrich, South Africa. The activated carbon was prepared in using pyrolysis method (Chapter 4). De-ionized water was used during the preparation processes. All chemicals were used as received, without any further purification.

5.2.2 Methods

5.2.2.1 Preparation of copper oxide nanoparticles (CuO NPs)

CuO nanostructures were synthesized at room temperature through a solution reduction process using sodium hydroxide as a reducing agent. The preparation of the CuO nanostructures was done according to previously documented methods (Sonia et al., [15]) but with some minor modifications. In a typical reaction, 2 M aqueous solution of NaOH was mixed slowly with 50 ml of 0.2 M aqueous solution of copper nitrate hexahydrate at room temperature and until a pH value of 12 was maintained. The mixture was the stirred for 12 hours at room temperature. The resultant solution was then sonicated for 30 min at room temperature, and the black-coloured precipitate obtained was washed with distilled water and ethanol several times and dried at 100 °C for 6 h, lastly, the sample was calcined at 400 °C in a muffle furnace for 2h. The reaction mechanism for the formation of copper oxide is as follows [16]:

$$Cu\,(NO_3)_2 + 2NaOH \longrightarrow Cu(OH)_2 + 2NaNO_3 \xrightarrow{\Delta} CuO + H_2O$$

NaOH plays an important role in the formation of CuO nanorods since OH^- concentration facilitates the reaction that produces nanostructures. The mechanism shows that, in an alkaline bath there is initially the formation of $Cu(OH)_2$ acting partly as nuclei for the growth of CuO nanoparticles [17].

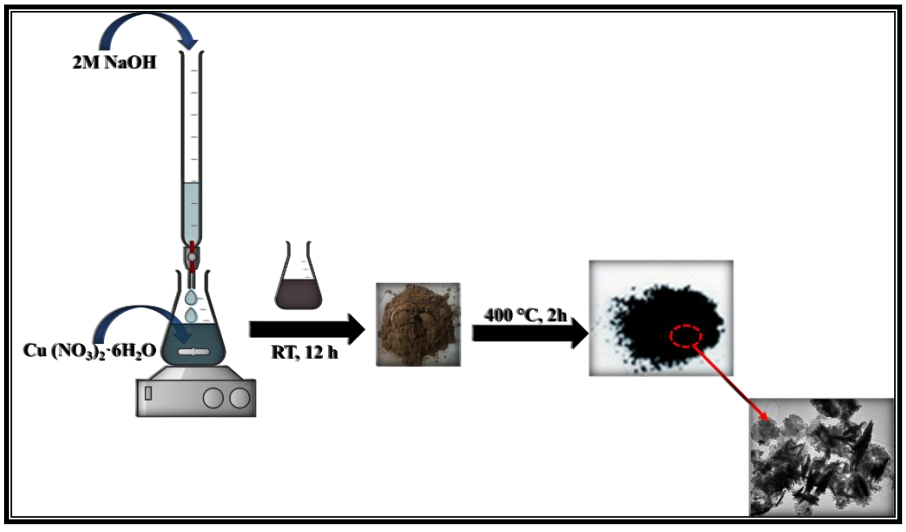

Figure 5.1: Graphical illustration of copper oxide nanoparticles.

5.2.2.2 Preparation of ACC/PVA/CuO composites and sensing devices

The ACC/CuO/PVA composites were prepared using previously documented methods by Linganiso et al., with some minor modifications [18]. Briefly, 50 mg AC were ultrasonicated in 10 mL dimethylformamide for about 15 minutes to allow particle dispersion. About 5 mg of PVA was then added to form continuous network and bed the dispersed particles and the mixture was stirred at 60 °C for about 6 hours to dissolve the PVA. The composites solutions were prepared in the proportions: 5%, 10%, and 15% of CuO in ACC/PVA (w:w). For device fabrication, interdigitated electrodes-printed circuit board (IDEs-PCB) substrates were bought with IDE already mounted on the PCB substrates. Two copper wires of the same size were each mounted on each electrode by soldering method. Prior to preparing sensor films, the sensor substrate was rinsed with acetone, and dried in a 100 °C oven for 2h. Preparation of sensor films was carried out by drop casting method of the as-prepared composites using a micro-pipette. Precisely, 5 µL of the sonicated composites was carefully dropped on the sensing layer of IDE-PCB, the sensors were allowed to dry at room temperature overnight and further dried in an oven at 60 °C for 4 h. Figure 5.2 shows the preparation of sensing electrode.

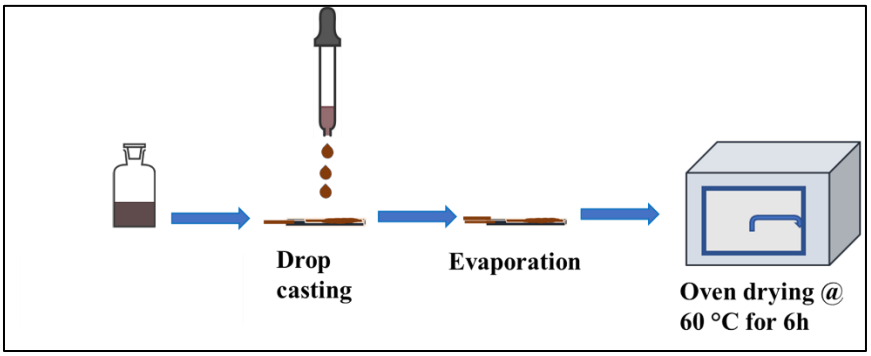

Figure 5.2: Preparation of sensing electrode

5.2.2.3 Gas sensing measurements

The gas sensing properties of the fabricated sensing devices were studied by exposing the devices to the analytes (ethanol, acetone, 2-butanol, and methanol) and analysing the change in electrical resistance. An LCR 6300 multimeter with an AC input signal was used for the electrical resistance measurements. Fig. 5.3 gives a schematic representation of the sensing system used, where the sensing electrode was placed inside a 5 L round bottom flask. The gas vapour of the different analytes was injected into the round bottom flask using a micro-syringe. To obtain desired concentrations of analytes in ppm, the concentration was calculated using to Eq. 5.1 [19].

$$(ppm) = \frac{22.4\ \rho TVs}{273MrV} \times 1000 \qquad \text{eq (5.1)}$$

Where C is the concentration of the analyte gas in parts per million (ppm), ρ the density of the analyte in g·mL^{-1}, T the testing temperature in Kelvin, Vs the injected volume of the analyte in μL, Mr the molar mass of the analyte gas in g·mol^{-1}, and V the volume of the round bottom flask of 5 L.

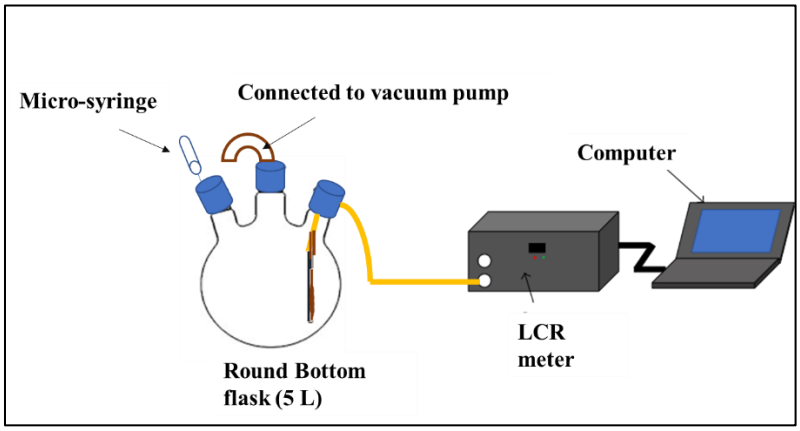

Figure 5.3: Graphical illustration of gas sensing setup

5.3 Characterization

The CuO NPs and composites were characterized using transmission electron microscopy (TEM) (FEI G^2 TECNAI Spirit T12) to determine the morphology, and X-ray diffraction (XRD) (Bruker D_2 Phaser) to determine the crystalline phase of the samples. Measurement of specific surface areas of the activated carbons and composites were determined using N_2 adsorption (at 77 K), using a surface and porosity analyser (A

Micromeritics Tristar 3000). The thermal stability of the materials was monitored using a Perkin Elmer 6000 thermogravimetric analyser (TGA).

5.4 Results and discussion

5.4.1 X-ray powder diffraction

The crystallographic and structural characteristics of the synthesized CuO rods and ACC/PVA/CuO composites were evaluated using XRD as shown in Figure 5.4. ACC exhibits broad and wide diffraction peaks around 23.8° and 42.5°, confirming the (002) and (100) phase of the graphitic domain. These peaks demonstrate the formation of small graphitic phase in ACC during calcination [20]. Comparison of XRD patterns of CuO and ACC/PVA/CuO samples in Figure 5.4 revealed that the CuO NPs in all samples represent a monoclinic structure that was indexed to copper oxide [CuO, PDF 01-073-6234]. The peaks appeared at 2θ (32.45°, 35.57°, 38.69°, 48.77°, 53.57°, 58.75°, 61.72°, 66.04°, 68.24°, 75.16°, and 83.53°) values and they were assigned to the corresponding (110), (002), (111), (-202), (020), (202), (-113), (310), (220) and (004) planes, respectively. All the observed peaks were assigned to the tenorite phase, in addition, a broad diffraction hump at 2θ range of 19.65° and a shoulder peak at 23.15° were observed in case of ACC/PVA/CuO samples, confirming presence of AC and PVA [21]. The mean CuO NPs crystallite size was calculated to be 20.90 nm, from the CuO (002 and 111) peaks using the Debye–Scherer equation (see equation 5.2) [22, 23].

$$D = \frac{k\lambda}{\beta \cos(\theta)} \qquad \text{eq (5.2)}$$

Where D is the average size of the ordered (crystalline) domains, K is the shape factor with a typical value of about 0.9, λ is the X-ray wavelength (0.154), β is the full width at half maximum (FWHM) of the reflection peak, and θ is the diffraction angle. The intensity of peaks of the CuO peaks in ACC/PVA/CuO tends to be increased with increasing amounts of CuO.

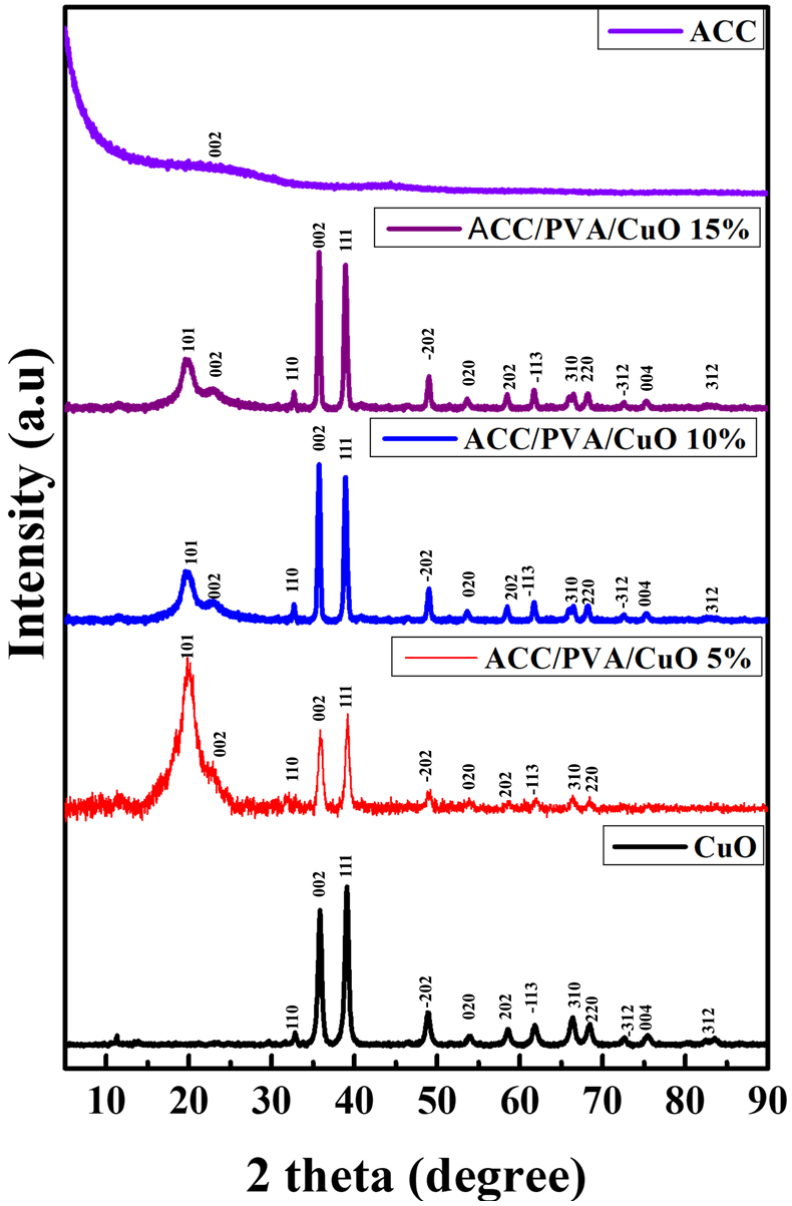

Figure 5.4: XRD patterns of ACC, ACC/PVA/CuO 5%, ACC/PVA/CuO 10%, ACC/PVA/CuO 15%, and CuO.

5.4.2 TEM analysis

To further investigate the as-prepared samples, the morphology of the materials was studied by TEM (Figure 5.5). The pristine activated carbon is shown in figure 5.5 a, exhibits uniform distribution of pores. The porous nature of ACC is more favourable for the adsorption of VOCs, and may prevent large agglomeration of CuO nanoparticles [24].

TEM analysis of CuO (Figure 5.5 b and c) confirmed the presence of flower like sample comprised of agglomerated, polydisperse rods with diameters ranging from 8.31 to 52.41 nm and an average size distribution of 21.79± 9.88 nm, which is comparable to the average crystallite size calculated using the Debye Scherrer equation. Similar properties were reported by Vasantharaj et al., [25]. The ACC/PVA/CuO composites show the homogenous deposition of the rod nanoparticles in the activated carbon matrix and demonstrated that the variation in the concentration of CuO has an influence on the morphology of the composites.

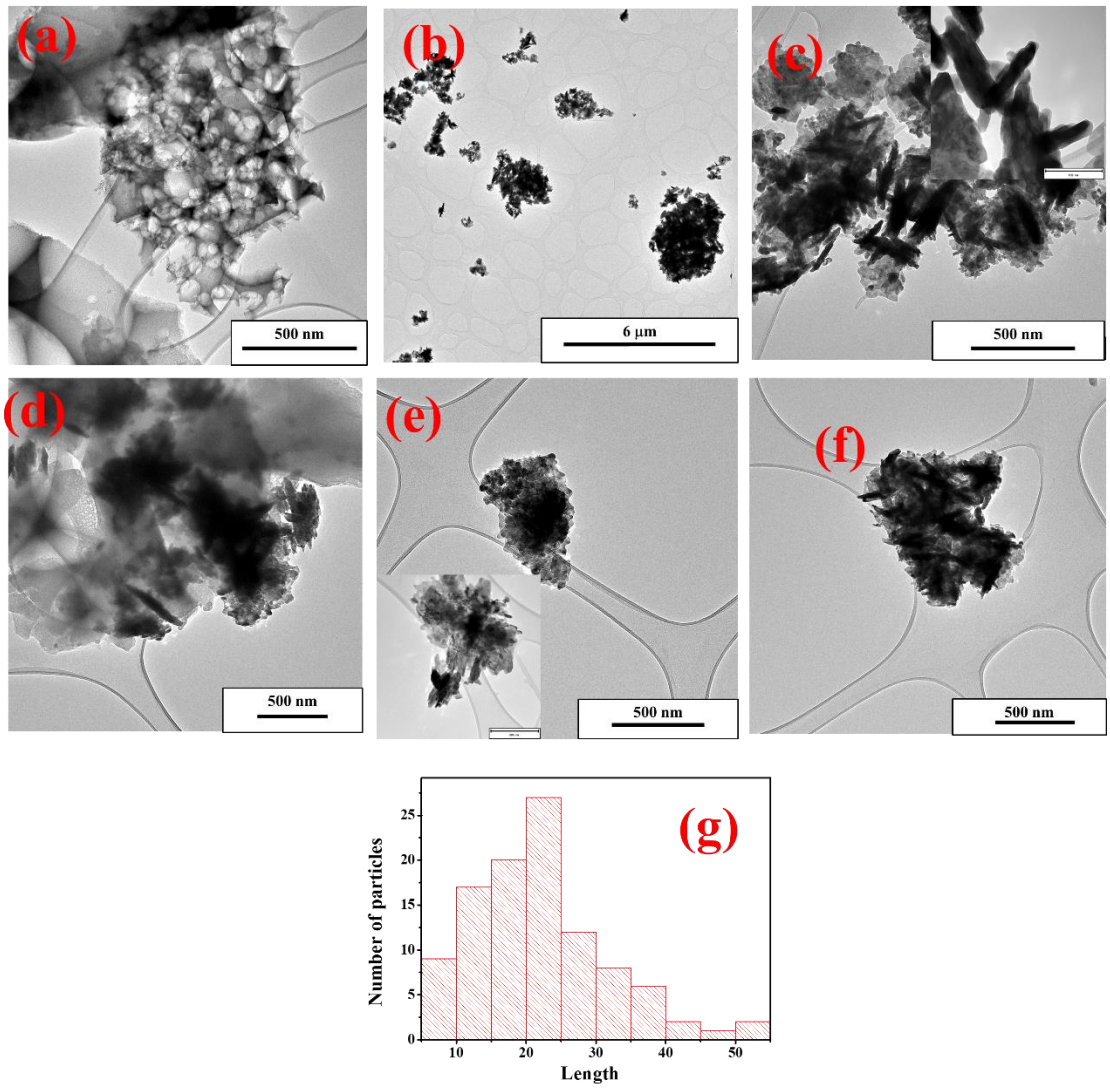

Figure 5.5: TEM images (a) ACC, (b-c) CuO NPs, (d) ACC/PVA/CuO 5%, (e) ACC/PVA/CuO 10%, (f) ACC/PVA/CuO 15%, and (g) show the particle size distribution of the CuO NPS. The inset in (c and e) show TEM images at a lower magnification scale

5.4.3 Thermal stability

The TGA and differential thermal analysis (DTG) analysis was performed to identify the thermal behaviour and stability of the composites in an air atmosphere. Figure 5.6 (a and b) presents TGA and DTG of the composites. The thermograms for all the composites show similar degradation patterns, the weight loss in the first region at a temperature around 100 ℃ is attributed to the elimination of adsorbed moisture. A second degradation peak around 175–387 °C can be attributed to the thermal degradation of the main chains of PVA [26]. The major weight loss between 400 and 600 ℃ is mainly related to the combustion of the activated carbon [27]. At the end of the degradation, the final residual mass of the ACC/PVA/CuO 5%, ACC/PVA/CuO 15%, and ACC/PVA/CuO 10% were 6.44%, 9.84 %, and 13.85% respectively.

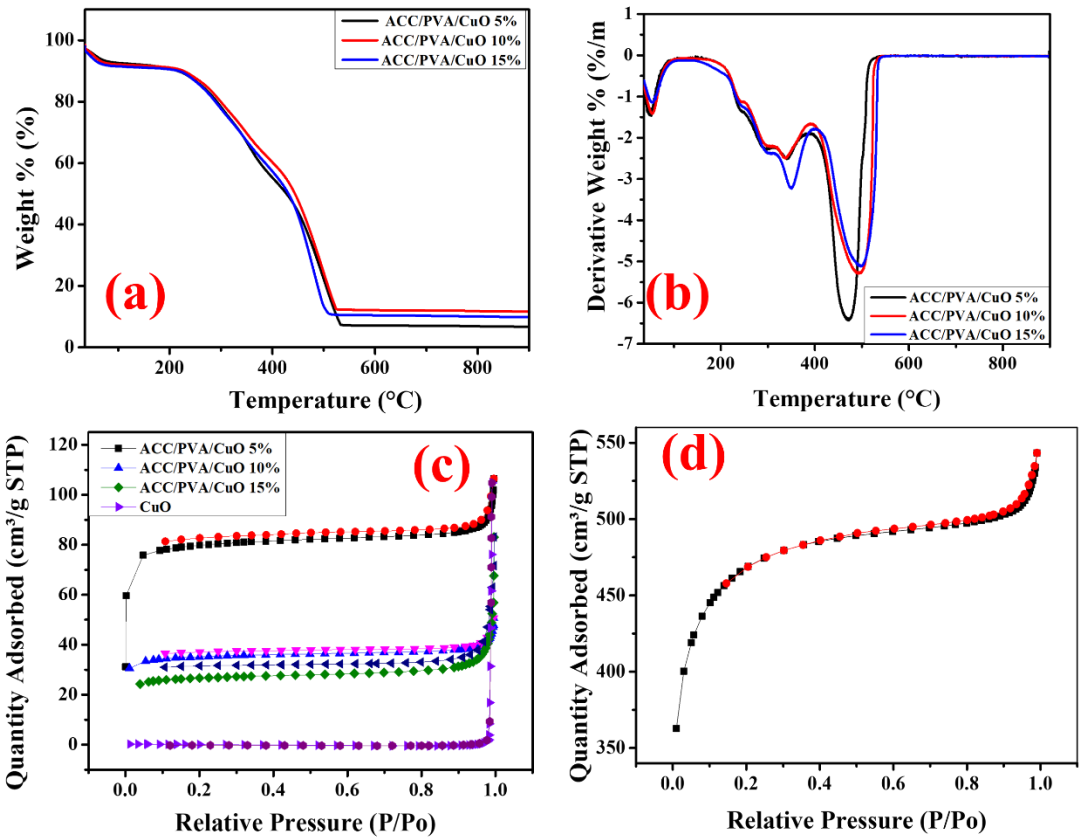

Figure 5.6: (a) TGA, (b) DTG of the composites, (c) N_2 adsorption–desorption isotherms of the CuO NPs and composites, and (d) N_2 adsorption–desorption isotherm of the ACC.

5.4.4 Pore structure characterization

Figure 5.6 c and d shows the nitrogen adsorption isotherms measured for all samples. The ACC and the modified ACC/PVA/CuO composite samples exhibit a type-IV isotherm profiles according to the International Union of Pure and Applied Chemistry (IUPAC) classification. In each of the samples, the gas quantity adsorbed increase evidently at low relative pressure ($P/P_0 < 0.2$) due to the abundance of meso-pores [28]. The ACC/PVA/CuO composites exhibited higher specific surface areas of 296.22, 132.64, 98.30 m^2/g for ACC/PVA/CuO 5%, ACC/PVA/CuO 10%, and ACC/PVA/CuO 15% respectively, when compared to the pristine CuO (0.624 m^2/g). This increase in the surface area of the ACC/PVA/CuO composites can be attributed to the addition of ACC (1508.53 m^2/g), which exhibits a much higher specific surface area. The nitrogen adsorption amount of the composites decreases gradually with an increase in the CuO loading, due to the loss of free space (intraparticle voids) after the CuO particle dispersion on the ACC [29]. The textural properties of the ACC, CuO, and ACC/PVA/CuO composites are summarized in table 5.1.

Table 5.1: Textural characteristics of activated carbon, CuO, and ACC/PVA/CuO composites.

	BET surface area (m^2/g)	**Pore volume (cm^3/g)**	**Pore size (nm)**
ACC	1508.53	0.72	2.17
CuO	0.624	0.12	1.44
ACC/PVA/CuO 5%	278.04	0.13	1.94
ACC/PVA/CuO 10%	132.64	0.061	1.83
ACC/PVA/CuO 15%	98.30	0.058	2.14

5.4.5 XPS analysis

XPS analysis is a powerful surface sensitive technique that has been used to confirm the chemical composition, purity, and oxidation state of the as-prepared CuO NPS. Figure 5.7 a shows XPS survey spectrum of CuO NPs, which have confirmed that the presence of copper (Cu), oxygen (O), and carbon (C). Figure 5.7 b–d show the high-resolution spectra of Cu 2p, O1s, and C 1s, respectively. The high-resolution spectra of Cu 2p revealed distinguishable Cu $2p_{3/2}$ and Cu $2p_{1/2}$ peaks at binding energies of 934.6 and 954.6 eV respectively with an energy difference of 20 eV, which correlated well with the standard Cu 2p peaks for CuO[28]. In the same spectra, there is a satellite peak of Cu $2p_{3/2}$ at the higher binding energies allocated at 943.4 eV, the presence of satellite feature of Cu 2p ruled out any possible Cu_2O phase[30]. The high-resolution spectrum of O1s as shown in Figure 5.7 was deconvoluted to three peaks at 533.3, 531.7, and 529.6 eV. The peak at 529.6 eV, can be assigned to the binding energy for lattice oxygen $(O_L)^{2-}$ in CuO lattice and is in good agreement with the binding energy of O^{2-} ion in the metal oxide sites (Cu^{2+}−O^{2-}) [31]. The peak at 531.7 and 533.3 eV can be assigned to the binding energy for oxygen defects/vacancies $(O_V)^{2-}$ within the matrix of CuO, and the binding energy for adsorbed residual carbon or other surface oxygen species, which can easily react with the CuO NPS [32]. All the peaks of the C 1s spectrum known as adventitious carbon contamination are typically used as a charge reference for XPS spectra on the surface of the sample [31]. Figure 5.7 d shows the high-resolution spectra of carbon (C 1s), which confirmed the presence of a referenced peak at 284.7 eV and other peaks at 284.3, 286.1, 287.9, and 288.67 eV, assigned to C–C sp^3 bond, C-C sp^2 bond, C=O, and O-C=O bond, respectively. The results measured from the XPS spectra confirmed the existence of the CuO structure.

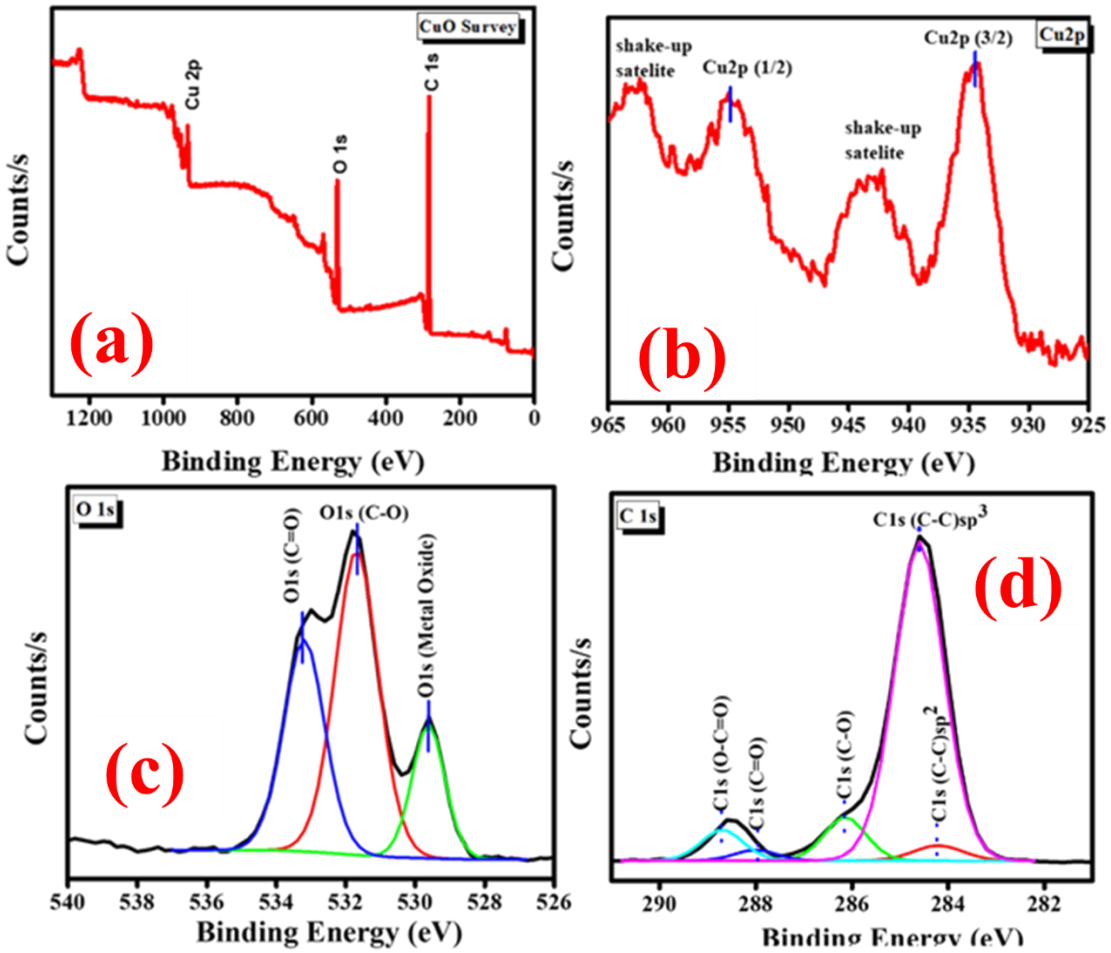

Figure 5.7: (a) XPS survey spectrum of CuO NPs. (b–d) High resolution (Core level) of Cu 2p, O 1s, and C 1s from as synthesized CuO NPs, respectively.

5.5 Gas sensing

For gas sensing investigations the fabricated gas sensors were mounted in the test chamber for 30 min before exposure to analyte gases in order to stabilize the electrical baseline [12]. Different VOCs (ethanol, acetone, 2-butanol, and methanol) were selected as test gases to demonstrate changes in selectivity and sensitivity of the ACC and the ACC/CuO composites, with exposure time of 5 min in vapour and 5 min in air. The gas response is presented as Response = (R_a- R_g / R_g)× 100%, were Rg and Ra are the resistances of the sensor specimen under gas exposure and in air, respectively. All the gas sensors exhibited a higher response percentage to ethanol when compared to acetone, 2-butanol, and methanol, thus confirming their selectivity to ethanol. The major preference of activated carbon-based sensors towards ethanol over the other is due to the presence of oxygen adsorption sites and dispersion interactions mainly through the hydrocarbon

chain on the activated carbon-based materials [33]. Figure 5.8 demonstrates that the sensor responses were found to be dependent on the CuO concentration. The maximum sensor response for all the VOCs was achieved for ACC/PVA/CuO 15%, compared to pristine activated carbon and the other composites, in which ACC/PVA/CuO 15% > ACC/PVA/CuO 10% > ACC/PVA/CuO 5% >ACC. It is clear that the response of the composites is highly affected by the amount of CuO in the composite as the response increased with CuO percentage loading. This confirms that the overall composite performance was improved by the addition of CuO. This further confirms that the CuO nanoparticles can be effectively applied in room temperature operable gas sensors when mixed with the ACC and PVA constituents.

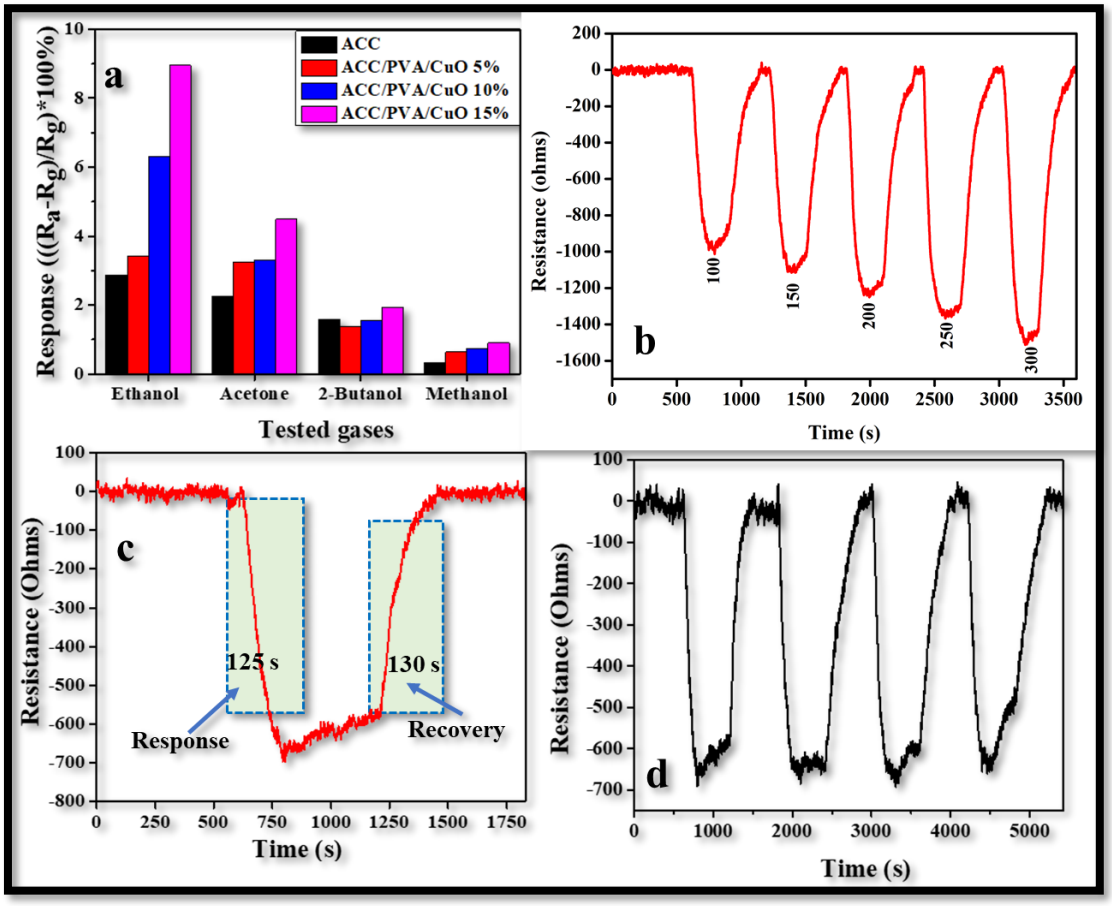

Figure 5.8: (a) Sensitivity of the sensor towards different gases at 300 ppm, (b) Ethanol dynamic response curve of the ACC/PVA/CuO 15% sensor, (c) Response and recovery time of ACC/PVA/CuO 15% to 100 ppm of ethanol gas, and (d) Reproducibility cycles of ACC/PVA/CuO 15% sensor towards 100 ppm ethanol at room temperature.

Figure 5.8 b illustrates the dependence of the sensor resistance on the ethanol concentration (ranging from 100-300 ppm) at ambient temperature for the ACC/PVA/CuO 15%. The electrical resistance of the

sensor decreases when in contact with the ethanol and increased when exposed to air, carbon materials and CuO are commonly p-type semiconductors, for various sensor-analyte pairs, an inversion from p to n (or n to p) type response has been previously reported, where the n or p type here refers simply to the reaction to the analyte and not to the conductivity type (electrons or holes) [34]. Excellent reversibility with stable response and complete recovery to the initial resistance state is observed, indicating a fast response and recovery processes, which is extremely important for a real-time sensing device. As the ethanol concentration increase, the ethanol could easily get adsorbed and react with formed oxygen species on the surface of sensor device, thus facilitating the sensing reactions, promoting the response significantly. This result demonstrates that ACC/PVA/CuO 15% can be considered as a potential sensor (breathalyser) to screen drunk drivers at normal at ambient temperatures. Response and recovery are the central parameters that define the performance of a chemical sensor, response time is defined as the amount of time required for sensor's resistance change to reach 90 % of the maximum response (saturation point) in the presence of a target gas and the recovery time is the time taken for lowering 90% of the final equilibrium value [35]. The response and recovery of the ACC/PVA/CuO 15% were 125 and 130 seconds, respectively, when exposed to 100 ppm of ethanol. To determine the repeatability of sensing material, the ACC/PVA/CuO 15% sensor was exposed to 100 ppm of ethanol. As seen in figure 5.7 d, the sensor demonstrated a reversible and stable sensor behavior after four cycles.

5.6 Proposed sensing mechanism

The gas-sensing mechanism of ACC/PVA/CuO 15% can be explained by the change in resistance arising from the adsorption and desorption of oxygen. As illustrated in figure 5.9, when the sensor is exposed to air, the oxygen molecules will be adsorbed on the surface of the sensor and then ionize into oxygen species in the form of O_2^-, O^-, O^{2-} by depriving electrons from the conduction band leading to a thick electron depletion region with high potential barrier formed on the surface of the sensing material, thereby leading to an increase in sensor resistance [36]. However, once the ethanol gas is injected into the test chamber, ethanol molecules react with the oxygen species on the surface, which releases the trapped electrons back to the conduction band of the sensor, leading to the decrease of the thickness of the depletion region as well as the potential barrier, resulting in the sensor resistance to decrease [37].

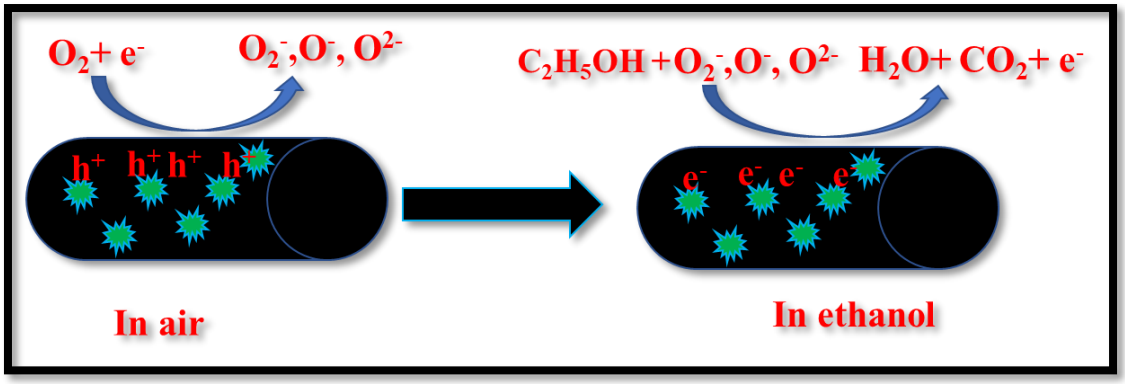

Figure 5.9: Graphical illustration of the gas sensing mechanism.

5.7 Conclusion

In this work, ACC/PVA/CuO composites were successfully prepared by a simple oil bath method. Nanosized CuO particles with an average diameter of about 21.79± 9.88 nm were successfully attached to the surface of ACC and PVA. The characteristics of the prepared composites were examined using TEM, TGA, N_2 adsorption-desorption, and XRD. The experimental results illustrated significant changes in the specific surface area (S_{BET}) as the concentration of CuO increase from 5-15%. The nitrogen adsorption capacity of the composites decreased gradually with an increase in the CuO loading due to ACC pore blockage as a result of the introduced CuO species, resulting in the reduction of the total pore volume and specific surface area when compared to the pristine ACC sample. The TEM images demonstrated that the variation in the concentration of CuO has an influence on the morphology of the composites. The composites were further explored for the detection of VOCs at room temperature. All the gas sensors exhibited a higher response percentage to ethanol, however, the ACC/PVA/CuO 15% composite-based sensor demonstrated high response (%) compared to pristine activated carbon and the other composites, in which ACC/PVA/CuO 15% > ACC/PVA/CuO 10% > ACC/PVA/CuO 5% >ACC. This is associated to the introduction of defects on the surface of activated carbon contributing to increased electrical conductivity, active sites, whereby the surface modifications promoted the adsorption and diffusion of vapour. The measured response and recovery time for the ACC/PVA/CuO 15% sensor in 100 ppm ethanol was to 125 s and 130 s, respectively. These results indicate that ACC/PVA/CuO 15 % has the potential for ethanol sensing application at room temperature.

5.8 References

[1] A. A. Khaleed, A. Belloa, J. K. Dangbegnon, D. Y. Momodu, M. J. Madito, F. U. Ugbo, A. A.A kande, B. P. Dhonge, F.Barzegara, O. Olaniyana, B. W. Mwakikunga, and N. Manyala, "Effect of activated carbon on the enhancement of CO sensing performance of NiO," *J. Alloys Compd.*, vol. 694, pp. 155–162, 2017, doi: 10.1016/J.JALLCOM.2016.09.310.

[2] S. Ahmad, M. Mujahid, A. Khan, and F. Mohammad, "Graphene/Nickel Oxide-Based Nanocomposite of Polyaniline with Special Reference to Ammonia Sensing," *ACS Omega*, vol. 21, pp. 39, 2018, doi: 10.1021/acsomega.8b00825.

[3] Y. J. Heo and S. J. Park, "Synthesis of activated carbon derived from rice husks for improving hydrogen storage capacity," *J. Ind. Eng. Chem.*, vol. 31, pp. 330–334, 2015, doi: 10.1016/J.JIEC.2015.07.006.

[4] S. Wang, H. Nam, and H. Nam, "Preparation of activated carbon from peanut shell with KOH activation and its application for H2S adsorption in confined space," *J. Environ. Chem. Eng.*, vol. 8, pp. 103683, 2020, doi: 10.1016/J.JECE.2020.103683.

[5] W. Zheng, J. Hu, S. Rappeport, Z. Zheng, Z. Wang, Z. Han, J. Langer, and J. Economy, "Activated carbon fiber composites for gas phase ammonia adsorption," *Microporous Mesoporous Mater.*, vol. 234, pp. 146–154, 2016, doi: 10.1016/J.MICROMESO.2016.07.011.

[6] N. A. Travlou, C. Ushay, M. Seredych, E. Rodríguez-Castello, and T. J. Bandosz, "Nitrogen-Doped Activated Carbon-Based Ammonia Sensors: Effect of Specific Surface Functional Groups on Carbon Electronic Properties," *ACS Sens.*, vol. 1, pp. 591–599, 2016, doi: 10.1021/acssensors.6b00093.

[7] T. Huang, Z. Qiu, D. Wu, and Z. Hu, "Bamboo-Based Activated Carbon @ MnO 2 Nanocomposites for Flexible High-Performance Supercapacitor Electrode Materials," *Int. J. Electrochem. Sci.*, vol. 10, pp. 6312 - 632, 2015.

[8] D. Letchumanan, S. P. M. Sok, S. Ibrahim, N. H. Nagoor, and N. M. Arshad, "Plant-Based Biosynthesis of Copper/Copper Oxide Nanoparticles: An Update on Their Applications in Biomedicine, Mechanisms, and Toxicity," *Biomolecules*., vol. 11, pp. 564, 2021, doi: 10.3390/biom11040564.

[9] S. A. Akintelu, A. S. Folorunso, F. A. Folorunso, and A. K. Oyebamiji, "Green synthesis of copper oxide nanoparticles for biomedical application and environmental remediation," *Heliyon*, vol. 6, pp. e04508, 2020, doi: 10.1016/J.HELIYON.2020.E04508.

[10] E. Rostami-Tapeh-Esmaeil, M. Golshan, M. Salami-Kalajahi, and H. Roghani-Mamaqani, "Synthesis of copper and copper oxide nanoparticles with different morphologies using aniline as reducing agent," *Solid State Commun.*, vol. 334–335, pp. 114364, 2021, doi: 10.1016/J.SSC.2021.114364.

[11] P. G. Bhavyasree and T. S. Xavier, "Green synthesis of Copper Oxide/Carbon nanocomposites using the leaf extract of Adhatoda vasica Nees, their characterization and antimicrobial activity," *Heliyon*, vol. 6, no. 2, pp. e03323, 2020, doi: 10.1016/J.HELIYON.2020.E03323.

[12] V. Cretu, V. Postica, A. K. Mishra, M. Hoppe, I. Tiginyanu, Y. K. Mishra, L. Chow, N. H. de Leeuw, R. Adelung, and O. Lupan, "Synthesis, characterization and DFT studies of zinc-doped copper oxide nanocrystals for gas sensing applications †," *J. Mater. Chem. A*, vol. 4, pp. 6527-6539, 2016, doi: 10.1039/c6ta01355d.

[13] W. Hittini, A. Abu-Hani, and S. Mahmoud, "cellulose-copper oxide hybrid nanocomposites membranes for H 2 S gas detection at low temperatures," *Scientific Rep*., vol. 10, pp. 2940, 2020, doi: 10.1038/s41598-020-60069-4.

[14] N. Sihar, T. Y. Tiong, C. F. Dee, P. C. Ooi, A. A. Hamzah, M. A. Mohamed, and B. Y, Majlis, "Ultraviolet Light-Assisted Copper Oxide Nanowires Hydrogen Gas Sensor," *Nanoscale Res Lett*., vol. 13, pp. 150, 2018, doi: 10.1186/s11671-018-2566-6.

[15] S. Sonia, N. D. Jayram, P. Suresh Kumar, D. Mangalaraj, N. Ponpandian, and C. Viswanathan, “Effect of NaOH concentration on structural, surface and antibacterial activity of CuO nanorods synthesized by direct sonochemical method,” *Superlattices Microstruct.*, vol. 66, pp. 1–9, 2014, doi: 10.1016/j.spmi.2013.10.020.

[16] A. El-Trass, H. Elshamy, I. El-Mehasseb, and M. El-Kemary, “CuO nanoparticles: Synthesis, characterization, optical properties and interaction with amino acids,” *Appl. Surf. Sci.*, vol. 258, no. 7, pp. 2997–3001, 2012, doi: 10.1016/J.APSUSC.2011.11.025.

[17] S. Sonia, N. D. Jayram, P. Suresh Kumar, D. Mangalaraj, N. Ponpandian, and C. Viswanathan, “Effect of NaOH concentration on structural, surface and antibacterial activity of CuO nanorods synthesized by direct sonochemical method,” *Superlattices Microstruct.*, vol. 66, pp. 1–9, 2014, doi: 10.1016/J.SPMI.2013.10.020.

[18] E. C. Linganiso, R. Rodrigues, S. D. Mhlanga, B. W. Mwakikunga, N. J. Coville, and I. A. Hümmelgen, “GaN nanostructures-poly(vinyl alcohol) composite based hydrostatic pressure sensor device,” *Mater. Chem. Phys.*, vol. 143, pp. 367–372, 2013, doi: 10.1016/J.MATCHEMPHYS.2013.09.011.

[19] V. O. Okechukwu, V. Mavumengwana, I. A. Hümmelgen, and M. A. Mamo, “Concomitant in Situ FTIR and Impedance Measurements to Address the 2-Methylcyclopentanone Vapor-Sensing Mechanism in MnO 2 -Polymer Nanocomposites,” *ACS Omega*, vol. 4, pp. 8324–8333, 2019, doi: 10.1021/acsomega.8b03589.

[20] Y. Luo, D. Li, Y. Chen, X. Sun, Q. Cao, and X. Liu, “The performance of phosphoric acid in the preparation of activated carbon-containing phosphorus species from rice husk residue,” doi: 10.1007/s10853-018-03220-x.

[21] M. Jain, M. Yadav, T. Kohout, M. Lahtinen, V. K. Garg, and M. Sillanpää, “Development of iron oxide/activated carbon nanoparticle composite for the

removal of Cr(VI), Cu(II) and Cd(II) ions from aqueous solution," *Water Resour. Ind.*, vol. 20, pp. 54–74, 2018, doi: 10.1016/J.WRI.2018.10.001.

[22] A Taylor and H Sinclair, " On the determination of lattice parameters by the debye-scherrer method," *Proc. Phys. Soc.*, vol. 57, pp. 126- 135, 1945, doi: 10.1088/0959-5309/57/2/306.

[23] I. B.Usman, B. J.Matsoso, R. Erasmus, N. J.Coville, and D. M.Wamwang, "The role of carrier gas on the structural properties of carbon coated GaN," *Mater. Today Commun.*, vol. 27, pp. 102325, 2021, doi: 10.1016/J.MTCOMM.2021.102325.

[24] K. Zhou, W. Ma, Z. Zeng, X. Ma, X. Xu, Y. Guo, H. Li, and L. Li, "Experimental and DFT study on the adsorption of VOCs on activated carbon/metal oxides composites," *Chem. Eng. J.*, vol. 372, pp. 1122–1133, 2019, doi: 10.1016/J.CEJ.2019.04.218.

[25] S. Vasantharaj, S. Sathiyavima1, M. Saravanan, P. Senthilkumar, K. Gnanasekaran, M. Shanmugave, E. Manikandan, and A. Pugazhendhi, "Synthesis of ecofriendly copper oxide nanoparticles for fabrication over textile fabrics: Characterization of antibacterial activity and dye degradation potential," *J. Photochem. Photobiol. B Biol.*, vol. 191, pp. 143–149, 2019, doi: 10.1016/J.JPHOTOBIOL.2018.12.026.

[26] X. Sheng, S. Li, Y. Zhao, D. Zhai, L. Zhang, and X. Lu, "Synergistic Effects of Two-Dimensional MXene and Ammonium Polyphosphate on Enhancing the Fire Safety of Polyvinyl Alcohol Composite Aerogels," *Polymers (Basel).*, vol. 11, p. 1964, 2019, doi: 10.3390/polym11121964.

[27] T. Yumak, D. Bragg, and E. M. Sabolsky, "Effect of synthesis methods on the surface and electrochemical characteristics of metal oxide/activated carbon composites for supercapacitor applications," *Appl. Surf. Sci.*, vol. 469, pp. 983–993, 2019, doi: 10.1016/J.APSUSC.2018.09.079.

[28] H. Li, F. Zheng, J. Wang, J. Zhou, X. Huang, L. Chen, P. Hu, J. Gao, Q. Zhen, S. Bashir, and J. L. Liu, "Facile preparation of zeolite-activated carbon composite from

coal gangue with enhanced adsorption performance," *Chem. Eng. J.*, vol. 390, pp. 124513, 2020, doi: 10.1016/J.CEJ.2020.124513.

[29] G. Chen, F. Wang, S. Wang, C. Ji, W. Wang, J. Dong, and F. Gao, "Facile fabrication of copper oxide modified activated carbon composite for efficient CO 2 adsorption," *Korean J. Chem. Eng*, vol. 38, no. 1, pp. 46–54, 2021, doi: 10.1007/s11814-020-0684-1.

[30] J. Sackey, A. C. Nwanya, A. K. H. Bashir, N. Matinise, J. B. Ngilirabang, A. E. Ameh, E. Coetse, and M. Maaza, "Electrochemical properties of Euphorbia pulcherrima mediated copper oxide nanoparticles," *Mater. Chem. Phys.*, vol. 244, p. 122714, Apr. 2020, doi: 10.1016/J.MATCHEMPHYS.2020.122714.

[31] K. Munawar, M. A. Mansoor, W. J. Basirun, M. Misran, N. M. Huang, and M. Mazhar, "Single step fabrication of CuO-MnO-2TiO 2 composite thin films with improved photoelectrochemical response †," *RSC Adv.*, vol. 7, pp. 15885-15893, 2017, doi: 10.1039/c6ra28752b.

[32] M. A. Khan, N. Nayan, M. K. Ahmad, and C. F. Soon, "Surface Study of CuO Nanopetals by Advanced Nanocharacterization Techniques with Enhanced Optical and Catalytic Properties," *Nanomater.*, vol. 10, pp. 1298, 2020, doi: 10.3390/nano10071298.

[33] M. Vaseem, A.R. Hong, R.T. Kim, and Y.B. Hahn, "Copper oxide quantum dot ink for inkjet-driven digitally controlled high mobility field effect transistors," *J. Mater. Chem. C*, vol. 1, pp. 2112, 2013, doi: 10.1039/c3tc00869j.

[34] A. Silvestre-Albero, J. Silvestre-Albero, A. Sepúlveda-Escribano, and F. Rodríguez-Reinoso, "Ethanol removal using activated carbon: Effect of porous structure and surface chemistry," *Microporous Mesoporous Mater.*, vol. 120, pp. 62–68, 2009, doi: 10.1016/J.MICROMESO.2008.10.012.

[35] J. Bartolomé, M. Taeño, R. Martínez-Casado, D. Maestre, and A. Cremades, "Ethanol gas sensing mechanisms of p-type NiO at room temperature," *Appl. Surf.*

Sci., vol. 579, pp. 152134, 2022, doi: 10.1016/J.APSUSC.2021.152134.

[36] S. R. Nalage, S. T. Navale, R. S. Mane, M. Naushad, F. J. Stadlar, and V. B. Patil, "Preparation of camphor-sulfonic acid doped PPy–NiO hybrid nanocomposite for detection of toxic nitrogen dioxide," *Synth. Met.*, vol. 209, pp. 426–433, 2015, doi: 10.1016/J.SYNTHMET.2015.08.018.

[37] L. Zhu, Y. Li, and W. Zeng, "Hydrothermal synthesis of hierarchical flower-like ZnO nanostructure and its enhanced ethanol gas-sensing properties," *Appl. Surf. Sci.*, vol. 427, pp. 281–287, 2018, doi: 10.1016/J.APSUSC.2017.08.229.

[38] S. Zhao, Y. Shen, X. Yan, P. Zhou, Y. Yin, R. Lu, C. Han, B. Cui, and D. Wei, "Complex-surfactant-assisted hydrothermal synthesis of one-dimensional ZnO nanorods for high-performance ethanol gas sensor," *Sensors Actuators B Chem.*, vol. 286, pp. 501–511, 2019, doi: 10.1016/J.SNB.2019.01.127.

Chapter 6: Synthesis and Characterization of biomass-based fluorescent carbon structures for the detection of Fe (III) in aqueous solutions

6.1 Introduction

With the increase in industrial and wastewater effluents, water pollution has become a serious threat for human and aquatic life [1]. One of the major concerns is the presence of heavy metal ions from industrial waste such as Fe^{3+}, Hg^{2+}, Pb^{2+}, Cu^{2+}, Cr^{6+}, Zn^{2+}, Co^{2+}, etc [2–7]. Ferric ion (Fe^{3+}) is the most abundant and essential metal ion in living organisms, it plays crucial roles such as cellular metabolism, oxygen transport, enzyme catalysis, deoxyribonucleic acid (DNA), and ribonucleic acid (RNA) synthesis [8–11]. Although Fe^{3+} plays vital roles in the biological system, excess Fe^{3+} cause liver damage, kidney failure, cell oxidation and annihilation of blood circulation in human body [12], [13]. Moreover, high concentrations of Fe^{3+} in water bodies plays a role in the primary productivity of phytoplankton besides nitrate, phosphate and silicate which negatively affects the environment and aquatic life [13]. Hence, it is a necessity to develop effective analytical methods for the detection of Fe^{3+} ions and other metal ions.

So far, several approaches for the determination of Fe^{3+} in aqueous solutions have been developed including plasma optical emission spectroscopy, atomic absorption spectrometry, inductively coupled plasma mass spectrometry, etc. [9, 14, 15]. However, these methods are complicated, expensive, and require several steps for sample preparation [16]. To overcome these shortcomings, fluorescence quenching has been used for the detection of Fe^{3+} owing to the high sensitivity, great simplicity, easy monitoring, and rapid response [17]. The most widely used fluorescence sensors include organic dyes, semiconductor quantum dots (QDs), fluorescent metal organic frameworks and fluorescence metal nanoclusters [1, 16, 18–20]. However, there are concerns rising from their photo instability, toxicity, low sensitivity, and environmental unfriendliness restricting their real applications [21, 22]. Thus, highly efficient, sensitive, photo-stable, and eco-friendly nanostructures are desirable.

Since their discovery in 2004 by Xu et al., during the purification of single-walled carbon nanotube (SWCNT) through preparative electrophoresis, and then via laser ablation of graphite powder and cement in 2006 by Sun et al., CQDs have gradually become a rising star in the carbon nanomaterials

family [23]. Owing to their unique tunable photoluminescent, size-dependent optical properties, good biocompatibility, facile synthesis, and low toxicity as compared to their counterparts, the semiconductor quantum dots (QDs) [24, 25]. Recently, CQDs have been widely used as fluorescent sensors in the detection of Fe^{3+} due to their fluorescence quenching effect which may originate from formation of CQD–Fe^{3+} complexes through the interaction of Fe^{3+} with surface functional groups of the CQDs such as phenolic hydroxyl, carboxyl, and amino groups [26]. Different synthesis methods have been developed for the preparation of CQDs such as microwave-assisted synthesis, hydrothermal method, solid-phase method, ultrasonic treatment, electrochemical method, and so on [10, 27]. Among these methods, microwave-assisted synthesis is highly desirable because of the simplicity and short synthesis time, which result in homogeneous and fast heating that is beneficial in the synthesis of CQDs [28, 29].

Nitrogen-doped CQDs (N-CQDs) have gained interest due to their ability to enhance the performance and stability of CQDs and broaden the potential applications of CQDs by replacing carbon atoms in the sp^2/sp^3 network [30]. In this study, a simple, one-step microwave-assisted method to prepare nitrogen-doped carbon quantum dots (N-CQDs) from microcrystalline cellulose-derived cellulose nanocrystals prepared in Chapter 3. The as-prepared N-CQDs exhibited an excitation wavelength dependent fluorescence. These N-CQDs were further explored for the detection of Fe^{3+}. The preparation of fluorescent nitrogen doped carbon materials from CC-CNCs was published on the IEEE sensors 2021 [31].

6.2 Materials and Methods

6.2.1 Materials and reagents

Microcrystalline cellulose, sulphuric acid (H_2SO_4, 98%), and urea (CH_4N_2O) were obtained from Sigma-Aldrich (South Africa). Metal salts, namely, KCl, $Ni(NO_3)_2{\cdot}6H_2O$, $CdCl_2.H_2O$, $Cu(NO_3)_2$, $Mg(NO_3)_2{\cdot}6H_2O$, $Zn(NO_3)_2{\cdot}6H_2O$, $Al(NO_3)_3.9H_2O$, $Ca(NO_3)_2$, $Fe(NO_3)_3$, $Co(NO_3)_2{\cdot}6H_2O$, and $NaNO_2$ were all purchased from Sigma-Aldrich (South Africa). All the chemicals and reagents were of analytical grade and used as received without further purification. Deionized water was used for the preparation of aqueous solutions.

6.2.2 Methods

6.2.2.1 Synthesis of nitrogen-doped carbon quantum dots (N-CQDs) from cellulose nanocrystals (CNCs)

Figure 6.1 illustrates the schematic diagram of the synthesis of N-CQDs from CNCs. Briefly, 0.5 g dry powdered CNCs was mixed with 0.35 g of urea and placed in a 35 mL microwave tube with 15 mL of distilled water. To perform the synthesis, the sample was heated from room temperature to 180 °C and maintained at this temperature for 10 minutes before fast cooling to room temperature. The reaction mixture was centrifuged to remove large particles and impurities, passed over a 0.22 µm filter membrane to isolate the N-CQDs, which were stored in the refrigerator or further analysis.

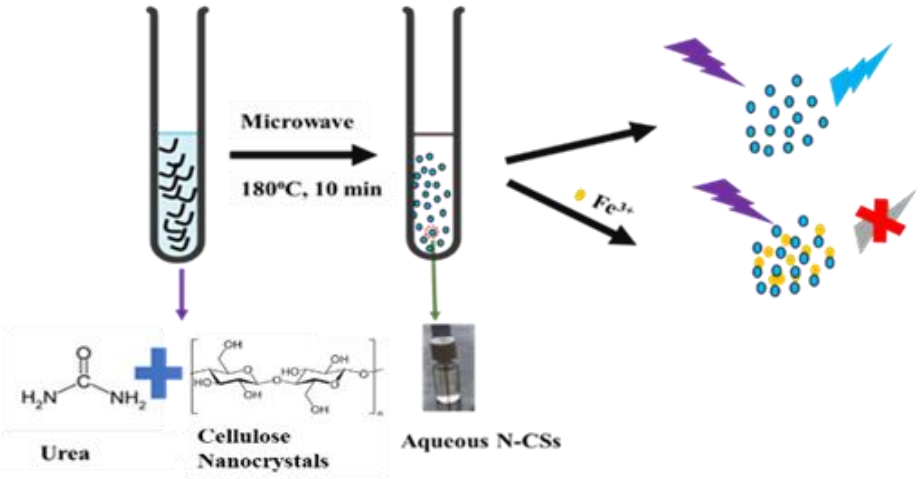

Figure 6.1: Synthesis of N-CQDs using microwave synthesis and their application in the detection of Fe^{3+} using photoluminescence spectroscopy

6.2.2.2 Detection of Fe^{3+} using N-CQDs

For the detection of Fe^{3+}, N-CQDs (100 µL of the original fluid was diluted with 2 mL of distilled water) and mixed with varying concentrations of ferric nitrate (0-3000 µM) at a 1:1 v/v ratio. To study the selectivity of the prepared N-CQDs towards the detection of Fe^{3+} in aqueous solution, other metal ions with the concentration of 1000 µM were prepared (K^+, Cd^{2+}, Mg^{2+}, Zn^{2+}, Ni^{2+}, Al^{3+}, Co^{2+}, Na^+, and Cu^{2+}), and examined similarly to Fe^{3+}. The fluorescence emission spectra of the above solutions were collected at the optimum excitation wavelength of 340 nm.

6.3 Characterization

The functional groups of N-CQDs were analyzed using a Fourier transform infrared spectroscopy (FT-IR) ((Brucker TENSOR 27 FT-IR). The materials were studied by powder X-ray diffraction (PXRD) (Bruker D2 phaser equipped with Cu-Kα radiation (λ = 1.5405 Å)), at an operating voltage of 30 kV and current of 10 mA. Transmission electron microscopy was used to determine the morphology of the particles (TEM, FEI Technai G2 Spirit) operated at 120 kV. ImageJ software was used to determine the particle size distribution from TEM images; more than 150 particles were measured. The fluorescence characteristics of the N-CQDs were analzsed using a photoluminescence (PL) spectrophotometer (Varian Cary 2656 Eclipse EL04103870 fluorescence spectrophotometer). The UV–vis absorption spectra of the N-CQDs were recorded using a spectrophotometer (SPECORD 210 plus UV–vis spectrophotometer).

6.4 Results and discussion

6.4.1 Properties of the N-CQDs

Transmission electron microscope (TEM) images (figure 6.2) demonstrate that the prepared N-CQDs exhibited spherical particles with diameters ranging from 1–5 nm and an average size of 2.30± 0.55 nm (the diameters of the particles were determined from the TEM images using ImageJ software as shown in the inset of figure 6.2 a). FT-IR spectroscopy was employed to determine the functional groups populating the surface of the CNCs and N-CQDs (figure 6.3 a). The characteristic absorption peaks of the CNCs at 3046-3675 cm^{-1}, and 2805-2990 cm^{-1} are attributed to the O-H and C-H stretching vibrations [32], these peaks slightly shifted on the N-CQDs appearing around 2735-3522 cm^{-1}, with an additional adsorption band around 3272-3389 cm^{-1} which is due to the N-H stretch [33]. Comparatively, the spectrum of N-CQDs consist of special bands between 1324 cm^{-1} and 1610 cm^{-1}, which correspond to the characteristic stretching vibration of C-N bonds and the N-H bonds respectively, suggesting nitrogen was successfully incorporated during the N-CQDs synthesis [34]. The XRD pattern of the N-CQDs is shown in figure 6.3 b. A broad diffraction peak around 23.0° and a weak shoulder peak around 42.0° were observed for the prepared NCQDs. These peaks were assigned to the (002) and (100) planes of graphitic carbon, revealing a graphitic nature of the N-CQDs with highly disordered carbon atoms [35, 36]. The inset in figure 6.3 b, shows the XRD reflections of the cellulose nanocrystals (CNCs), three reflection peaks at 16, 22, and 34 °

which were assigned to the amorphous and crystalline carbon framework. This indicates that the CNCs were fully carbonized during the synthesis of N-CQDs [37]. The optical properties of the as-prepared N-CQDs were studied using both UV–vis and photoluminescence spectroscopy.

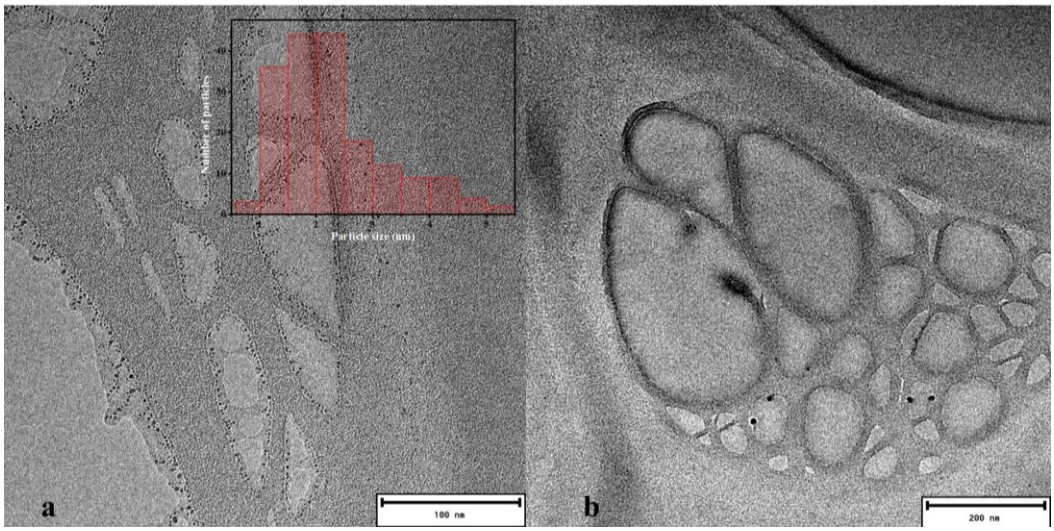

Figure 6.2: (a-b) TEM images of the N-CQDs, the inset in (a) shows the particle size distribution of the N-CQDs

Figure 6.3 c shows the UV-Vis absorption spectra of the N-CQDs, two characteristic peaks at 220 and 285 nm were observed. These were assigned to the π - π * transition of the C=C or C=N bonds in the carbon core and the n- π * transition of the C=O or amine groups on the surface of the N-CQDs [34]. Under the UV lamp (365 nm) the N-CQDs exhibited a blue fluorescence (shown in the inset of figure 6.3 c). Figure 6.3 d, shows the excitation dependent fluorescence emission spectra of N-CQDs obtained at varying excitation wavelengths from 300 nm to 400 nm with an increment of 10 nm, which resulted in an emission redshift [35]. This property may be due to the distribution of different functional groups with different emission traps, the difference in particle size, and multi fluorescence components in N-CQDs [27].

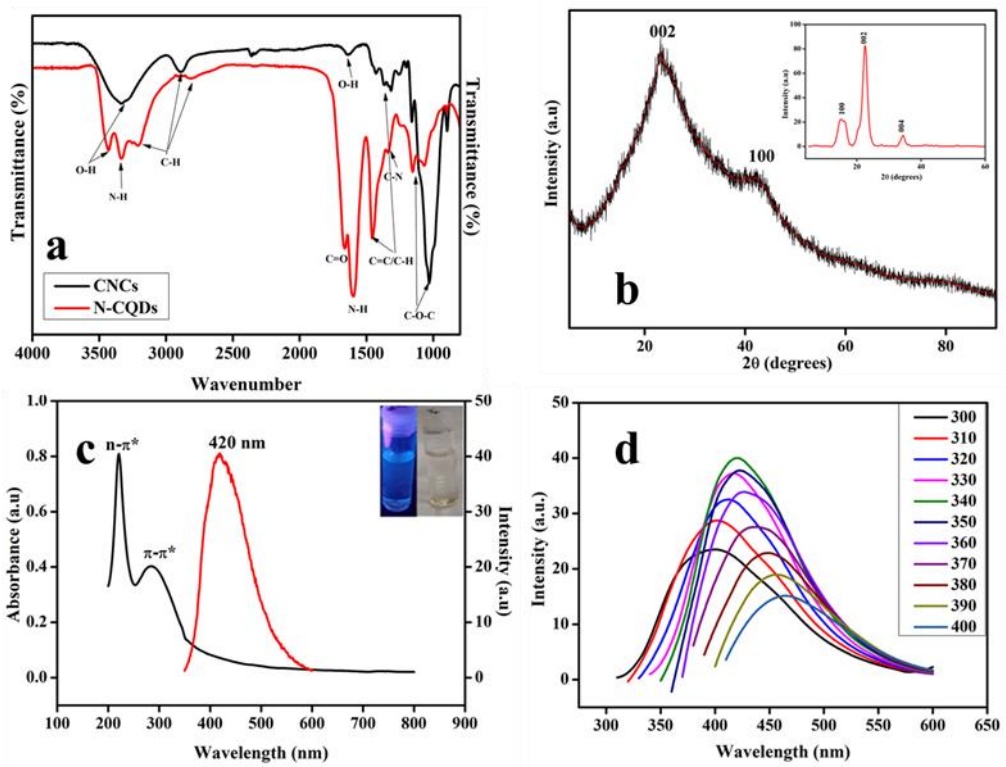

Figure 6.3: (a) FT-IR of CNCs and the N-CQDs, (b) XRD of the N-CQDs, (c) UV–vis absorption spectra of the as-prepared N-CQDs sample in water (black) and fluorescence emission of the N-CQDs at 340nm excitation wavelength (red) and (d) is the fluorescence spectra obtained from different wavelengths of excitation 300–400 nm (with 10 nm increments starting from 300 nm). The inset in (c) shows the N-CQDs sample solution in water during daylight and under a UV lamp (365 nm) and the inset in (b) shows the XRD profile of the cellulose nanocrystals

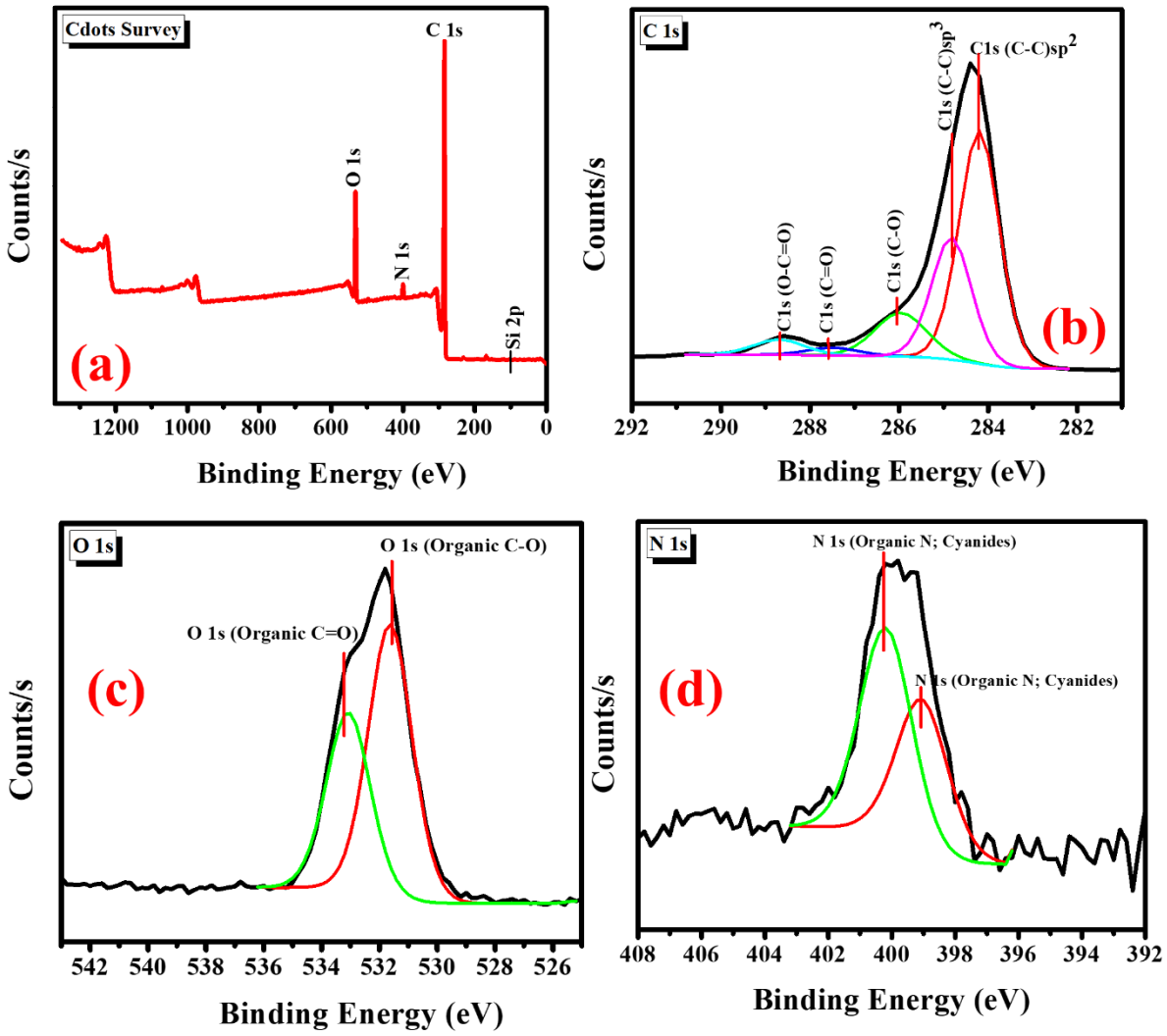

Figure 6.4: (a) XPS survey spectrum of N-CQDs. (b–d) High resolution (Core level) of C 1s, O 1s, and N 1s from as synthesized N-CQDs, respectively

XPS analysis is a powerful surface sensitive technique that has been used to confirm the chemical composition, nature of bonding, and purity of the as-prepared N-CQDs. Figure 6.4 a shows XPS survey spectrum of N-CQDs, which have confirmed that the presence of carbon (C), oxygen (O), Nitrogen (N), and Silicon (Si). With atomic percentage of 83.8 % of carbon, 12.2 % of oxygen, 2.9 % of nitrogen, and Si (< 1%) impurities due to the starting material (corncob) used during preparation. Figure 6.4 b–d show the high-resolution spectra of C 1s, O 1s, and N 1s, respectively. The high-resolution spectra of C 1s revealed distinguishable six peaks at 284.6, 284.2, 284.8, 286.0, 287.6 and 288.7 eV, assigned to C–C sp^2 bond, C-C sp^3 bond, C-O, C=O and O-C=O bonds, respectively which is consistent with the FT-IR results. The high-resolution spectrum of O 1s as shown in figure 6.4 (b) was deconvoluted to three peaks at 531.6 and 533.17 eV assigned to the C-O and C=O bonds. The high-resolution spectrum of N 1s (figure 6.3 d) was deconvoluted to two peaks centered at 399.1 and 400.2 eV associated to pyrrolic and graphitic N [36]. Figure 6.5 demonstrates the possible position of surface functional groups on N-doped

Cdots as determined by N1s XPS survey deconvolution, which confirmed the incorporation of nitrogen functional groups (N-H) similar to the FTIR.

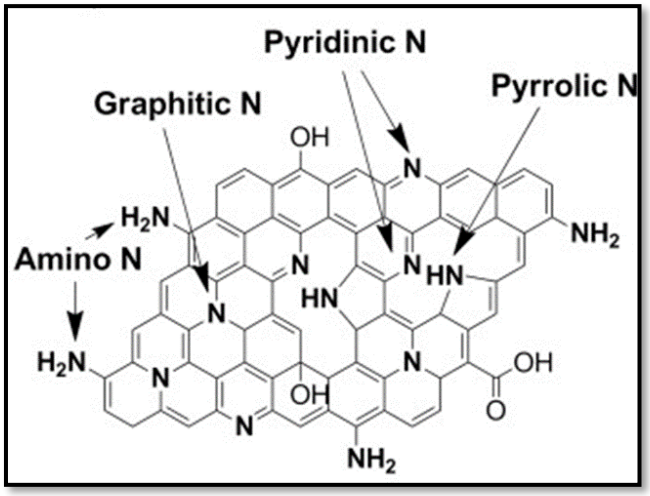

Figure 6.5: Types of nitrogen dopants in N-CQDs.

6.5 N-CQDs based fluorescent chemosensor for sensitive and selective detection of Fe^{3+}

6.5.1 Sensitivity of the N-CQDs for Fe^{3+} detection

The sensitivity of the N-CQDs towards Fe^{3+} was studied by adding different concentrations of Fe^{3+} (0 µM to 3000 µM) to the N-CQDs suspension and measuring the fluorescence emission intensity at the optimum excitation wavelength of 340 nm. As shown in figure 6.6 a, the fluorescence intensity of the N-CQDs decreased gradually with increasing concentration of the Fe^{3+}, indicating that the addition of Fe^{3+} ions can effectively quench the fluorescence emission of the N-CQDs. Based on previous studies the mechanism of fluorescence quenching of N-CQDs in the presence of Fe^{3+} is caused by the formation of the N-CQDs-Fe^{3+} complexes, which facilitate electron transfer between N-CQDs and Fe^{3+} and restrict excitation recombination, leading to fluorescence quenching [10, 14]. The quenching constant was calculated using the Stern-Volmer equation: $F_0/F - 1 = Ksv\,[Fe^{3+}]$, where Ksv represents the static Stern-Volmer constant, F_0 and F represent the fluorescence intensities of the N-CQDs in the absence and presence of Fe^{3+} ions respectively. The Stern-Volmer plots in figure 6.6 b showed a good linearity in the Fe^{3+} range of 0–500 µM with Ksv equal to $0.164 \times 10^4\ M^{-1}$ and a correlation coefficient (R^2) value of 0.995. The limit of detection (LOD) was calculated to be 75 nM using the formula LOD= 3σ/s (where σ is the standard deviation and s is the slope of the linear response) which is comparable to previously

reported fluorescence methods of Fe^{3+} ions' detection as shown in table 6.1 [8, 9, 12, 13, 34–37]. UV-Vis absorption was used to further study the mechanism of fluorescence quenching of the N-CQDs in the presence and absence of Fe^{3+} (Figure 6.6 c). After adding 1000 µM Fe^{3+}, the absorption peak at 285 nm disappeared and the spectrum resembled the absorption spectrum of the undiluted Fe^{3+}, indicating that Fe^{3+} ions saturated the surface of N-CQDs, which resulted in colour change from bright blue to brown colour under the UV irradiation (the inset of figure 6.6 c).

Table 6.1: Comparison of different methods used for the detection of Fe^{3+}

Detection method	**sensors**	**Linear range (µM)**	**LOD (µM)**	**Reference**
Fluorescence	CDs from pinewood	0-1000	0.36	[15]
Fluorescence	CDs from sweet potato	0-100	0.32	[37]
Fluorescence	N-GQDs from marigold	0-20	0.041	[38]
Fluorescence	N-CQDs from chitosan	1-200	0.15	[39]
Fluorescence	N-CQDs from watermelon juice	0-300	0.16	[21]
Fluorescence	N-CQDs from cellulose nanocrystals	0-500	0.075	This work

6.5.2 Selectivity of the N-CQDs towards Fe^{3+}

To investigate the selectivity of the N-CQDs towards Fe^{3+}, the fluorescence emission of different metal ions with the potential of interfering with Fe^{3+} (1000 µM of Ca^{2+}, Cd^{2+}, Cu^{2+}, Co^{2+}, Mg^{2+}, Ni^{2+}, Zn^{2+}, Al^{3+}, K^{+}, or Na^{+}) were measured at the optimum excitation wavelength of 340 nm. Fig. 6.6 d shows the quenching effect of the different metal ions. It is seen that Fe^{3+}, Cu^{2+}, Ni^{2+}, and Co^{2+} tend to decrease the fluorescent intensity, with Fe^{3+} showing the strongest effect. Cd^{2+}, Ca^{2+}, and K^{+} slightly increase the fluorescent intensity, and no effect was observed after adding Na^{+}, Mg^{2+}, Zn^{2+}, and Al^{3+}. The reason for this quenching is ascribed to the strong affinity of N-CQDs toward Fe^{3+}, facilitating electron transfer between N-CQDs and the half-filled 3d orbital of Fe^{3+} ion and restrict excitation recombination, leading to fluorescence quenching [14]. To further study the interference of Fe^{3+} with other metal ions, Fe^{3+} detection in the presence of other ions was also measured. As shown in figure 6.6 d after the addition of Fe^{3+}, the other metal ions start to exhibit a slight quenching effect on the fluorescence of the N-CQDs. The obtained results indicate that the prepared N-CQDs have a high sensitivity and selectivity towards the detection of Fe^{3+} and can be used as a chemosensor in an aqueous environment with competing ions.

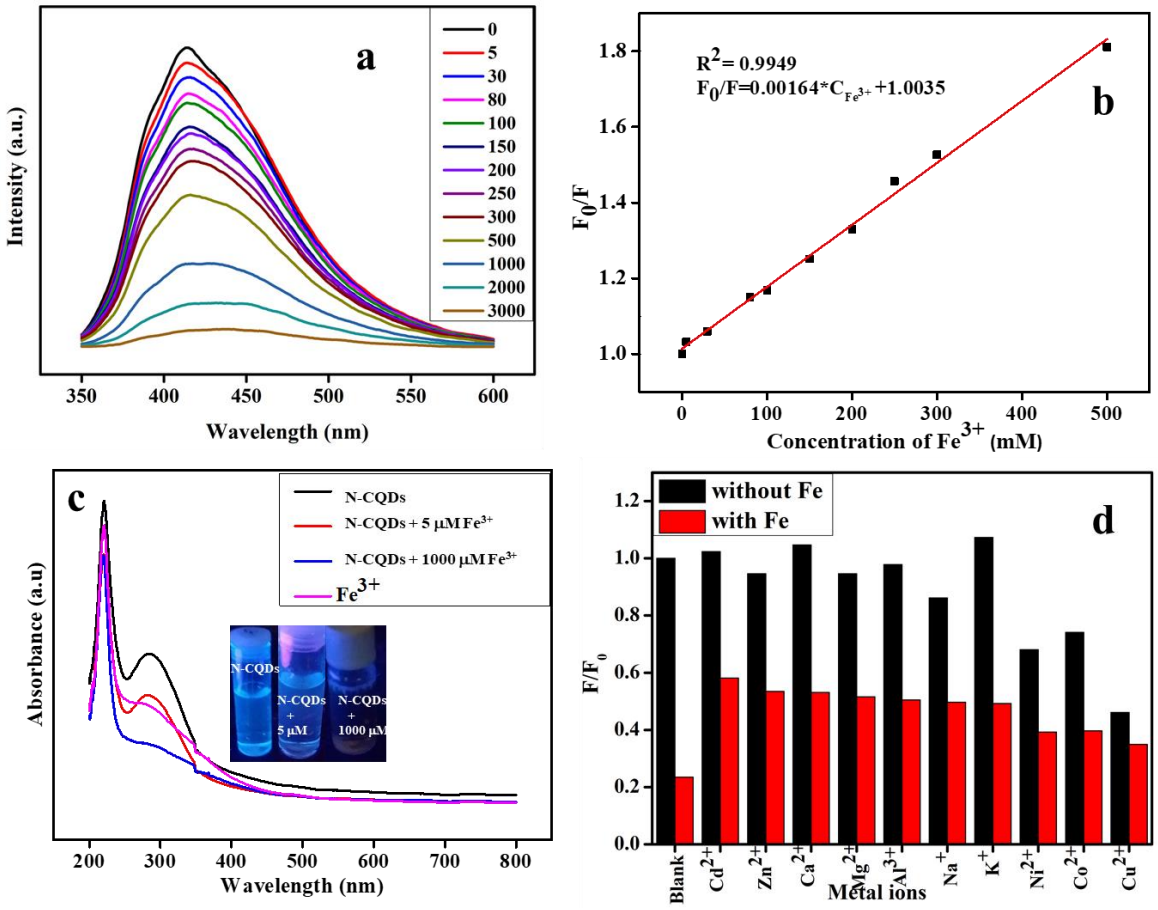

Figure 6.6: (a) Fluorescence spectra of N-CQDs in different concentrations of Fe3+ (5–3000 μM), (b) Linear relationship between F0/F and Fe3+ concentration (5-500 μM), (c)UV-vis spectra of the N-CQDs with and without different concentrations of Fe3+, and (d) Changes in the fluorescence intensity ratio (I/I0) of N-CQDs after the addition of various metal ions. The inset in (c) shows the N-CQDs sample with different concentrations of Fe3+ under the UV lamp (365 nm)

6.6 Conclusion

In this study, highly photoluminescent N-CQDs with high sensitivity towards Fe^{3+} in aqueous solutions and a bright blue emission were synthesized by a one-step microwave synthesis from a mixture of cellulose nanocrystals and urea. The LOD was determined to be 75 nM which is comparable to previously reported Fe^{3+} fluorescence detection methods. The study demonstrated that the prepared N-CQDs have a potential to be applied as chemosensors for detection of metal ions in aqueous environments. Future studies will investigate the effect of varying reaction parameters on the sensitivity, selectivity and the quantum yield of the N-CQDs. Heteroatom doping effect on the properties of CQDs will also be investigated.

6.7 References

[1] M. A. Akram, J.Ye, G.Wang, L. Shi, Z. Liu, H. Lu, S. Zhang, and G. Ning, "Bifunctional chemosensor based on a dye-encapsulated metal-organic framework for highly selective and sensitive detection of Cr2O72− and Fe3+ ions," *Polyhedron*, vol. 185, p. 114604, 2020, doi: 10.1016/J.POLY.2020.114604.

[2] H. Guo, X. Wang, N. Wu, M. Xu, M. Wang, L. Zhang, and W. Yang, "In-situ synthesis of carbon dots-embedded europium metal-organic frameworks for ratiometric fluorescence detection of Hg2+ in aqueous environment," *Anal. Chim. Acta*, vol. 1141, pp. 13–20, 2021, doi: 10.1016/j.aca.2020.10.028.

[3] Y. Jiang, Y. Wang, F. Meng, B. Wang, Y. Cheng, and C. Zhu, "N-doped carbon dots synthesized by rapid microwave irradiation as highly fluorescent probes for Pb 2+ detection †," *New J. Chem*, vol. 39, p. 3357, 2015, doi: 10.1039/c5nj00170f.

[4] S. Chaudhary, M. Kumari, P. Chauhan, and G. Ram Chaudhary, "Upcycling of plastic waste into fluorescent carbon dots: An environmentally viable transformation to biocompatible C-dots with potential prospective in analytical applications," *Waste Manag.*, vol. 120, pp. 675–686, 2021, doi: 10.1016/j.wasman.2020.10.038.

[5] X. Ji, S. Wang, Y. Luo, X. Yuan, Y. Wei, Q. Zhang, K. Qin, Y. Tu, "Green synthesis of weissella-derived fluorescence carbon dots for microbial staining, cell imaging and dual sensing of vitamin B12 and hexavalent chromium," *Dye. Pigment.*, vol. 184, pp. 108818, 2021, doi: 10.1016/j.dyepig.2020.108818.

[6] Y. Wang, S. Lao, W. Ding, Z. Zhang, and S. Liu, "A novel ratiometric fluorescent probe for detection of iron ions and zinc ions based on dual-emission carbon dots," *Sensors Actuators, B Chem.*, vol. 284, pp. 186–192, 2019, doi: 10.1016/j.snb.2018.12.139.

[7] S. Saxena and S. F. D'Souza, "Heavy metal pollution abatement using rock phosphate mineral," in *Environment International*, vol. 32, pp. 199–202, 2006, doi: 10.1016/j.envint.2005.08.011.

[8] Y. Jiang, Q. Han, C. Jin, J. Zhang, and B. Wang, "A fluorescence turn-off chemosensor based on N-doped carbon quantum dots for detection of Fe3+ in aqueous solution," *Mater. Lett.*, vol. 141, pp. 366–368, 2015, doi: 10.1016/j.matlet.2014.10.168.

[9] H. Qi, M. Teng, M. Liu, S. Liu, J. Li, H. Yu, C. Teng, Z. Huang, H. Liu, Q. Shao, A. Umar, T. Ding, Q. Gaog, and Z. Guo,"Biomass-derived nitrogen-doped carbon quantum dots: highly

selective fluorescent probe for detecting Fe 3+ ions and tetracyclines," *J. Colloid Interface Sci.*, vol. 539, pp. 332–341, 2019, doi: 10.1016/j.jcis.2018.12.047.

[10] F. Wu, M. Yang, H. Zhang, S. Zhu, X. Zhu, and K. Wang, "Facile synthesis of sulfur-doped carbon quantum dots from vitamin B1 for highly selective detection of Fe3+ ion," *Opt. Mater. (Amst).*, vol. 77, pp. 258–263, 2018, doi: 10.1016/j.optmat.2018.01.048.

[11] G. Gao, Y. W. Jiang, H. R. Jia, J. Yang, and F. G. Wu, "On-off-on fluorescent nanosensor for Fe3+ detection and cancer/normal cell differentiation via silicon-doped carbon quantum dots," *Carbon N. Y.*, vol. 134, pp. 232–243, 2018, doi: 10.1016/j.carbon.2018.02.063.

[12] M. Zulfajri, G. Gedda, C.-J. Chang, Y.-P. Chang, and G. G. Huang, "Cranberry Beans Derived Carbon Dots as a Potential Fluorescence Sensor for Selective Detection of Fe 3+ Ions in Aqueous Solution," ACS Omega., vol. 4, pp. 15382–15392, 2019, doi: 10.1021/acsomega.9b01333.

[13] T. T. Xu, X. Yang, J.M. Song, J. S. Chen, H. L. Niu, C. J. Mao, S. Y. Zhang, and Y. H. Shen, "Synthesis of high fluorescence graphene quantum dots and their selective detection for Fe3+ in aqueous solution," *Sensors Actuators B Chem.*, vol. 243, pp. 863–872, 2017, doi: 10.1016/J.SNB.2016.12.048.

[14] X. Deng, Y. Feng, H. Li, Z. Du, Q. Teng, and H. Wang, "N-doped carbon quantum dots as fluorescent probes for highly selective and sensitive detection of Fe3+ ions," *Particuology*, vol. 41, pp. 94–100, 2018, doi: 10.1016/j.partic.2017.12.009.

[15] S. Zhao, X. Song, X. Chai, P. Zhao, H. He, and Z. Liu, "Green production of fluorescent carbon quantum dots based on pine wood and its application in the detection of Fe3+," *J. Clean. Prod.*, vol. 263, p. 121561, 2020, doi: 10.1016/j.jclepro.2020.121561.

[16] K. Wang, J. Chen, H. Li, M. Zhang, and Q. Liao, "A fluorescent probe for selective detection of Fe 3+ by using a self-assembled nitrogen-doped carbon quantum dots-3,4,9,10-perylenetetracarboxylic acid composite," *Ionics (Kiel).*, vol. 1, pp. 3, 2021, doi: 10.1007/s11581-021-04233-4.

[17] F. Wu, M. Yang, H. Zhang, S. Zhu, X. Zhu, and K. Wang, "Facile synthesis of sulfur-doped carbon quantum dots from vitamin B1 for highly selective detection of Fe3+ ion," *Opt. Mater. (Amst).*, vol. 77, pp. 258–263, 2018, doi: 10.1016/J.OPTMAT.2018.01.048.

[18] R. Guo, S. Zhou, Y. Li, X. Li, L. Fan, and N. H. Voelcker, "Rhodamine-Functionalized Graphene Quantum Dots for Detection of Fe 3+ in Cancer Stem Cells," *ACS Appl. Mater. Interfaces.*, vol. 7, pp. 23958–23966, -+-*2015, doi: 10.1021/acsami.5b06523.

[19] W. J. Ji, W. W Pei, Q. B. Wang, G. F. Liu, B. Yan, S. G. Yao, and Q. G. Zhao, "Decoration of bare carboxyl group on the pore surface of metal-organic frameworks for high selective fluorescence Fe3+ detection," *J. Solid State Chem.*, vol. 274, pp. 18–25, Jun. 2019, doi: 10.1016/J.JSSC.2019.02.035.

[20] J. J. Ma, and W. Liu, "Two water-stable Cd(II)-MOFs as multiresponsive chemosensor with high sensitively and selectively detection of Fe3+, Cr2O72− and MnO4− ions," *J. Solid State Chem.*, vol. 303, pp. 122538, 2021, doi: 10.1016/J.JSSC.2021.122538.

[21] M. Lu, Y. Duan, Y. Song, J. Tan, and L. Zhou, "Green preparation of versatile nitrogen-doped carbon quantum dots from watermelon juice for cell imaging, detection of Fe3+ ions and cysteine, and optical thermometry," *J. Mol. Liq.*, vol. 269, pp. 766–774, 2018, doi: 10.1016/j.molliq.2018.08.101.

[22] Y. Chen, X. Sun, W. Pan, G. Yu, and J. Wang, "Sensitive Carbon Dots for Detection of Fe 3+ in Aqueous Solution and Intracellular Imaging of Fe 3+ Inside Fungal Cells," *Front. Chem*, vol. 7, pp. 911, 2020, doi: 10.3389/fchem.2019.00911.

[23] X. Xu, R. Ray, Y. Gu, H. J. Ploehn, L. Gearheart, K. Raker, and W. A. Scrivens "Electrophoretic Analysis and Purification of Fluorescent Single-Walled Carbon Nanotube Fragments," *J. AM. CHEM. SOC*, vol. 126, pp. 12736–12737, 2004, doi: 10.1021/ja040082h.

[24] Y. Zhuo, H. Miao, D. Zhong, S. Zhu, and X. Yang, "One-step synthesis of high quantum-yield and excitation-independent emission carbon dots for cell imaging," *Mater. Lett.*, vol. 139, pp. 197–200, 2015, doi: 10.1016/J.MATLET.2014.10.048.

[25] X. W. Tan, A. N. B. Romainor, S. F. Chin, and S. M. Ng, "Carbon dots production via pyrolysis of sago waste as potential probe for metal ions sensing," *J. Anal. Appl. Pyrolysis*, vol. 105, pp. 157–165, 2014, doi: 10.1016/J.JAAP.2013.11.001.

[26] X. Deng, Y. Feng, H. Li, Z. Du, Q. Teng, and H. Wang, "N-doped carbon quantum dots as fluorescent probes for highly selective and sensitive detection of Fe3+ ions," *Particuology*, vol. 41, pp. 94–100, 2018, doi: 10.1016/J.PARTIC.2017.12.009.

[27] Y. Guo, F. Cao, and Y. Li, "Solid phase synthesis of nitrogen and phosphor co-doped carbon quantum dots for sensing Fe3+ and the enhanced photocatalytic degradation of dyes," *Sensors Actuators, B Chem.*, vol. 255, pp. 1105–1111, 2018, doi: 10.1016/j.snb.2017.08.104.

[28] Y. Liu, N. Xiao, N. Gong, H. Wang, X. Shi, W. Gu, and L. Ye, "One-step microwave-assisted polyol synthesis of green luminescent carbon dots as optical nanoprobes," *Carbon N. Y.*, vol. 68,

pp. 258–264, 2014, doi: 10.1016/j.carbon.2013.10.086.

[29] S. Qu, X. Wang, Q. Lu, X. Liu, and L. Wang,“Carbon Nanodots A Biocompatible Fluorescent Ink Based on Water-Soluble Luminescent Carbon Nanodots**,” *Angewandte Chemie International Edition*, vol. 124, pp. 12381–12384, 2012, doi: 10.1002/ange.201206791.

[30] S. Li, L. Li, H. Tu, H. Zhang, D. S.Silvester, C. E.Banks, G. Zou, H. Hou, and X. Ji, “The development of carbon dots: From the perspective of materials chemistry,” *Mater. Today*, vol. 51, pp. 188–207, 2021, doi: 10.1016/J.MATTOD.2021.07.028

[31] L. P. Magagula, N. Moloto, S. Gqoba, P. J. Kooyman, T. E. Motaung, and E. C. Linganiso, “Synthesis of fluorescent nitrogen-doped carbon spheres from corncob residue for the detection of Fe (III) in aqueous solutions,” *IEEE Sensors*, pp. 1–4, 2021, doi: 10.1109/SENSORS47087.2021.9639764.

[32] N. Johar, I. Ahmad, and A. Dufresne, “Extraction, preparation and characterization of cellulose fibres and nanocrystals from rice husk,” *Ind. Crops Prod.*, vol. 37, no. 1, pp. 93–99, 2012, doi: 10.1016/j.indcrop.2011.12.016.

[33] J. Xu, E. F. Krietemeyer, V. M. Boddu, S. X. Liu, and W. C. Liu, “Production and characterization of cellulose nanofibril (CNF) from agricultural waste corn stover,” *Carbohydr. Polym.*, vol. 192, pp. 202–207, 2018, doi: 10.1016/J.CARBPOL.2018.03.017.

[34] Y. Yuan, Y. Sun, Z. Feng, X. Li, R. Yu, W. Sun, C. Zhao, and L. Yang, “Nitrogen-doped hierarchical porous activated carbon derived from paddy for high-performance supercapacitors,” *Materials (Basel).*, vol. 14, pp. 1–12, 2021, doi: 10.3390/ma14020318.

[35] C. Hu, Y. Zhu, and X. Zhao, “On-off-on nanosensors of carbon quantum dots derived from coal tar pitch for the detection of Cu2+, Fe3+, and L-ascorbic acid,” *Spectrochim. Acta - Part A Mol. Biomol. Spectrosc.*, vol. 250, pp. 119325, 2021, doi: 10.1016/j.saa.2020.119325.

[36] N. Far’ain Md Noor, M. A. Saiful Badri, M. M. Salleh, and A. A. Umar, “Synthesis of white fluorescent pyrrolic nitrogen-doped graphene quantum dots,” *Opt. Mater. (Amst).*, vol. 83, pp. 306–314, Sep. 2018, doi: 10.1016/J.OPTMAT.2018.06.040.

[37] J. Shen, S. Shang, X. Chen, D. Wang, and Y. Cai, “Facile synthesis of fluorescence carbon dots from sweet potato for Fe3 + sensing and cell imaging,” *Mater. Sci. Eng. C*, vol. 76, pp. 856–864, 2017, doi: 10.1016/j.msec.2017.03.178.

[38] Y. P. Zhang, J. M. Ma, Y. S.Yang, J. X. Rub, X. Y. Liu, Y. Ma, and H. C. Guob, “Synthesis of nitrogen-doped graphene quantum dots (N-GQDs) from marigold for detection of Fe 3+ ion and

bioimaging," *Spectrochim. Acta - Part A Mol. Biomol. Spectrosc.*, vol. 217, pp. 60–67, 2019, doi: 10.1016/j.saa.2019.03.044.

[39] L. Zhao, Y. Wang, X. Zhao, Y. Deng, and Y. Xia, "Facile Synthesis of Nitrogen-Doped Carbon Quantum Dots with Chitosan for Fluorescent Detection of Fe 3+," *Polymers*, vol.11, pp. 1731, 2019, doi: 10.3390/polym11111731.

Chapter 7: Conclusions and recommendation

7.1 Conclusions

Developing countries such as South Africa experience significant negative impacts associated with poor agricultural waste management. The growing environmental awareness has resulted in growing research interest in the use of agricultural waste to prepare renewable and green resources for sustainable economies. Agricultural waste has been utilized in this study to prepare cellulose nanocrystals and different types of carbon materials (activated carbon (AC) and carbon quantum dots (CQDs)). The aim study was of this study was to improve the economical use of corncob waste as a feedstock for preparation of CQDs and activated carbon for sensing applications. Acid hydrolysis was used to extract CNCs from corncob which were compared to the CNCs prepared from commercial microcrystalline cellulose. The CNCs samples revealed comparable thermal, surface/structural, and crystallinity. These were confirmed by various characterizations techniques including SEM, TEM, XRD, TGA, and FT-IR analysis. The as-prepared CNCs were then utilized to prepare highly luminescent N-CQDs with a high degree of functional groups, sensitivity, and selectivity towards Fe^{3+}. CQDs showed great potential for fluorescent sensor applications. Incorporation of surface functional groups such as nitrogen and oxygen containing groups were confirmed by FT-IR and XPS analysis which showed that the prepared N-CQDs were highly functionalized with these heteroatoms, resulting in emission redshift as the excitation wavelength increased from 300-400 nm.

Due to its natural porous nature, the corncob was also utilized to prepare activated carbons by chemical activation with potassium carbonate (activating agent) at 800 °C using varied ratios of impregnation. Highly porous AC material with BET surface area of 1523.2 m^2 /g and a pore volume = 0.81 cm^3 /g was obtained in this study. Decoration of the activated carbon with CuO NPs was achieved, in which the effect of CuO NPs loading was investigated using TEM, XRD, BET, and TGA. The prepared ACC/CuO composites exhibited higher BET specific surface areas when compared to pristine CuO NPs. Sensing of VOCs at room temperature conditions was studied using different sensors designed from the pristine ACC, ACC/PVA/CuO 5%, ACC/PVA/CuO 10%, and ACC/PVA/CuO 15 %. The results showed that CuO NPs play an important role in enhancing sensor performance of the ACC since its incorporation improved on

the conductivity and response when compared to the ACC-based sensor. The ACC/PVA/CuO 15% sensor exhibited better sensing performance compared to all the sensors due the introduction of more defects on the surface of activated carbon contributing to increased electrical conductivity, active sites, whereby the surface modifications promoted the adsorption and diffusion of vapour. The ACC/PVA/CuO sensor demonstrated good reproducibility of the sensing signal when exposed to 100 ppm ethanol vapours for up to four cycles. Hence, the ACC/CuO composites could be a future candidate for ethanol gas sensing application at room temperature.

7.2 Recommendation for future work

Having described the potential of acid hydrolysis and chemical activation for applicability in the conversion of agricultural waste to value added products that have a potential to be utilized as chemical sensors, it is important to note that there is required work for further scope in the development of value-added products from agricultural waste in South Africa. Efficient methods for converting lignocellulosic waste to CNCs are still desirable. Future work should look into minimizing the number of steps required to produce CNCs from corncob. The nitro-oxidation method can be investigated further as an alternative to the conventional acid hydrolysis method.

The effect of microwave reaction parameters and heteroatom dopants on the quantum yield and subsequent application of CQDs is yet to be fully explored. Multi-heteroatom co-doping, and surfactant coordination on CQDs can be investigated for improved selectivity in heavy metal ion detection. Further, photoluminescence lifetime measurements are necessary to ensure successful application of CQDs.

Our sensing data showed an increasing response with increasing CuO concentration in the prepared composites, low concentrations of heavy metal oxides are usually desirable in order to minimise the toxicity and possible leaking of the heavy metals, however, increasing the CuO concentration in the composites should be studied in order to evaluate the highest possible response of the materials.

Synthesis of fluorescent nitrogen-doped carbon spheres from corncob residue for the detection of Fe (III) in aqueous solutions

Lindokuhle P. Magagula[1], Nosipho Moloto[1], Siziwe Gqoba[1], Patricia J. Kooyman[2], Tshwafo E Motaung[3,4] and Ella C. Linganiso[1,4,5]*

[1]Molecular Sciences Institute, School of Chemistry, University of the Witwatersrand, Braamfontein, 2050, South Africa

[2]Department of Chemical Engineering, University of Cape Town, Rondebosch, 7701, Cape Town, South Africa

[3]Department of Chemistry, School of Science in the College of Science Engineering and Technology, University of South Africa, Preller Street, Muckleneuk Ridge, City of Tshwane, UNISA 0003, South Africa

[4]Department of Chemistry, Sefako Makgatho Health Science University, Medunsa 0204, South Africa

[5]Microscopy and Microanalysis Unit, University of the Witwatersrand, Braamfontein, 2050, South Africa

Cebisa.Linganiso@wits.ac.za*

***Abstract*— Water contamination has become more severe as modern industrial technology has progressed over the years. Among water contaminants are heavy metal ions such as Fe^{3+}, which is commonly used in industries such as mining, chemical processing, and battery manufacturing. Fe^{3+} is the principal contaminant of concern in acid mine drainage from coal mines, causing siderosis and organ damage. The current study prepared highly photoluminescent nitrogen-doped functionalized carbon spheres (N-CSs) from corncob residue using a facile, green, and low-cost microwave synthesis. The as-prepared N-CSs exhibited an excitation-dependent fluorescence with a maximum emission and excitation at 420 and 340 nm, respectively and showed good selectivity and sensitivity towards the detection of Fe^{3+} with a 70 nM limit of detection.**

Keywords*— *Corncob residue, Carbon spheres, Sensor, Fe^{3+}, Fluorescence quenching

I. Introduction

Maize (Zea mays), also known as corn, is a widely distributed crop, with a global production of approximately 10.99×10^8 tons in the 2018-2019 season [27]. In South Africa, corn is a staple food with over 16 million tons produced in the 2019-2020 period, which an 38% increase

compared to the 2018-2019 crop [7].

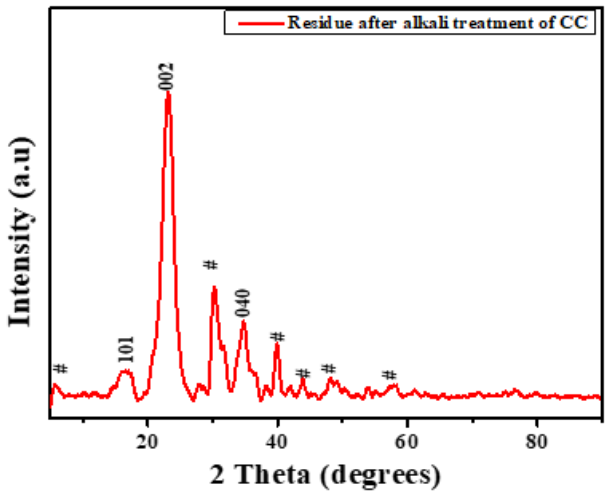

Figure S3.1: XRD pattern of the residue after alkali treatment

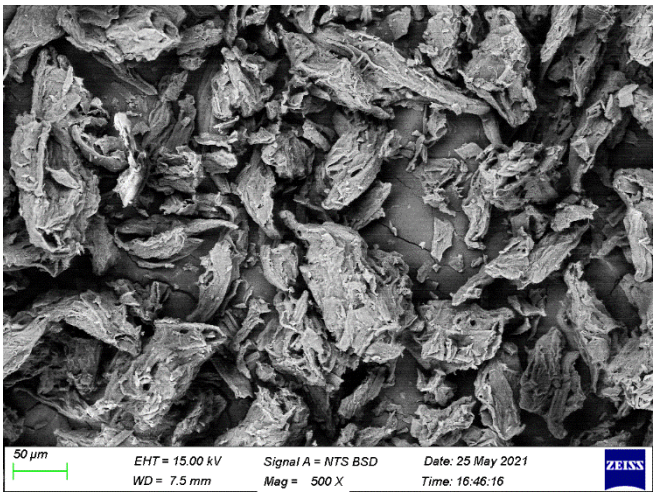

Figure S3.2: SEM image of MCC